NASA Contractor Report 182252

Concentration Measurements in a Cold Flow Model Annular Combustor Using Laser Induced Fluorescence

Douglas C. Morgan
Purdue University
West Lafayette, Indiana

September 1996

Prepared for
Lewis Research Center
Under Contract NAS3–24350

National Aeronautics and
Space Administration

CONCENTRATION MEASUREMENTS IN A COLD FLOW MODEL ANNULAR COMBUSTOR USING LASER INDUCED FLUORESCENCE

A Thesis

Submitted to the Faculty

of

Purdue University

by

Douglas C. Morgan

In Partial Fulfillment of the

Requirements for the Degree

of

Master of Science in Mechanical Engineering

August 1988

ACKNOWLEDGMENTS

The author would like to express his gratitude to his major professor, Dr. John P. Sullivan. His technical guidance, criticism and support is greatly appreciated.

The author would also like to thank Dr. S. Fleeter, Dr. S. N. B. Murthy and Dr. W. G. Tiederman for their participation on his advisory committee.

This research was sponsored by the Air Force Office of Scientific Research (AFOSR) through the Air Force Research in Aeropropulsion Technology (AFRAPT) program. The test rig used in this research was provided by NASA Lewis Research Center and Allison Gas Turbine Division.

Special thanks are in order for the author's wife, Maryann, without whose patience, support and assistance the work contained in this thesis would not have been possible.

TABLE OF CONTENTS

LIST OF TABLES

LIST OF FIGURES

Figure Page

Figure Page

Figure Page

ABSTRACT

Morgan, Douglas C. MSME. Purdue University. August 1988. *Concentration Measurements in a Cold Flow Model Annular Combustor using Laser Induced Fluorescence.* Major Professors: Dr. John P. Sullivan, School of Aeronautics and Astronautics and Dr. S. Fleeter, School of Mechanical Engineering.

A nonintrusive concentration measurement method is developed for determining the concentration distribution in a complex flow field. The measurement method consists of marking a liquid flow with a water soluble fluorescent dye. The dye is excited by a two dimensional sheet of laser light. The fluorescent intensity is shown to be proportional to the relative concentration level. The fluorescent field is recorded on a video cassette recorder through a video camera. The recorded images are analyzed with image processing hardware and software to obtain intensity levels. Mean and root mean square (rms) values are calculated from these intensity levels.

The method is tested on a single round turbulent jet because previous concentration measurements have been made on this configuration by other investigators. The previous results were used for comparison to qualify the current method. These comparisons showed that this method provides satisfactory results.

The concentration measurement system was used to measure the concentrations in the complex flow field of a model gas turbine annular combustor. The model annular combustor consists of opposing primary jets and an annular jet which discharges perpendicular to the primary jets. The mixing between the different jet flows can be visualized from the calculated mean and rms profiles. Concentration field visualization

images obtained from the image processing provide further qualitative information about the flow field.

CHAPTER 1: INTRODUCTION

This thesis investigates the mixing which occurs between a turbulent jet and its surroundings. This configuration occurs in the combustion chamber of gas turbine engines, with the primary air jets discharging into the combustor. The mixing between the primary air and the fuel/secondary air mixture influences the flame stability and burning efficiency. Other engineering applications of this technique include dilution of a smokestack discharge in the atmosphere or dilution of a pipeline discharge in a river; but here the combustor application is of primary interest.

The objective is to develop a nonintrusive method to measure concentration in a complex three dimensional flow field. This method will then be used to measure the concentration field in a model gas turbine annular combustor.

The concentration field of a round turbulent jet discharging into a stagnant reservoir has been measured previously. Becker, Hottel and Williams[2] explain in great detail the concentration measurement method known as marker nephelometry. This involves measuring the light scattered by marker particles in the fluid flow. The marker particles must have small inertia and small tendency to evaporate, coagulate, sublime or react chemically. The size of the particles must be maintained in a range to prevent excessive coagulation. The intensity of the scattered light is proportional to the number density of the particles, if the density is kept sufficiently low to meet the conditions for independent scattering. At the same time, a minimal number of particles must be present

in the probe volume to represent a continuum. Becker, Hottel, and Williams[3] utilized the light scattering technique to measure concentrations in an air jet, with oil smoke particles as a marker. Birch, et al.[5] measured concentrations in a natural gas turbulent free jet by detecting Raman scattered laser light. Long, Chu and Chang[9] , and Long, Webber and Chang[10] measured concentration distributions in a jet, seeded with sugar aerosols; by detecting the Mie scattered laser light. Chigier and Beer[6] made concentration measurements along the centerline of a coaxial air jet arrangement by introducing CO_2 as a tracer gas. The case with annular flow equal to zero, corresponds to a single turbulent jet.

The method of concentration measurement used in this thesis utilizes a fluorescent dye for a flow marker. The dye is excited by a sheet of laser light causing the dye to fluoresce. The local fluorescent intensity is proportional to the local dye concentration. The constraints mentioned above for marker particles do not apply, since the marker size is molecular. The dye concentration does have to be kept low enough to prevent significant absorption of the laser intensity by the dye. The fluorescent field is recorded on videotape and the images are digitized, with a numerical value, based on the local intensity, assigned to each pixel location. Dahm and Dimotakis[7] used a fluorescent dye excited by a laser beam, which was scanned by a linear photodiode array, to measure the radial concentration distribution across a turbulent jet. The array was scanned very fast giving a nearly instantaneous image, but this gives only one dimension of information (along the beam).

Balint, Ayrault and Schon[1] obtained a two dimensional concentration field by recording the laser light scattered by aloxite particles in an air jet. The laser light was spread into a sheet by a set of rotating mirrors. The scattered light was recorded with a 16 mm motion picture camera providing a two dimensional representation of the

concentration field. Borleteau[6] recorded light scattered by oil droplets, on a video tape to obtain a two dimensional concentration field. A rotating cylindrical lens was used to form the laser sheet. Seal[17] measured the concentration field in an air jet by using seed particles, which were created by atomizing a combination of ethyl alcohol and a petroleum distillate mixture, to mark the jet flow and recording the light scattered from a sheet of laser light, on a videotape. He provided only qualitative concentration distributions with these recorded images.

Brandt[8] combined the benefits of fluorescent dye with the two dimensional image capability of a video camera to record the concentration field in both a laminar jet and a turbulent jet. This thesis extends Brandt's method to include comparing quantitative results from a round turbulent jet with those measured by others. This case was used to validate the measurement system.

The same concentration measurement method was also applied to a flow system consisting of two opposing impinging round turbulent jets in a channel. An annular jet discharges into the channel from one end, perpendicular to the round jets. This flow system was designed to model the flow in a gas turbine annular combustor, with the round jets representing the primary air jets and the annular jet representing the fuel/secondary air mixture flow.

CHAPTER 2: MEASUREMENT SYSTEM

The measurement system was developed to determine the relative concentration levels in a turbulent jet flow. This was accomplished through the use of a fluorescent dye as a marker of the jet flow. The measurement method was tested on a round turbulent jet, a configuration in which the concentration distribution has been previously measured by other investigators. The system was then applied to the more complex case of a model gas turbine annular combustor flow field.

2.1 Experimental Apparatus

A fluorescent dye (Rhodamine 6-G) was injected into the jet flow far upstream (22 jet diameters) of the jet exit to allow thorough mixing. The beam of a Spectra-Physics argon ion laser was passed through a cylindrical lens, producing a thin sheet of light aligned with the jet axis. The sheet of laser light was spread much wider than the measurement region to reduce the effect of the Gaussian intensity variations across the laser sheet. The laser light causes the dye to fluoresce, such that the fluorescent intensity is proportional to the laser power and the local concentration of dye, for laser intensities below the fluorescence saturation level as described by Walker[21]. Koochesfahani and Dimotakis[13] developed an expression for the dye concentration at a point, i.

$$C(i) = K(i)\,\frac{V(i) - D(i)}{\beta(i)} \qquad (2.1.1)$$

where:

C(i) = local dye concentration

K(i) = attenuation factor for absorption of the laser intensity by the dye

V(i) = i^{th} pixel output

D(i) = dark response of i^{th} pixel

The quantity β (i) contains the effects of nonuniformity of imaging and pixel sensitivity and laser sheet thickness variations. These effects were experimentally determined to be negligible by observing the measured fluorescent intensity variations across the test section with a uniform dye concentration (see Appendix). The attenuation factor, K(i), was kept very near 1.0 by injecting dye at a very low rate (approx. 20 ppb), thus reducing the amount of dye available to absorb the laser power. The choice of Rhodamine 6-G for the dye, also reduced the absorption. Figure 2.1 shows the mean concentration profile of Fluorescein, another fluorescent dye. The laser light entered the jet from the right side of the axis. The apparent variation in concentration across the jet is due to the absorption of the laser intensity by the Fluorescein. This did not occur with the Rhodamine 6-G, which will be shown by the results later in this chapter. To determine absolute concentration levels, the system would have to be calibrated to provide concentration for a given local laser power. However, only relative values of concentration are required for this thesis. Therefore, the local relative dye concentration is the difference between the pixel output and the dark response. The dark response was obtained by recording the camera output with no dye in the test section.

Figure 2.2 shows a schematic diagram of the test equipment setup. The fluorescent intensity was recorded through a Panasonic digital video camera, with a pickup element consisting of a 499 x 574 matrix of charge coupled devices, which will be referred to as segments of the pickup element. The camera was operated in the strobe effect shutter

mode, which records each field in .001 second instead of the normal 1/60 second. This reduces the time averaging across each field. The fields are still 1/60 second apart to remain compatible with standard video cassette recorders (VCR's). Two consecutive fields are interlaced to produce a frame. Figure 2.3 illustrates how the camera acquires the fields and how they are interlaced. The effect of the 1/60 second between fields can be seen by plotting the odd and even pixels separately on a vertical scan across the image. This is shown in Figure 2.4, where the concentration values for a single frame are plotted. The largest changes between fields occur at the jet edges, as expected. This will have no effect on the mean and rms calculations.

The camera output was recorded by a GE VCR onto standard ½ inch tape. The recorded images were digitized through an IBM PC/AT equipped with Data Translation's DT-IRIS image processing software and hardware. The digitized image is the result of assigning a value from 0 to 255 (8 bits) to each pixel (480 lines by 512 pixels) based on the recorded intensity. Mean and root mean square (rms) values at selected pixel locations can then be computed from the digitized images. These quantities were calculated from 50 frames each spaced approximately 1.4 seconds apart. The time between processed frames is due to the computer processing time. Only 50 frames were used, because extensive dye recirculation within the test section was encountered after approximately 70 seconds. Mean and rms values were calculated as follows.

$$\bar{C} = \frac{1}{N} \sum_{i=1}^{N} C_i \qquad (2.1.2)$$

$$c' = \left[\frac{\sum_{i=1}^{N} C_i^2 - \frac{1}{N}\left[\sum_{i=1}^{N} C_i\right]^2}{N-1} \right]^{1/2} \qquad (2.1.3)$$

where :

$\overline{C}$ = relative mean concentration

c' = rms concentration; $\left[\sqrt{\overline{c^2}}\right]$

N = number of frames

C_i = i^{th} instantaneous relative concentration ; (V(i) – D(i))

Visualization images are produced by mapping the intensity levels to colors, which are combinations of red, green and blue, to provide pseudo-color representations of the concentration field. Pink indicates the highest concentration and dark blue corresponds to the lowest. These color enhanced images allow visualization of the concentration distribution. Figure 2.5 shows the 127 frame average pseudo-color image of the single jet dark response.

It is desirable to have the concentration measurement system be independent of the flow velocity, especially for this thesis since no velocity measurements were made. To verify that the measurement system is independent of velocity, the fluorescent light energy incident on a pickup segment is calculated. The fluorescent light intensity received by a single segment of the pickup element is:

$$I(t) = [I_0(t) * \varepsilon] \int_{p.v.} C(x,y,z,t)\, dx\, dy\, dz \qquad (2.1.4)$$

where several quantities are defined as follows.

$I(t)$ = fluorescent intensity at the pickup segment

$I_0(t)$ = incident laser light intensity

ε = fluorescent efficiency

C = dye concentration in the probe volume

p.v. = probe volume

Let:

$$\int_{p.v.} C(x,y,z,t)\, dx\, dy\, dz = \hat{C}(t)$$

Then the total fluorescent light energy incident on the pickup segment during the camera exposure time, t_{exp} is:

$$E_{TOT} = A_{ps} \int_0^{t_{exp}} I(t)\, dt = A_{ps} \int_0^{t_{exp}} [I_0(t) * \varepsilon]\, \hat{C}(t)\, dt \qquad (2.1.5)$$

where:

A_{ps} = pickup segment area

Assume that the incident laser intensity is constant with time. The total fluorescent light energy can then be written as:

$$E_{TOT} = (I_0 * \varepsilon)\, \bar{\hat{C}}\, t_{exp}\, A_{ps} \qquad (2.1.6)$$

where:

$\bar{\hat{C}}$ = $\hat{C}$ time averaged over t_{exp}

From the above expression, it is apparent that the concentration measurement system is independent of velocity. It is also shown that the concentration measurement is averaged

over the exposure time and over the probe volume.

Table 2.1 shows the sampling time and exposure time requirements for measuring various quantities. There are no sampling time requirements for determination of the mean. The only requirement for rms determination is that the exposure time should be less than the flow time scale. To maintain the influence of the smallest scale fluctuations, this would require that the exposure time be less than the Kolmogorov time microscale. The spectrum can be determined if the time between samples is also small enough.

2.2 Test Case - Single Turbulent Jet

The measurement system was tested on a single round turbulent jet because concentration measurements have been made for this configuration by others. This demonstrates the validity of the measurements.

The experimental configuration consisted of a jet of water issuing from a 0.43 inch inside diameter tube, with a length to diameter ratio of 25. The water flow was supplied to the tube from a constant head tank. The tank level was maintained constant by a pump which supplied water to the tank, and an overflow pipe which discharges to the holding tank. The jet discharged vertically into a clear plexiglass water reservoir. The apparatus is shown in Figures 2.6 and 2.7. Mass flow rate was determined by weighing a sample of water collected over a timed interval. The mass-averaged jet velocity was 1.78 ft/sec, giving a Reynolds number based on jet diameter of 5300. The dye mixture, which was 3.8 ppm dye, was injected at the rate of 0.00058 lb/sec giving a dye concentration upstream to the jet exit of 20 ppb.

For this test case, the receiving optics were arranged such that the length of the probe volume was 0.006 inches. This was determined by counting the pixels in the digitized image corresponding to a known dimension, the jet diameter. As stated previously, the camera was operated in strobe effect shutter mode, which gave an effective exposure time of 0.001 seconds.

The Kolmogorov microscales were calculated to determine the smallest scales of fluctuations in the flow. Using an estimate of turbulence dissipation from Tennekes and Lumley[19], the length and time microscales are given respectively by,

$$\eta = \left[\frac{\nu^3 l}{u^3} \right]^{1/4} \tag{2.2.1}$$

$$\tau = \left[\frac{\nu l}{u^3} \right]^{1/2} \tag{2.2.2}$$

where:

ν = kinematic viscosity

l = width of flow (taken as jet diameter)

u = velocity fluctuation

The centerline turbulence intensity, (u/U), increases through the measurement section, which extends 5.5 jet diameters downstream. From Hinze[12], the maximum value within the measurement region would occur at 5.5 diameters and be approximately 15%. Borrego and Olivari[7] show that at 5.5 diameters downstream the centerline velocity would still be equal to the exit velocity. Therefore, the mean velocity U is the exit velocity of 1.78 ft/sec. From the above equations, the Kolmogorov length and time microscales are respectively, 0.003 inches and 0.0045 seconds. This indicates that all but

the smallest scale fluctuations are being recorded. As indicated in the previous section, this has no effect on the determination of the mean. The effect on the rms value will be minimal, since only the smallest scale fluctuations are being averaged across the exposure time. Since these scales are smaller than the measurement system can resolve, it is desirable to determine how much of the fluctuation energy is being recorded. Becker, et al.[3] present a concentration fluctuation spectrum recorded on the jet centerline, plotted against $\Lambda_\gamma\kappa$, which is the product of the axial integral scale and the wavenumber, (Figure 2.8). They developed a linear relationship for Λ_γ,

$$\Lambda_\gamma = 0.0445\ x \tag{2.2.3}$$

where:

x = axial distance from the jet exit

Based on the 1/60 second between image fields, assume that the highest frequency which can be resolved is 20 Hz. This would give a wavenumber of 71 ft^{-1}. The spectrum presented by Becker, et al. was measured at 32 diameters downstream. Therefore, the current value of $\Lambda_\gamma\kappa$ must be multiplied by (32/5.5) to be compatible with their spectrum. This ratioed value for $\Lambda_\gamma\kappa$ is 3.6, giving a fluctuation energy level which is less than one-tenth of the energy level at low wavenumbers. Therefore the vast majority of the fluctuation energy is being recorded.

The results of this test case are presented in Figures 2.9 through 2.17 with results from other investigators where available. Figures 2.9 and 2.10 are visualization images of the jet concentration field. Figure 2.9 shows a single frame of data, while Figure 2.10 is the result of averaging 127 frames.

Figure 2.11 presents the mean and fluctuation intensity ($c'/\overline{C}$) data in a three dimensional graphical format. The mean profile can be seen to flatten and spread downstream as expected. The fluctuation intensity increases outside of the peaks at the jet edges. This is due to the nearly zero rms being divided by a decreasing mean value.

Figure 2.12 presents the concentration profile near the jet exit (x/d = 0.1). The shape of the mean concentration profile (flat across the jet and nearly zero outside of the jet) indicates that the dye was thoroughly mixed with the jet flow. The fluctuation intensity has an asymmetric feature, this is due to the mean concentration curve. The value of $\overline{C}$ on the left side of the jet axis is slightly higher than that on the right side. The jet did spread faster on this side and it was visible in the flow visualization provided by the fluorescent dye. This was apparently due to a manufacturing defect inside the tube near the exit.

Figures 2.13 and 2.14 compare results with those obtained by Rosensweig, Hottel and Williams[16]. They measured concentrations in an air jet marked with smoke particles by recording the scattered light from the particles. Figure 2.13 presents the mean concentration profile at x/d = 1.0. The data from Rosensweig, et al. are asymmetric. The authors do not discuss this feature but it may be due in part to the fact that the projected slit width of their receiving optics was 14% of the jet diameter. This would make it difficult to accurately measure the concentration at the jet edges. The present data do agree fairly well on the left side of the jet axis. Figure 2.14 presents the fluctuation intensity profile at x/d = 1.5. As with the jet exit profile, there is a slight asymmetry in the profile at this location due to the defect in the tube. For the present data, a 95% certainty band was calculated by assuming a normal distribution for C, and utilizing Student's t and the χ^2 distributions. The values on the right side of the jet axis show good agreement with those obtained by Rosensweig, et al.

Measurements made at downstream locations of 2 and 4 jet diameters are compared with those made by Borrego and Olivari[7] in figures 2.15 and 2.16. They measured oil smoke concentrations, in a round turbulent air jet exhausting into ambient still air, with a light scatter meter. The radial locations are normalized by δ_c, the location at which the mean concentration is one-half of the centerline value. This allows direct comparison with Borrego and Olivari's results. The present mean concentration levels outside of the jet are higher than those measured by Borrego and Olivari. This is due to the recirculation of the dye within the reservoir, causing a higher background concentration. Their jet exhausted into a room and therefore did not have this condition. Also included for comparison are concentration profiles from data recorded by Seal[17]. The configuration was an air jet exhausting into still ambient air. The light scattered by marker particles was recorded on video tape. The videotaped data were processed for comparison with measurements made in this thesis. Seal's data agree quite well with the present results, with the exception that at x/d = 2.0, the light intensity saturated the image processing system near the jet centerline. This results in a flat mean profile and zero rms. Most of Borrego and Olivari's rms data fall within the 95% certainty band about the current data.

Figure 2.17 shows the jet half width growth along with data from Seal[17] and Birch, et al.[5] and analytical results from Squire and Trouncer[18] which are taken from Forstall and Shapiro[11]. The current data agree well with the trend from others. As explained above, the current test hardware had a slight flaw causing the jet to spread slightly faster than would be expected.

Based on the results of this test case and the comparisons with previous investigators, the measurement system has been found to provide concentration measurements with satisfactory accuracy.

Table 2.1 Sampling Requirements for Determination of Various Quantities.

Quantity	Sampling Time Req't	Exposure Time Req't
$\bar{c}$	None	None
c'	None	< Flow time scale
Spectrum	< Flow time scale	< Flow time scale

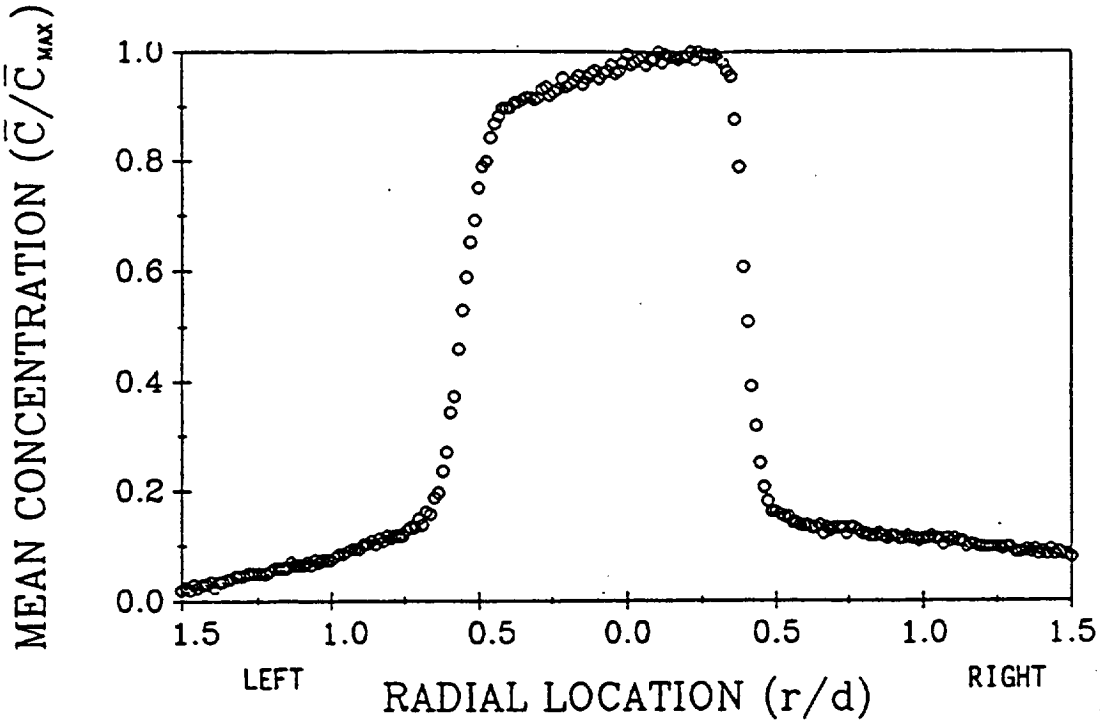

Figure 2.1. Mean Concentration of Fluorescein Dye in Round Jet (x/d = 0.5)

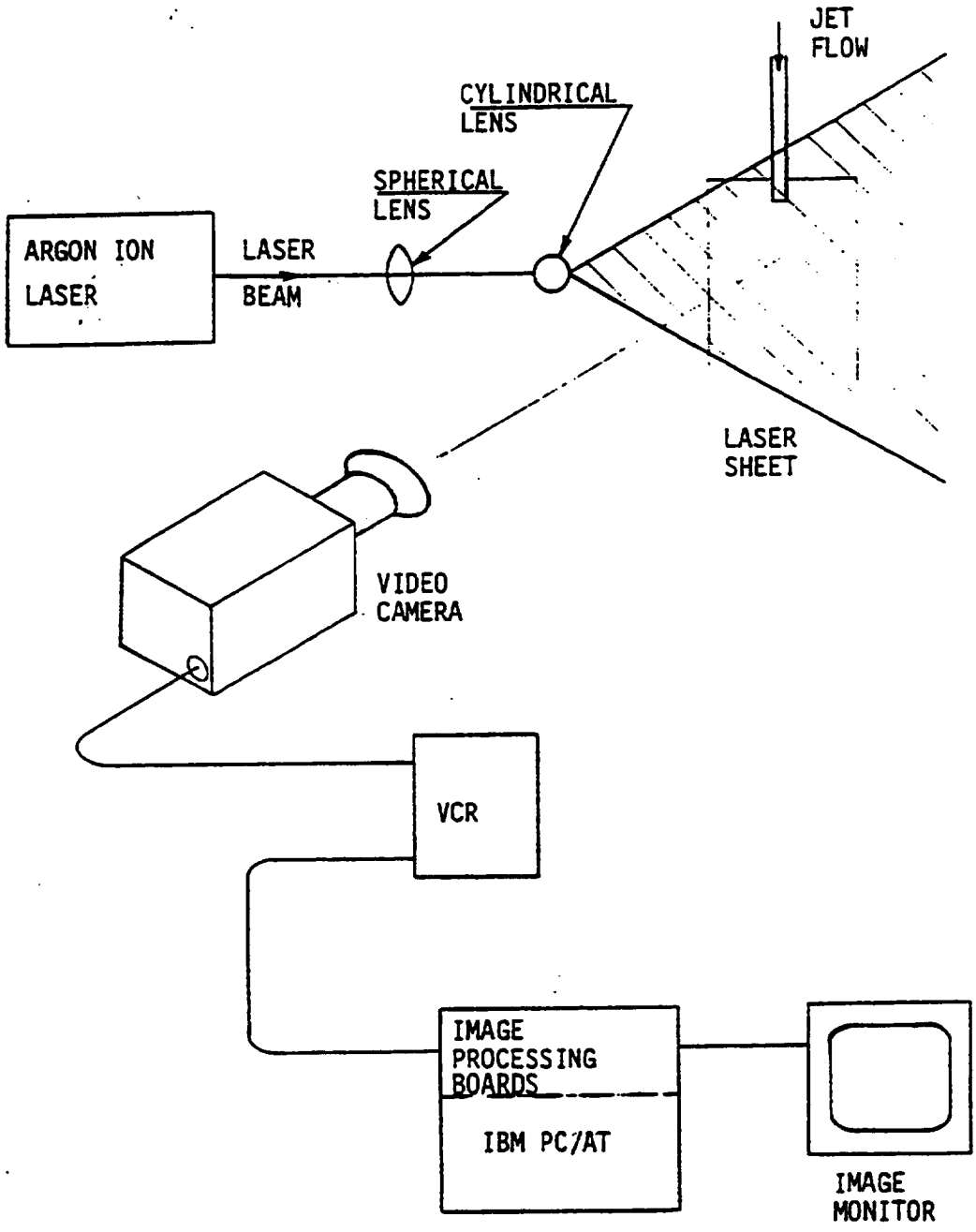

Figure 2.2. Test Equipment Schematic Diagram

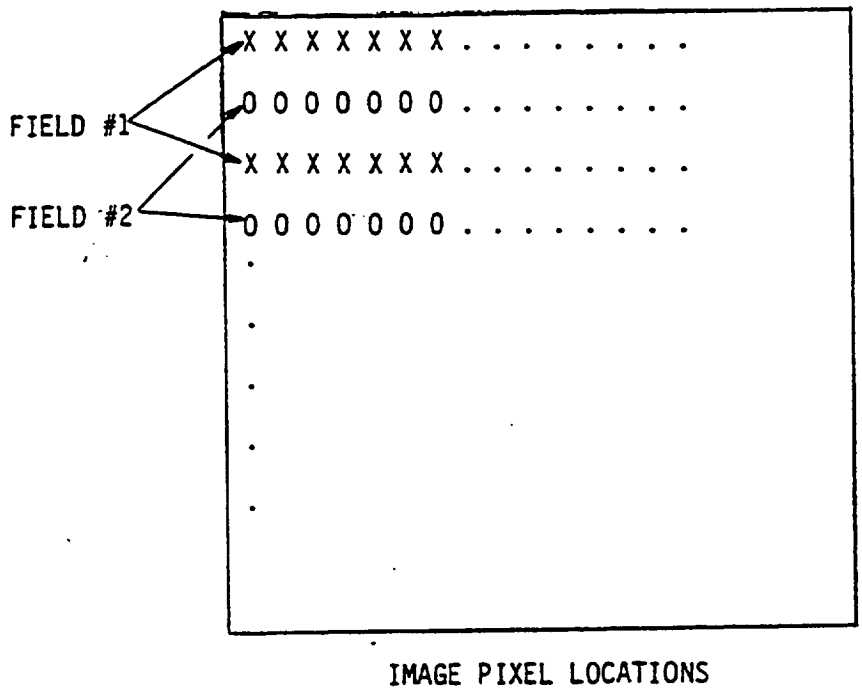

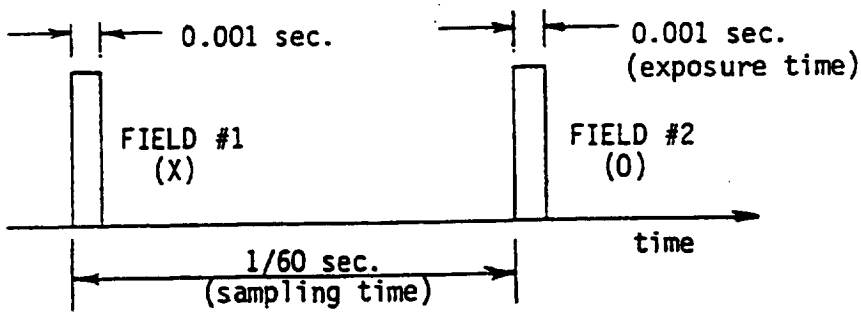

Figure 2.3. Temporal and Spatial Image Acquisition Scheme

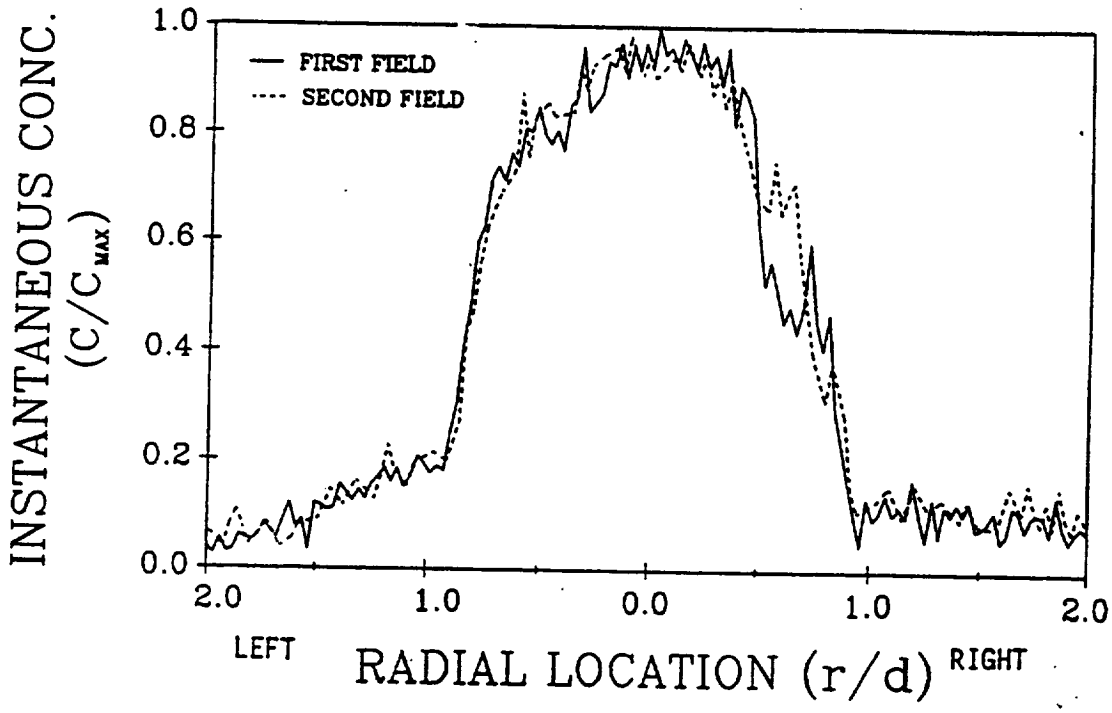

Figure 2.4. Instantaneous Concentration Profiles for Consecutive Image Fields (x/d = 1.5)

TE92-2522

Figure 2.5. 127 Frame Average Dark Response Image of Single Jet Setup

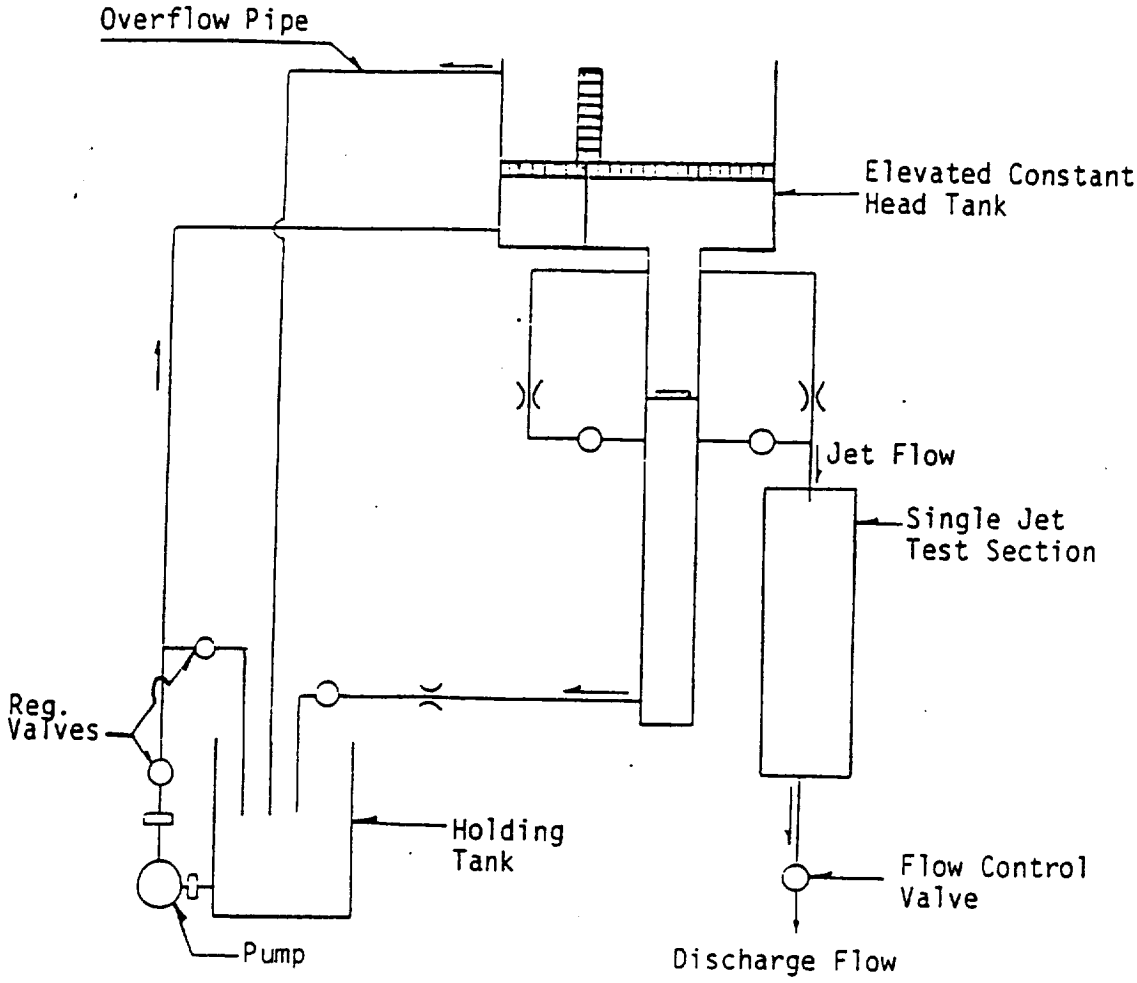

Figure 2.6. Schematic Diagram of Single Jet Test Apparatus

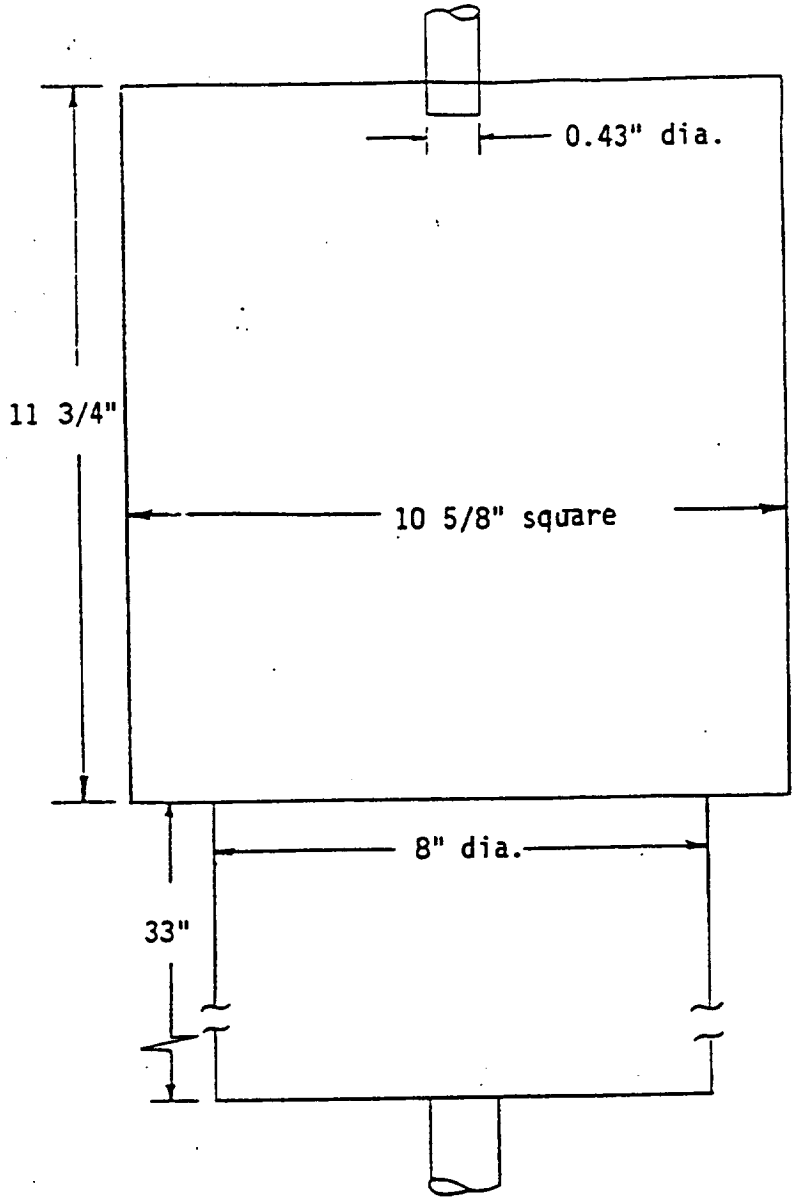

Note: All dimensions are internal dimensions.

Figure 2.7. Detail of Single Jet Test Section

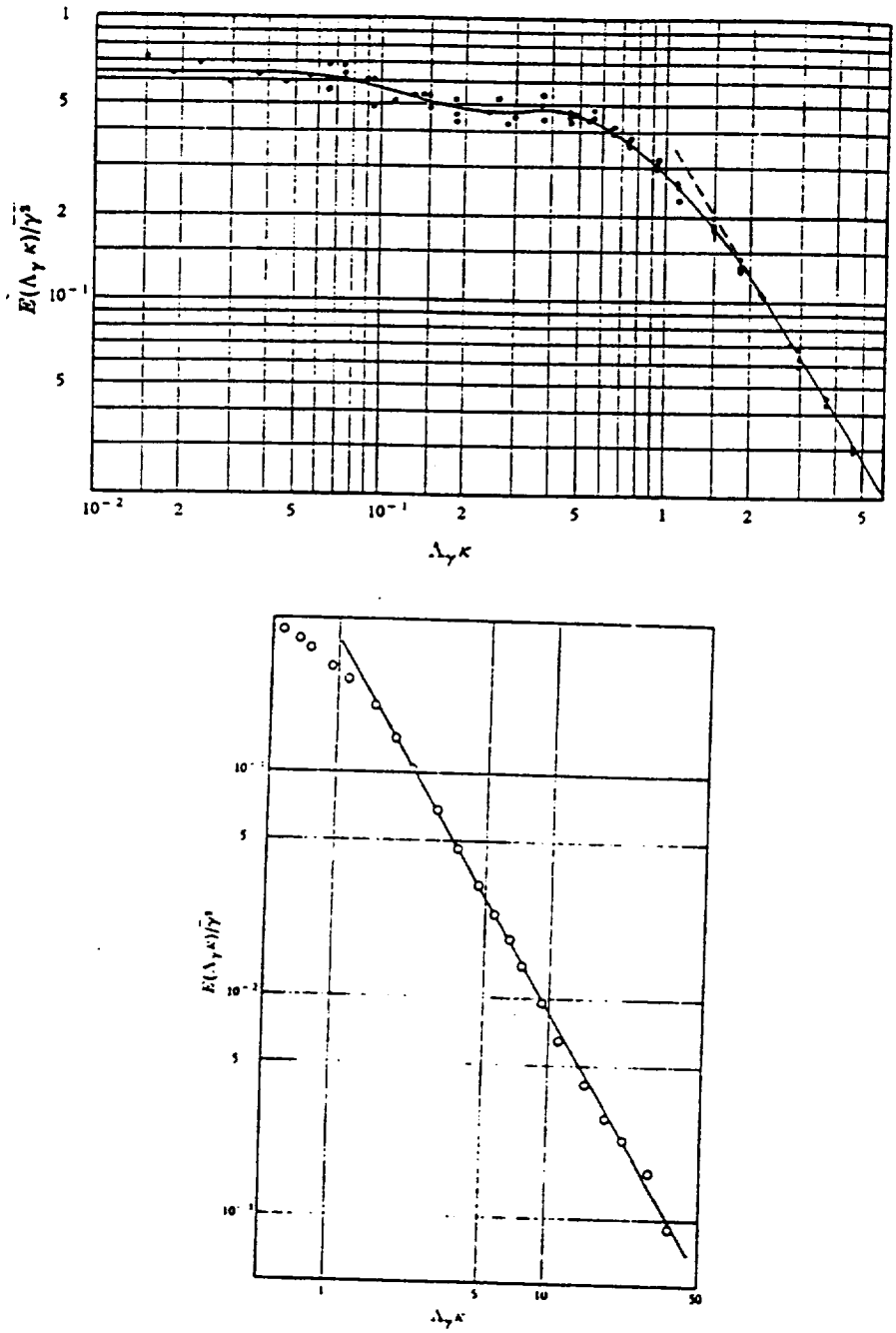

Figure 2.8. Concentration Fluctuation Spectrum on Jet Centerline (x/d = 32), from Becker, et al.[3]

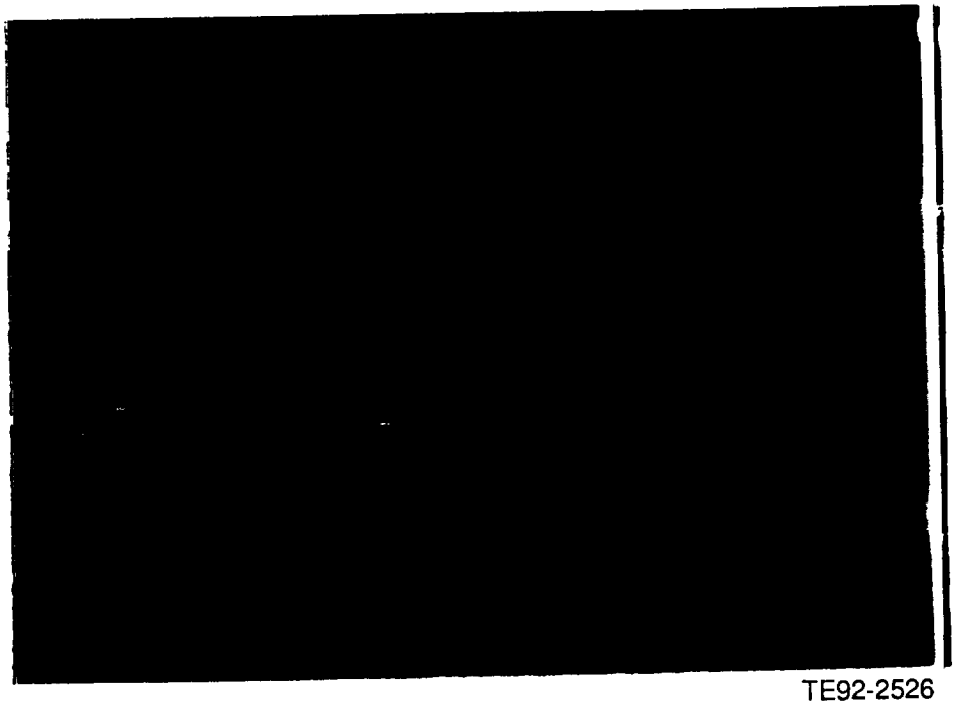

TE92-2526

Figure 2.9. Single Frame Concentration Field Visualization Image

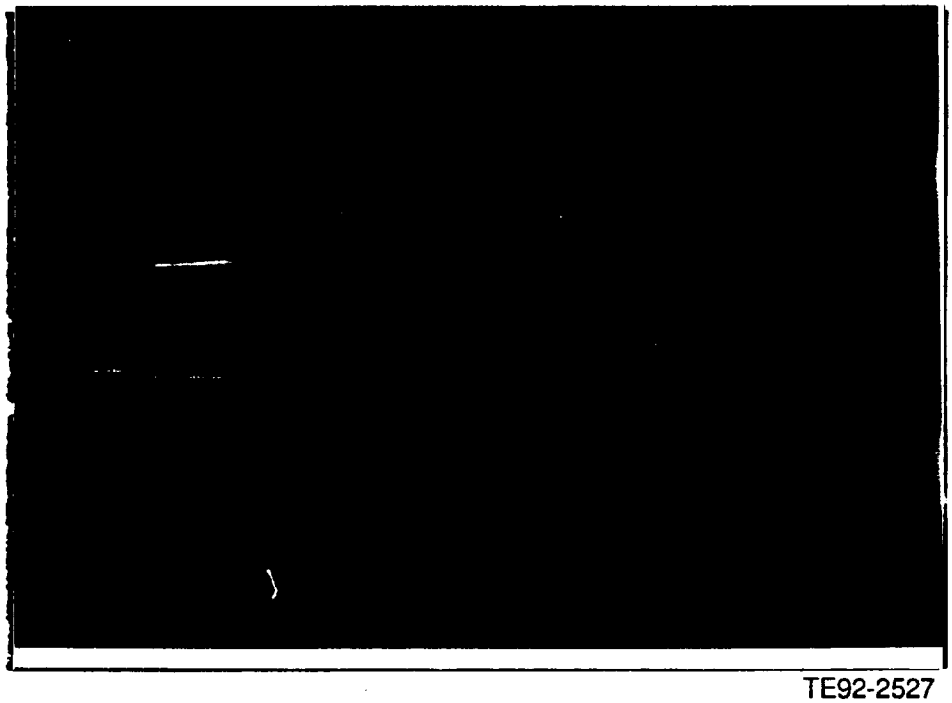

TE92-2527

Figure 2.10. 127 Frames Averaged Concentration Field Visualization Image

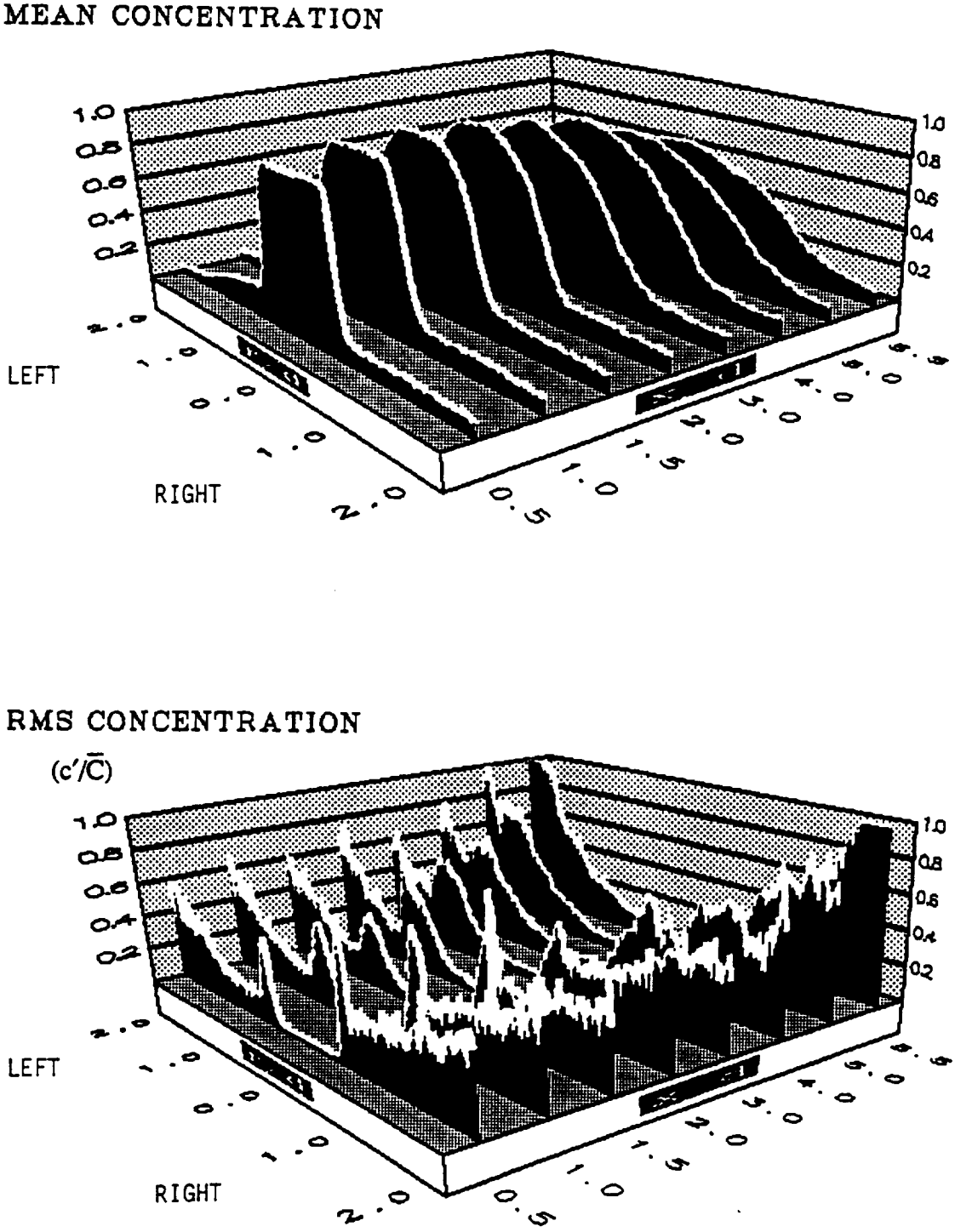

Figure 2.11. 3D Representation of Mean and RMS Concentration Profiles

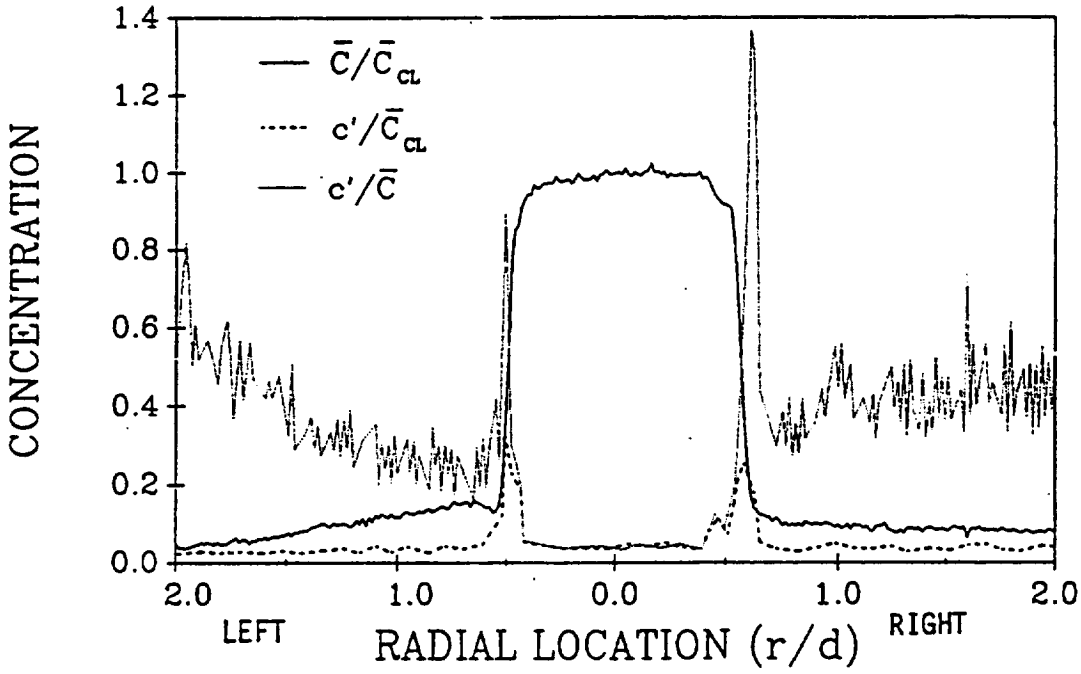

Figure 2.12. Mean and RMS Concentration Profiles at Jet Exit (x/d = 0.1)

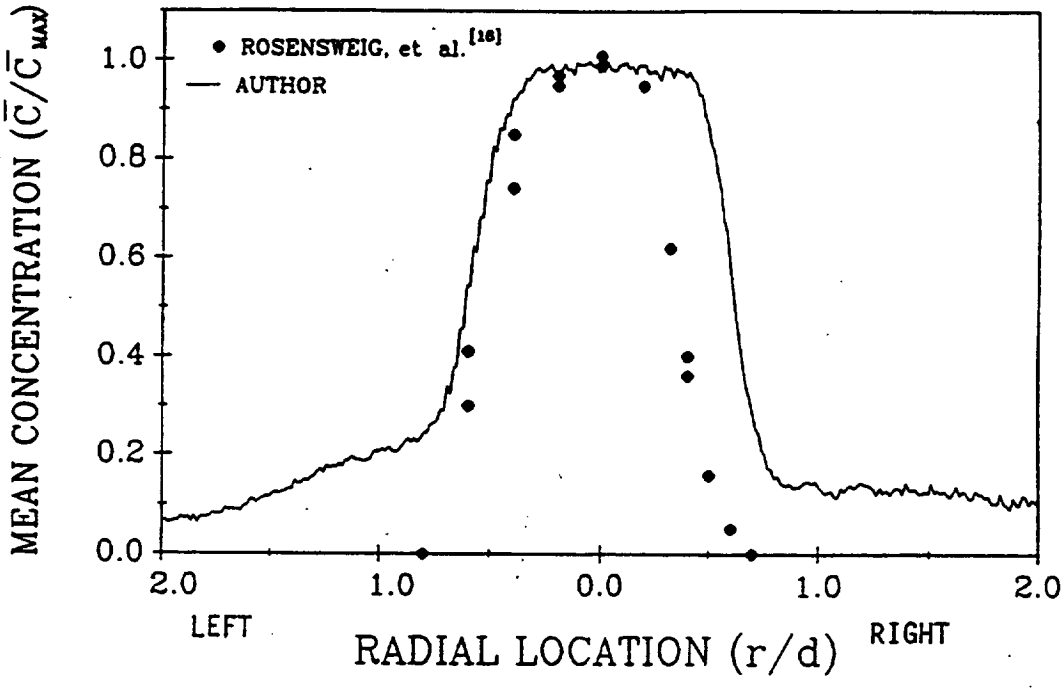

Figure 2.13. Mean Concentration Profile at x/d = 1.0

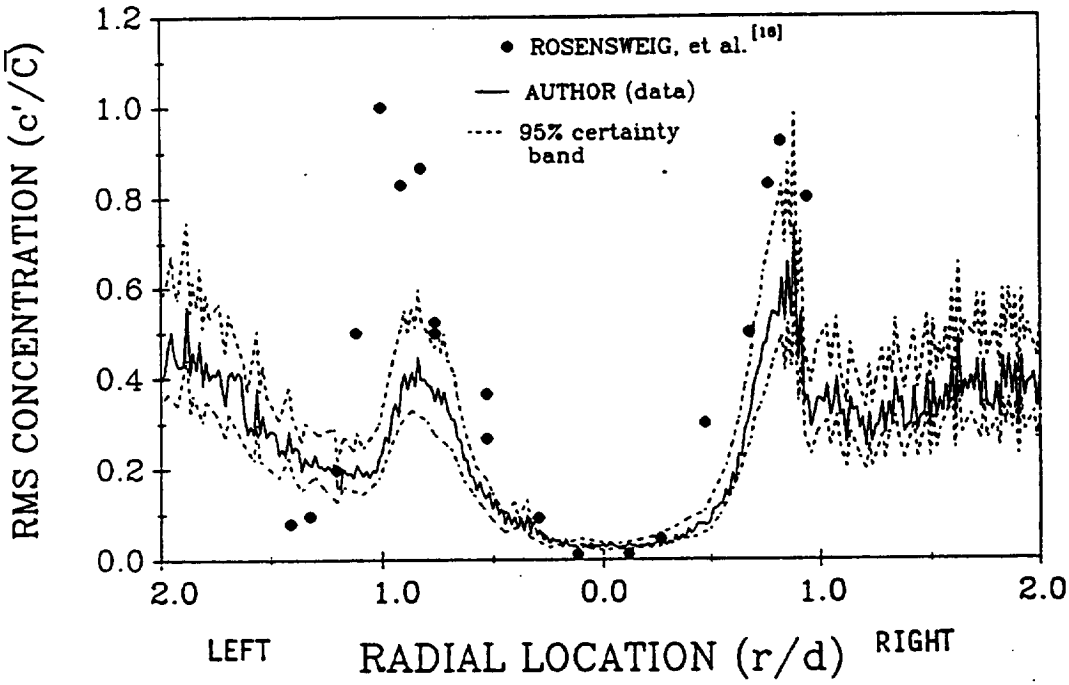

Figure 2.14. RMS Concentration Profile at x/d = 1.5

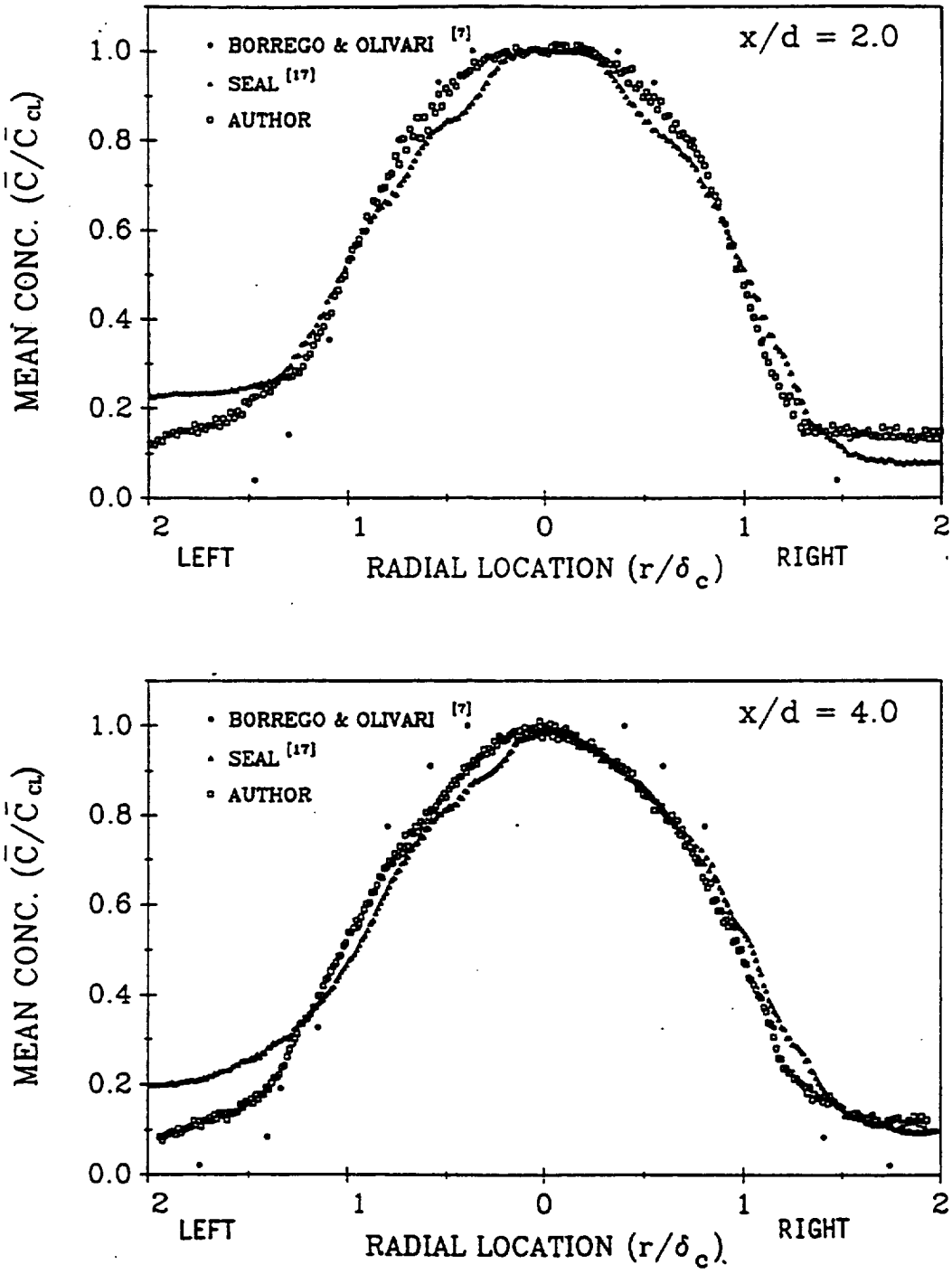

Figure 2.15. Mean Concentration Profiles at x/d = 2.0 and 4.0

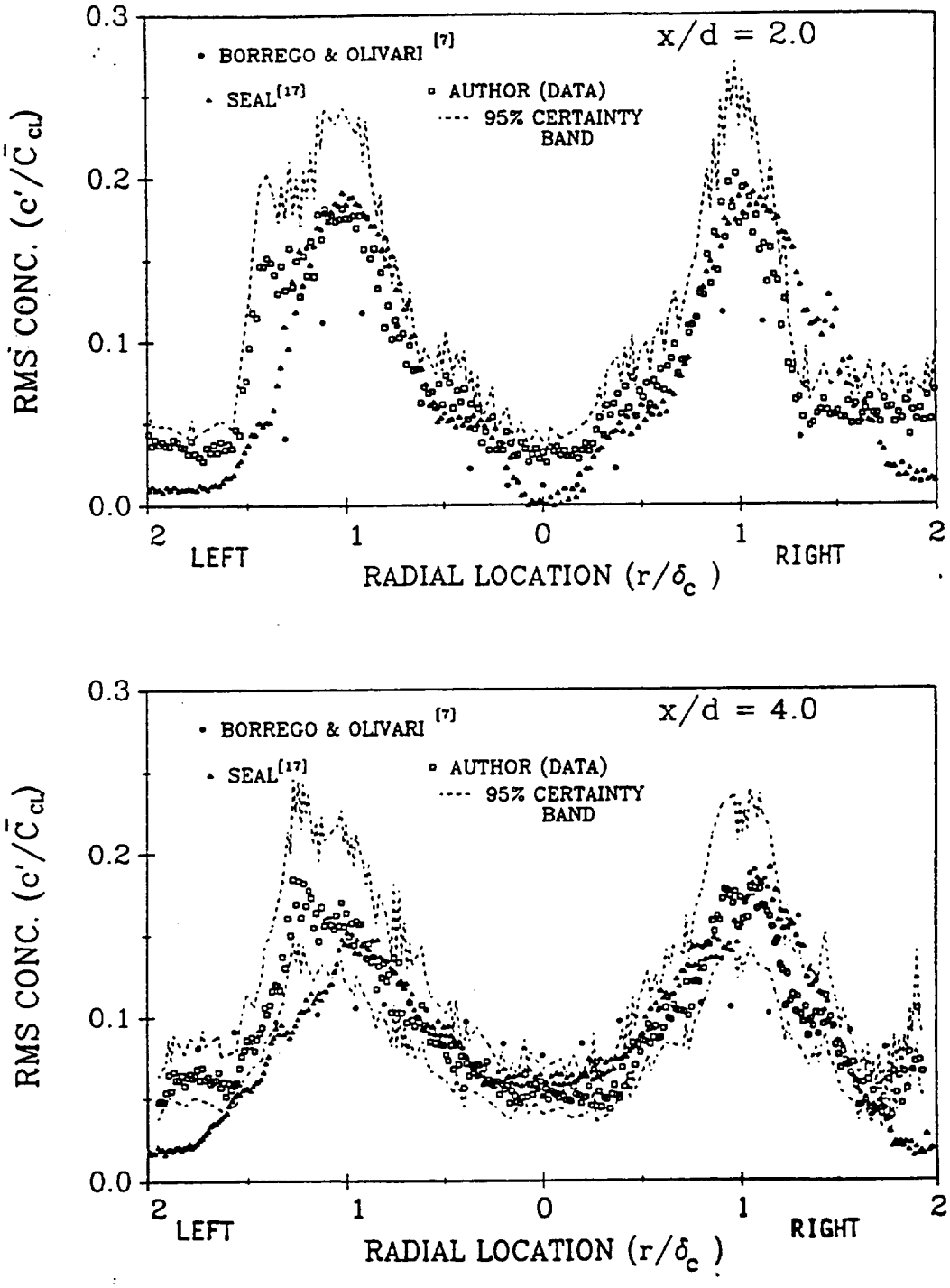

Figure 2.16. RMS Concentration Profiles at x/d = 2.0 and 4.0

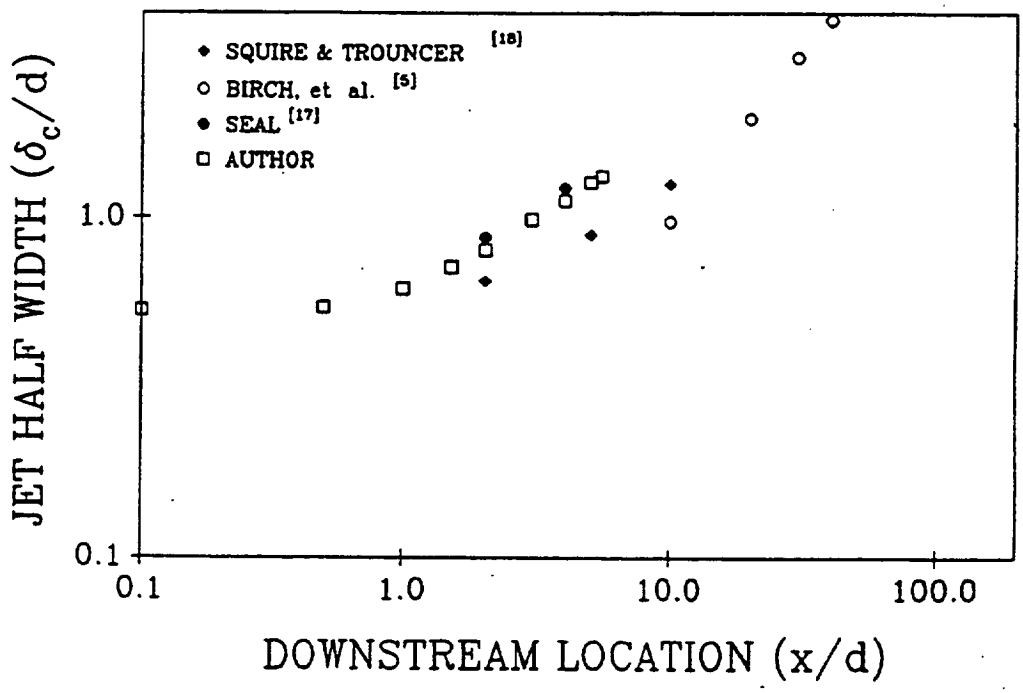

Figure 2.17. Jet Concentration Half Width Growth

CHAPTER 3: EXPERIMENT

The measurement system developed in the previous chapter was used to measure the concentration field in a model gas turbine annular combustor. This chapter describes the test apparatus and the tests performed.

3.1 Experimental Apparatus

The experimental apparatus is shown in Figures 3.1 through 3.4. This is the same test apparatus that was used for the single jet test, with a different test section. The test section for this test is a model of a gas turbine annular combustor. The effects of curvature have been assumed to be negligible and the annular flow channel was modeled as a rectangular channel (3 inches by 15 inches) constructed of clear plexiglass. At the top of the channel are 5 annular jets which would provide the fuel/secondary air mixture in the real combustor. Located one channel width, 3 inches, downstream of the annular jets are a pair of opposing round jets for each annular jet, aligned with the annular jet. These round jets would provide the primary air in the actual combustor. The primary jets had the same dimensions as the one used in the single jet test section (diameter = 0.43 inches; length/diameter = 25). The annular jet had an inner diameter of 1.084 inches and an outer diameter of 1.459 inches. The annular jets were located 3 inches apart, center to center. This same model combustor was used by Seal[17] to make velocity measurements in the flow field. His experiment used air as the working fluid and he had swirlers instead

of annular jets. The model consists of 5 annular jet/primary jet cells to reduce end wall effects. All measurements were made in the center cell.

Total water flow rate for all jets was determined from the venturi downstream of the test section. The primary jets' flow rate was determined from the pressure drop in the supply lines to each bank of jets. The venturi and each jet supply line were connected to manometers for flowrate determination. Figures 3.5 and 3.6 present the calibration curves for each flow measurement. The calibration data points are shown along with the equations which were used to determine the flow rates from the manometer readings. The total flow venturi output was determined from the difference between the manometer readings at the venturi's large and small diameters. The primary jet flow pressure drops were referenced to the constant head tank level. Readings were taken from the scale mounted next to the manometer tubes which has divisions that were used as units.

3.2 Test Configurations

The concentration field in the model combustor was first measured with the annular jet flow turned off. This configuration demonstrated the interactions between two opposing impinging round turbulent jets. The total flow rate was 1.7 lb/sec, giving a Reynolds number based on jet diameter of 8000 for each jet. The flow control valves were adjusted to position the interface between the jets at approximately the center of the channel. Figure 3.7 presents the coordinate system used for defining locations within the test section. Measurements were made with the laser sheet at z locations of 6.0, 6.5, 7.0 and 7.5 inches. These locations span the area from the center jets axes to the midway point between adjacent jet pairs. Symmetry was assumed and measurements were made on only one side of the jet axes.

The annular jets were turned on for the second configuration. This allowed visualization of the mixing between the primary jets and the annular jet. The total annular jet flow (5 jets) was 1.57 lb/sec and the primary jet flow was 1.10 lb/sec, giving Reynolds numbers based on hydraulic diameter of 2500 and 5200 for each annular jet and primary jet, respectively. A higher annular jet Reynolds number could not be attained without washing the primary jet flows downstream and eliminating the interaction between the three jets. The ratio of total primary jet momentum to annular jet momentum was 1.26. The primary jet flow rate to annular jet flow rate ratio was 0.7. Concentration measurements were made with the dye being injected first through one primary jet and then through the annular jet. As with the no annular jet flow case, the laser sheet was positioned at z locations of 6.0, 6.5, 7.0 and 7.5 inches for concentration measurements.

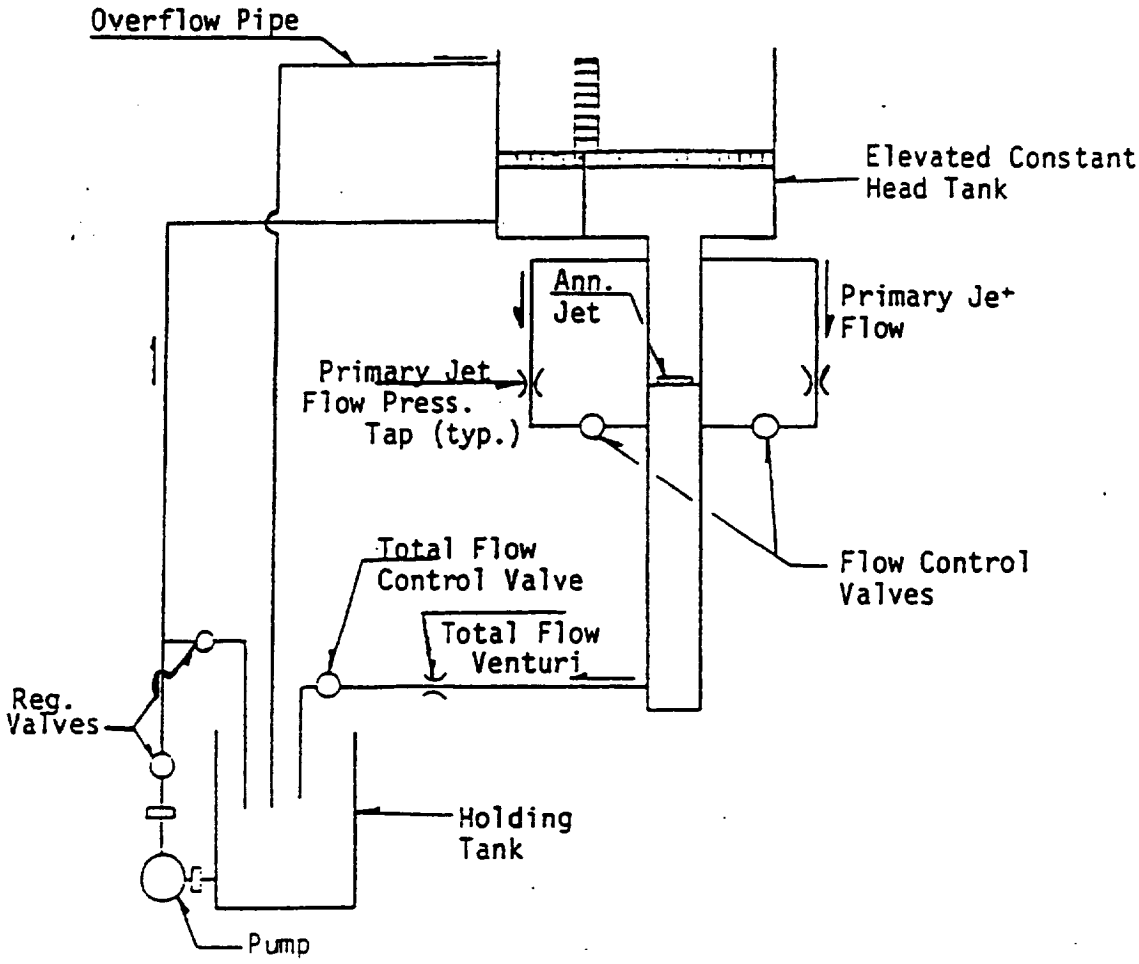

Figure 3.1. Model Annular Combustor Test Rig Schematic

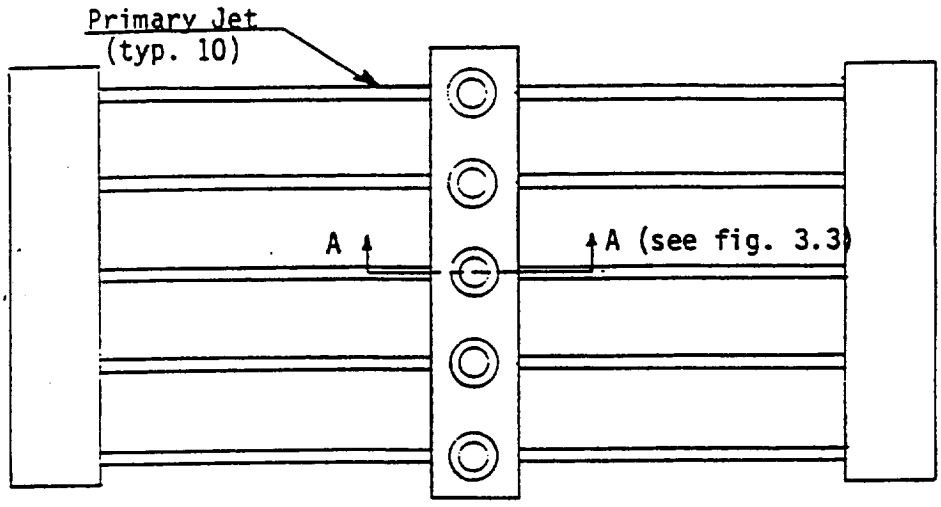

Top View

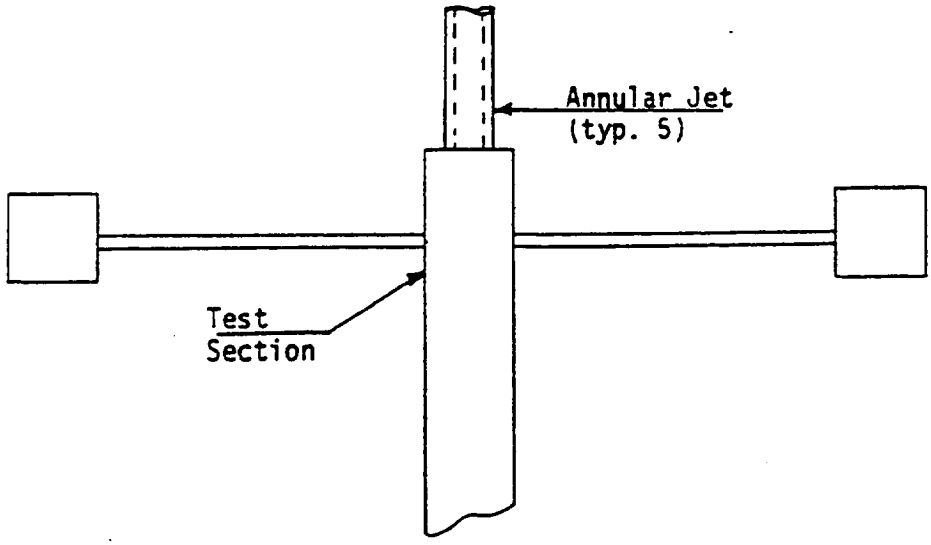

End View

Figure 3.2. Detail of Model Annular Combustor Test Section

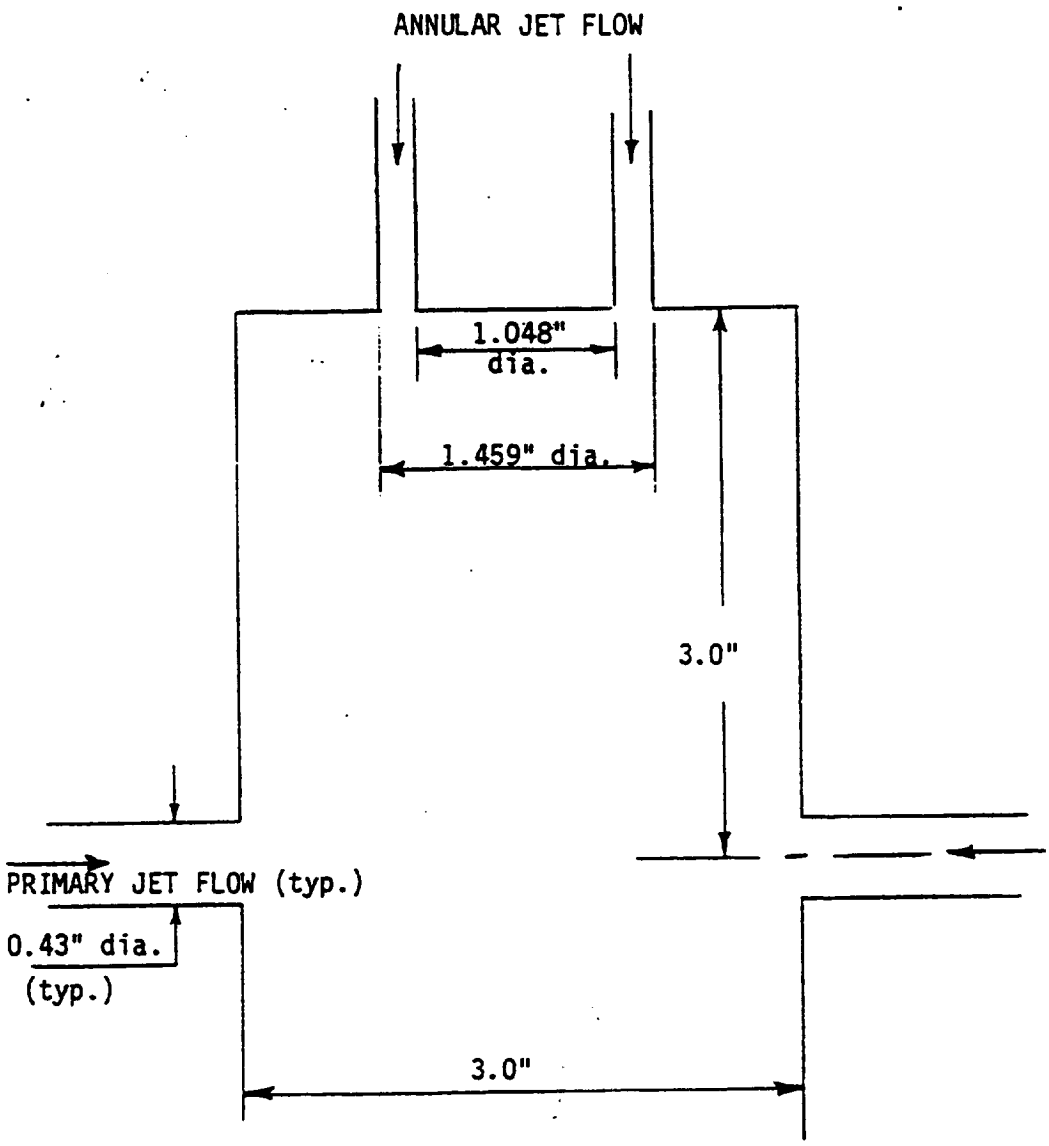

SECTION A-A (ref. figure 3.2)

NOTE: All dimensions are internal dimensions

Figure 3.3. Section of Model Annular Combustor Test Section

Figure 3.4. Photograph of Model Annular Combustor Test Section

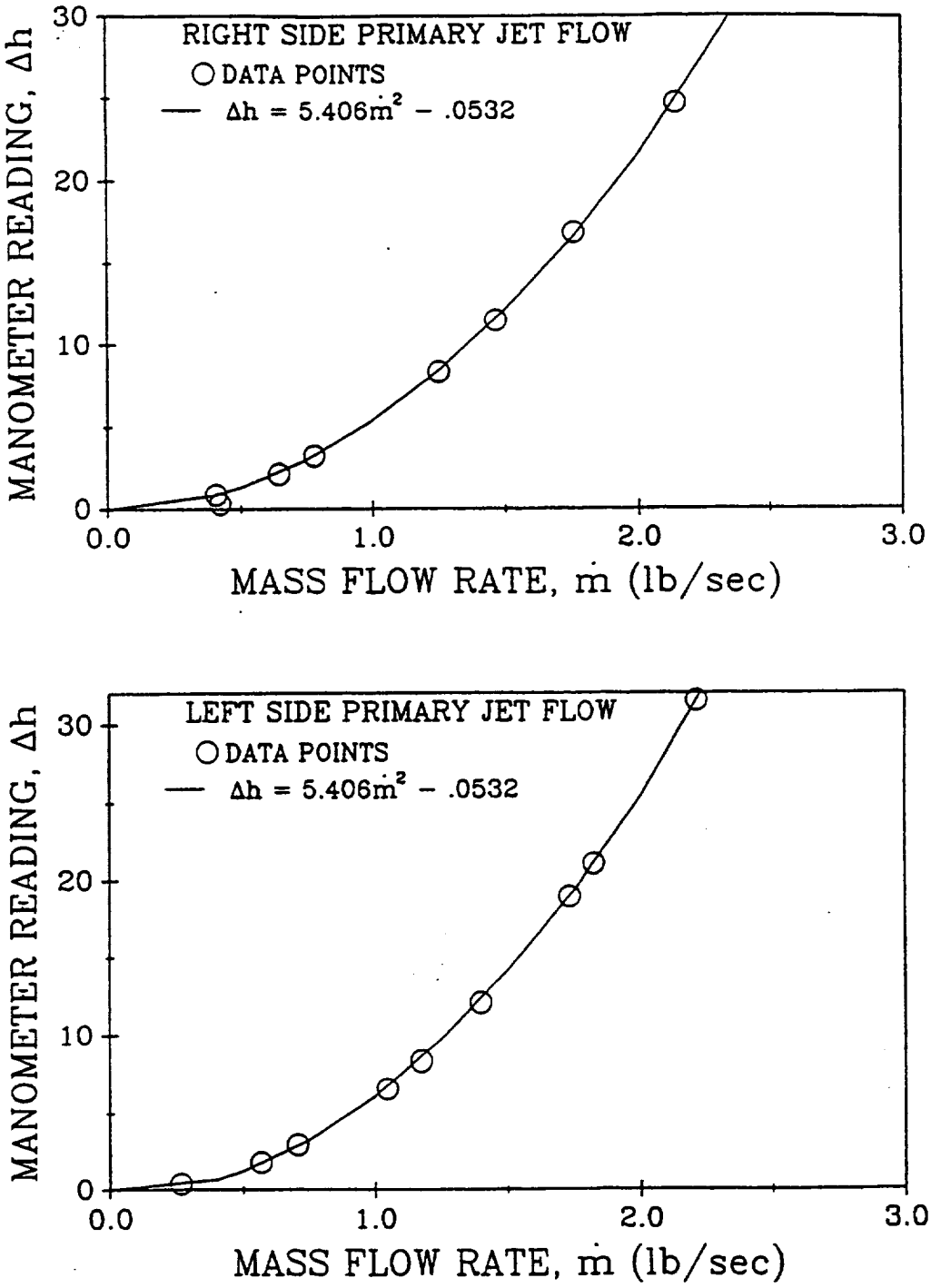

Figure 3.5. Flow Calibration Curves for Primary Jet Flow

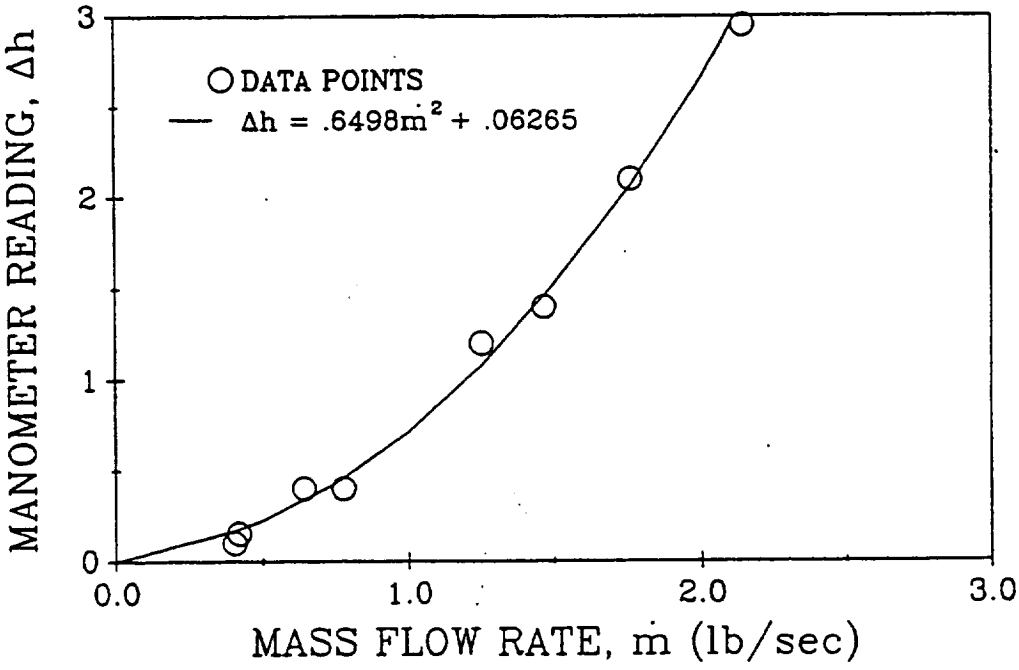

Figure 3.6. Venturi Calibration Curve for Total Jet Flow

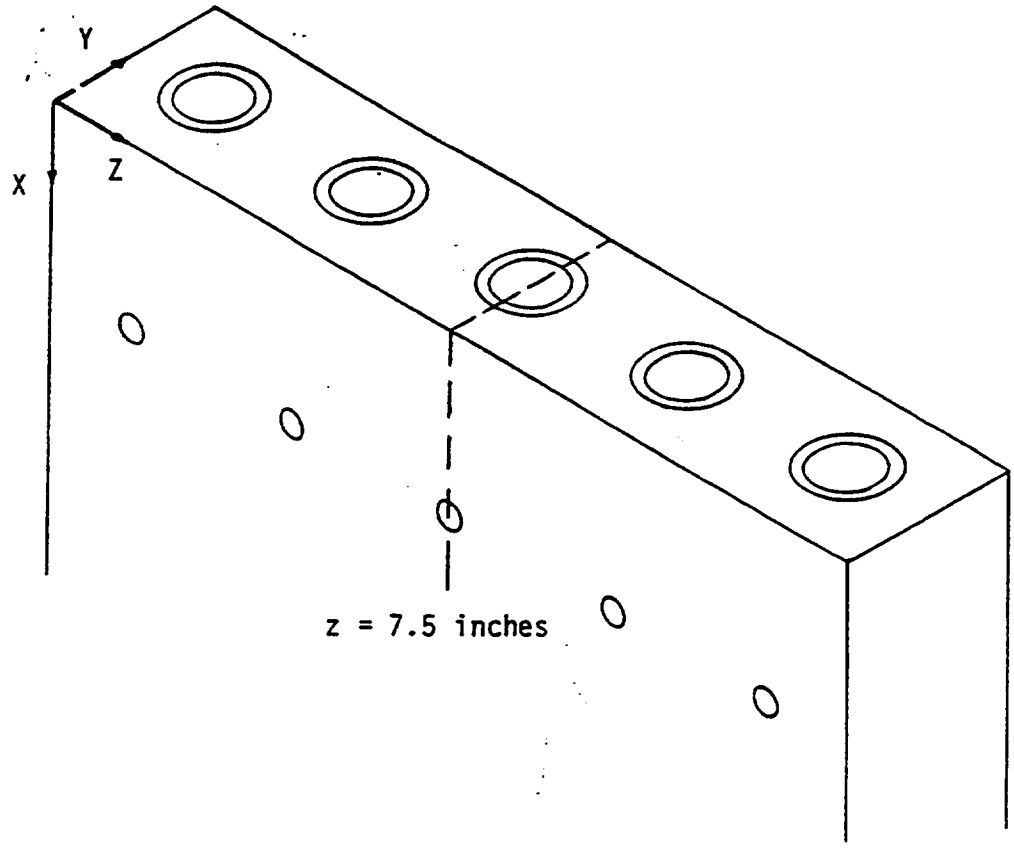

Figure 3.7. Model Annular Combustor Coordinate System

CHAPTER 4: RESULTS & DISCUSSION

This chapter discusses the results obtained from the experiments described in the previous chapter, which were conducted in the model annular combustor. The coordinate system used for the presentation and discussion of the results is the one presented in Chapter 3.

4.1 Opposing Jets

The results from the measurements made with no annular jet flow are presented in Figures 4.1 through 4.9. At each z location, the data were reduced along lines of constant y, for y values of 0.5, 1.0, 1.5 and 2.0 inches. The data reduction scheme is presented in Chapter 2. This provided radial distributions across the jet entering at y = 0.0 inches. In addition to these radial profiles, data were reduced along a line of constant x, at x = 3.0 inches, corresponding to the jets axes and lines parallel to the axes.

Mean and rms concentration profiles were calculated along each of the lines mentioned above. The mean concentration values are presented as a ratio to the maximum mean value on the jet centerline, $\overline{C}_{CL,MAX}$. The rms quantities are divided by the local mean value to provide a fluctuation intensity quantity, $c'/\overline{C}$.

Figures 4.1 through 4.4 are visualization images of the primary jet concentration field. Figures 4.1 and 4.2 are a single frame and a 127 frame average, respectively, with

both figures being taken through the jet axis. The single frame image is much different from the average image, indicating the highly turbulent nature of this flow field. The spread of the jet at the impingement point is barely observable in the average image because it switches from top to bottom and in the average is greatly reduced. Figures 4.3 and 4.4 are one-half inch from the jet axis. The spread from the jet impingement can be clearly seen in the single frame image (Figure 4.3). Due to the very turbulent nature of this interface, the mean image (Figure 4.4) shows that the concentration is spread over a relatively large area.

Figures 4.5 through 4.9 present the mean concentration profiles at the four z locations of the laser sheet. In each figure, the profiles are presented as line plots and as a three dimensional graph. Also included on each figure is a diagram indicating where the profiles are located in the test section. The concentration profiles in Figure 4.5 are calculated across the jet axis and are similar to those expected for a single jet at y = 0.5 and 1.0 inches. At higher values of y, the decrease at the location of the jet axis (x = 3.0 inches) is caused by the opposing jet which does not contain dye. With decreasing z, the profiles flatten as the dye mixes out toward a constant value. Figure 4.9 shows the axial mean profile along the jet axis and lines parallel to the axis. The jet spreads in the x-z plane when it impacts the opposing jet. The presence of this spread can be seen in the z = 7.0 inches profile. The mean appears to increase initially from the exit value. This effect was also observed by Borleteau[6] and Long, Chu and Chang[14]. This is probably due to the camera response which is expected to be attenuated at the image edge. Long, et al. noticed that even after correction of original digital images, the response of the camera was still attenuated at the edges. The laser sheet reflected off of the plexiglass walls, resulting in a higher laser intensity near the wall. This introduced a non-linearity near the walls which caused the signal to be attenuated (see Appendix). The combination

of the camera response and the reflection from the plexiglass walls results in the signal attenuation near the walls.

Figures 4.10 through 4.14 present the fluctuation intensity profiles for the case with no annular jet flow. Figure 4.10 is taken through the jet axis and shows a profile similar to that expected for a single jet at y = 0.5 and 1.0 inches. The interface between the two jets is apparently between y = 1.0 and 1.5 inches. The large peak which would occur at the interface is not observable. The mixing region can be seen at y = 1.5 inches for the decreasing values of z. Figure 4.14 is measured along the jet axis and lines parallel to the axis. The peak at y = 1.25 inches for the z = 7.5 inches profile indicates that the jet/jet interface is in fact between y = 1.0 and 1.5 inches. The increase for higher values of y is due to the near zero mean value which is the denominator of the plotted quantity.

4.2 Annular Jet /Primary Jets Interaction

The results for the configuration with annular jet flow and primary jet flow are presented in Figures 4.15 through 4.45. For the test with dye injection through a primary jet, data reductions were performed along radial and axial lines as described for the no annular jet flow case. The test with dye in the annular jet flow was analyzed by reducing data along lines of constant x, for x values of 1.0, 2.0, 3.0 and 4.0 inches. This provided radial distributions across the annular jet. An axial profile was also calculated along the annular jet's axis (y = 1.5 inches) and lines parallel to the axis. Mean values were normalized by the maximum annular jet centerline mean value, $\overline{C}_{CL\_MAX}$.

4.2.1 Primary Jet Concentration. Figures 4.15 through 4.29 present the results from the test with the dye being injected into a primary jet. Figures 4.15 through 4.18 are visualization images of the primary jet concentration field. As with the previous case, the

average images are greatly different from the single images indicating a highly unsteady flowfield. The effect of the annular jet is clearly evident in these images. The primary jet flow is driven downstream by the annular jet. The figures at z = 7.0 inches (Figures 4.17 and 4.18) show much less primary jet flow at this location than the case without annular jet flow. This indicates that the primary jet is more thoroughly mixed at z = 7.0 inches, due to the annular jet flow.

Figures 4.19 through 4.23 present the mean concentration profiles. Figure 4.19 shows the profiles through the jet axis. These are similar to the case without annular jet flow, except that above the primary jets the mean value is nearly zero due to the annular jet flow. The mean values drop off with decreasing z as before. This case results in a faster decrease due to the mixing with the annular jet. Figure 4.23 shows profiles along the jet axis and lines parallel to the axis. The value at the edge is attenuated as discussed in section 4.1.

Figures 4.24 through 4.29 present the fluctuation intensity profiles. Figure 4.24 shows profiles similar to the expected curves for a single jet at y = 0.5 and 1.0 inches. The peak on the lower x side of the jet is higher due to the increased mixing with the annular jet. This can be still be seen at z = 7.0 inches (Figure 4.25). At z = 6.5 inches, the fluctuation intensity profiles are nearly zero, indicating that the mixing is nearly zero. Figures 4.28 and 4.29 are both fluctuation intensity profiles along the plane of the jet axis. Figure 4.28 only goes to y = 1.7 inches because the quantity, $(c'/\overline{C})$, was very high and erratic beyond that point due to the nearly zero mean value. Figure 4.29 shows the rms normalized by $\overline{C}_{CL,MAX}$ instead of $\overline{C}$ to give a better indication of the shape of the rms profile.

Figures 4.30 and 4.31 compare the primary jet concentration results from the test cases with and without annular jet flow. Figure 4.30 compares mean and fluctuation intensity profiles across the primary jet axis (z = 7.5 inches). The effect of the annular jet flow is seen in the mean as a decrease on the low x value side of the jet. The fluctuation intensity peak on this side of the jet is higher, with the annular jet flow, due to the increased mixing. Figure 4.31 presents mean and fluctuation intensity profiles along the primary jet axis and lines parallel to the axis. The mean profiles at z = 7.5 inches show that the annular jet flow does not have a very large effect at this location. That is because the annular jet momentum, although greater, is spread over a larger area than that of the primary jet. The fluctuation intensity peak at the intersection of the three jets is higher due to a more turbulent flow with the annular jet flow. At the lower z values, the profiles for the case with annular jet flow show lower mean values and higher fluctuation intensity values. Both of these trends indicate more mixing with the annular jet flow, as expected.

4.2.2 Annular Jet Concentration. The results for the case with dye in the annular jet flow are presented in Figures 4.32 through 4.45. Figures 4.32 through 4.35 are concentration field visualization images of the annular jet. The unsteady nature of this field can be deduced from the large differences between the single frame image and the average image. This flow does not appear as turbulent as the primary jet flow and indeed the Reynolds number is significantly lower for the annular jet flow. The images appear asymmetric with more dye on the right side of the flow. This is apparently due to an uneven flow distribution at the annular jet exit. This could be due to the annular jet being nearly completely closed. If the jet control valve had been opened wider, the higher annular jet flow would have washed the primary jet flows downstreams and eliminated any interaction between the jets, in the field of observation.

The mean concentration profiles are presented in Figures 4.36 through 4.40. Figure 4.36 shows the mean profiles through the annular jet axis. The double peaked curve at x = 1.0 inch is slightly asymmetric, indicating the uneven flow distribution discussed above. The profile flattens and spreads downstream until at x = 4.0 inches (downstream of the primary jets), the profile is essentially flat. At z = 7.0 inches, there is only a single peak because the laser sheet intersects the annulus of the annular jet in just one area. This peak is off-center due to the uneven flow distribution from the annular jet. Again the profile spreads and flattens downstream. At z = 6.5 inches (Figure 4.38), the profile increases at x = 3.0 inches due to the primary jets carrying the annular jet flow across the channel to this location. This increase is not as significant at z = 6.0 inches due to the increased distance from the primary jet pair and the effect of the adjacent primary jet pair, since this location is midway between two jet pairs. Figure 4.40 shows mean profiles along the annular jet axis and lines parallel to the axis. The effect of the primary jet pair can be seen in the profiles at z = 7.0 and 6.5 inches as an increased concentration level extending across the channel at x = 3.0 inches.

Fluctuation intensity profiles are presented in Figures 4.41 through 4.45. Figure 4.41 presents measurements made with the laser sheet aligned with the annular jet axis. The edges of the jet can be seen as peaks. The overall level increases at x = 3.0 inches, due to the mixing with the primary jets at this location. The level drops again at x = 4.0 inches, downstream of the primary jets. The fluctuation intensity levels decrease with decreasing z, as the concentration reaches a steady value and the mixing drops off. At z = 6.0 inches, the curves are low in the middle and increase towards the sides due to the low mean value in these areas. Figure 4.45 presents fluctuation intensity profiles along the annular jet axis and lines parallel to the axis. The profile at z = 7.5 inches (the annular jet axis) has the expected shape, nearly zero until the primary jet location at x =

3.0 inches. The peak at this location indicates the highly turbulent mixing occurring where all three jets intersect.

4.3 Conclusions and Recommendations

This thesis presents a non-intrusive method for measuring the two dimensional concentration distribution in a very complex flow field. The method utilizes a fluorescent dye as a flow marker, which is excited by a two dimensional sheet of laser light. The fluorescent intensity field is recorded through a video camera on a video cassette recorder. The recorded images are analyzed with image processing hardware and software to obtain relative intensity values. The relative dye concentration has been shown to be proportional to the intensity. These intensity levels are then manipulated to obtain mean and rms concentration values.

This measurement method was verified on a single round turbulent jet for which previous measurements have been made by others. The results of the single round jet concentration measurements indicated that the measurement system provided satisfactory results.

The concentration measurement system was applied to the complex flow field in a model gas turbine annular combustor. The model consisted of opposing round primary jets and an annular jet discharging perpendicular to the primary jets. The test was run both with and without annular jet flow. The mixing between the jet flows could be visualized from the rms and mean profiles calculated across the flow field. Concentration field visualization images, obtained from the image processing procedures provided qualitative information about the flow field. These images together with the rms and mean profiles showed that this flowfield is highly turbulent and very complex.

This method of concentration measurement has proven to be very useful for obtaining information about a complex flow field. The method utilized is for a liquid flow, since a water soluble dye was used.

This method could possibly be improved by having higher laser power in the test section. This would require either a higher power laser or a reduction in the transmission losses between the laser and the test section. Higher laser power would result in higher fluorescent intensity for a given concentration, providing better system resolution. The full scale intensity value of the digitized image is 255 and the maximum level obtained in these tests was about 150 . Therefore, only about one-half of the available scale was utilized. The intensity level could also be increased by injecting a higher concentration of dye. However, this would result in more absorption of the laser intensity to the point where absorption may not be negligible in the data reduction.

Further improvements in this method could also be obtained by accounting for the camera response nonuniformities and the laser sheet nonuniformities. The data in this thesis were not corrected for these effects. The appendix investigates these effects and show that they are not significant. The reflection of the laser sheet from the plexiglass walls does introduce a significant nonlinearity, near the walls. This could probably be improved by masking the laser sheet to keep it narrower than the flow channel at the test section.

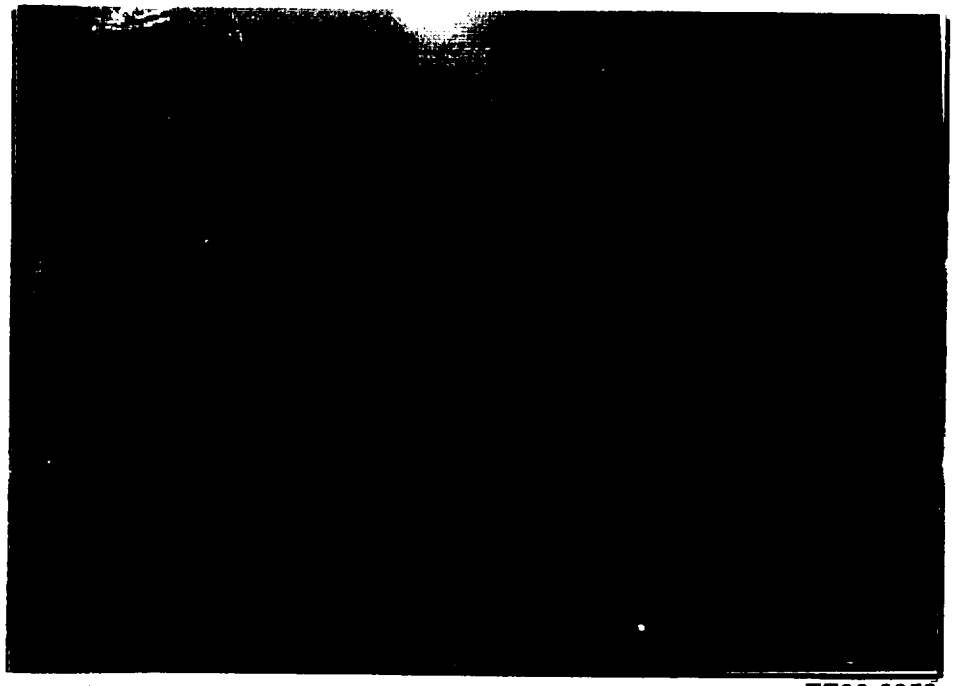

TE92-2359

Figure 4.1. Single Frame Primary Jet Concentration Field Visualization Image without Annular Jet Flow (z = 7.5 inches)

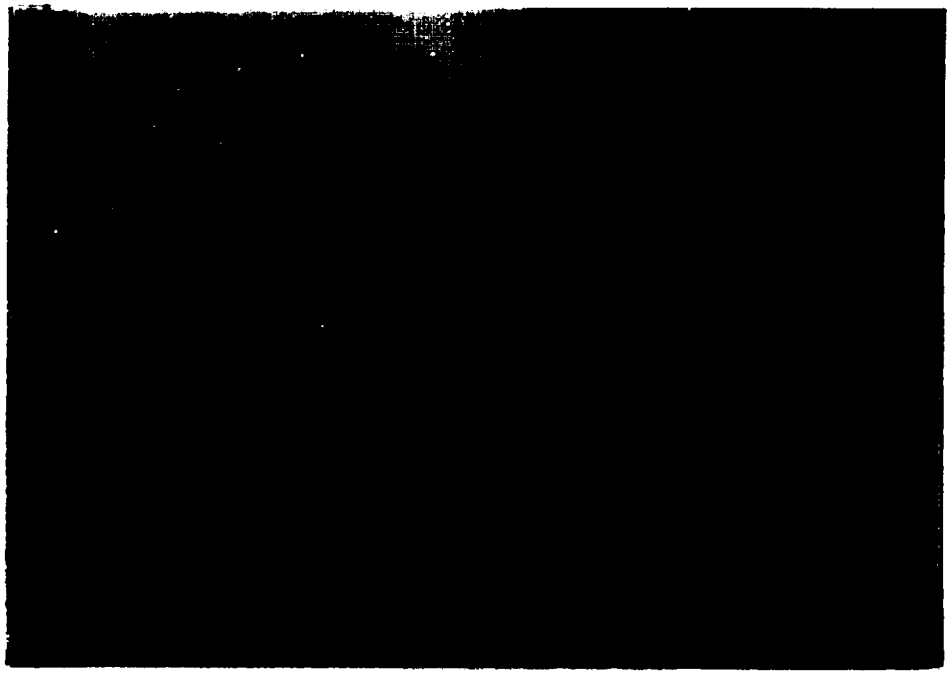

TE92-2360

Figure 4.2. 127 Frame Average Primary Jet Concentration Field Visualization Image without Annular Jet Flow (z = 7.5 inches)

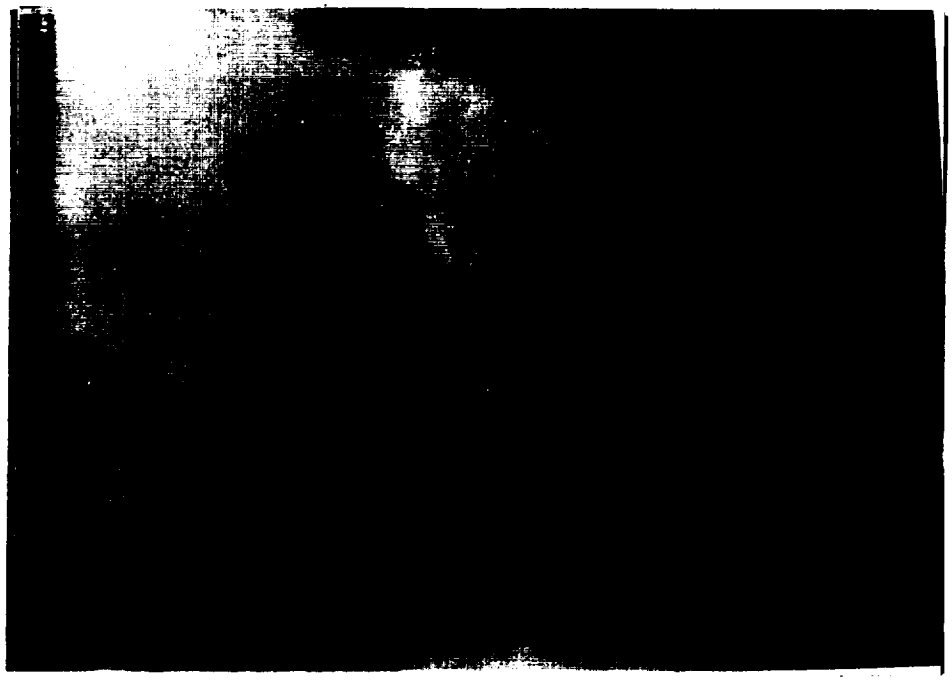

Figure 4.3. Single Frame Primary Jet Concentration Field Visualization Image without Annular Jet Flow (z = 7.0 inches)

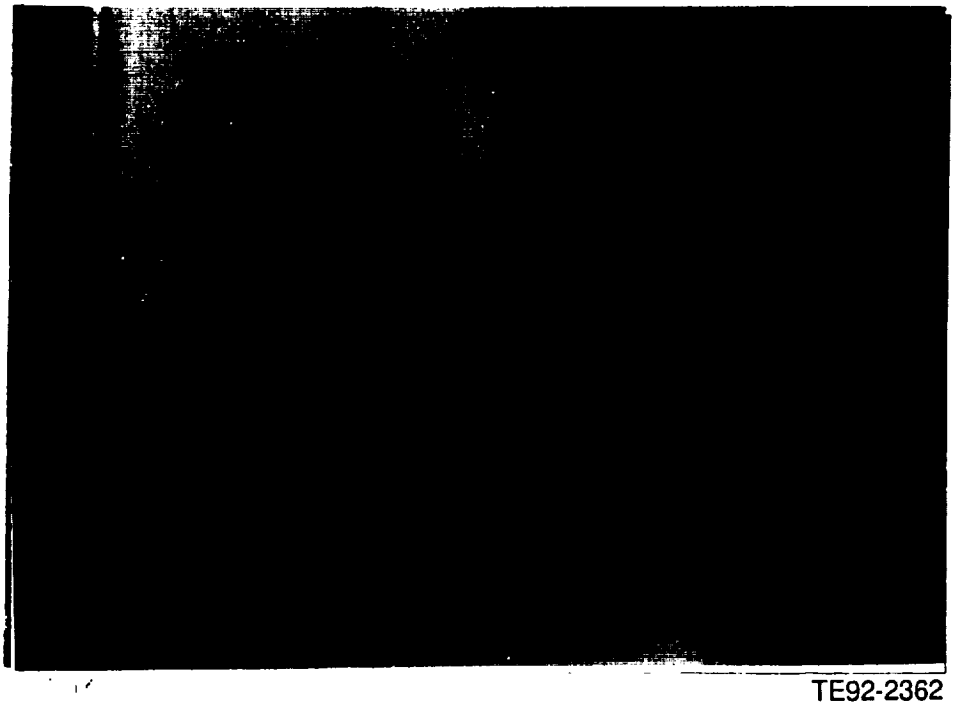

Figure 4.4. 127 Frame Average Primary Jet Concentration Field Visualization Image without Annular Jet Flow (z = 7.0 inches)

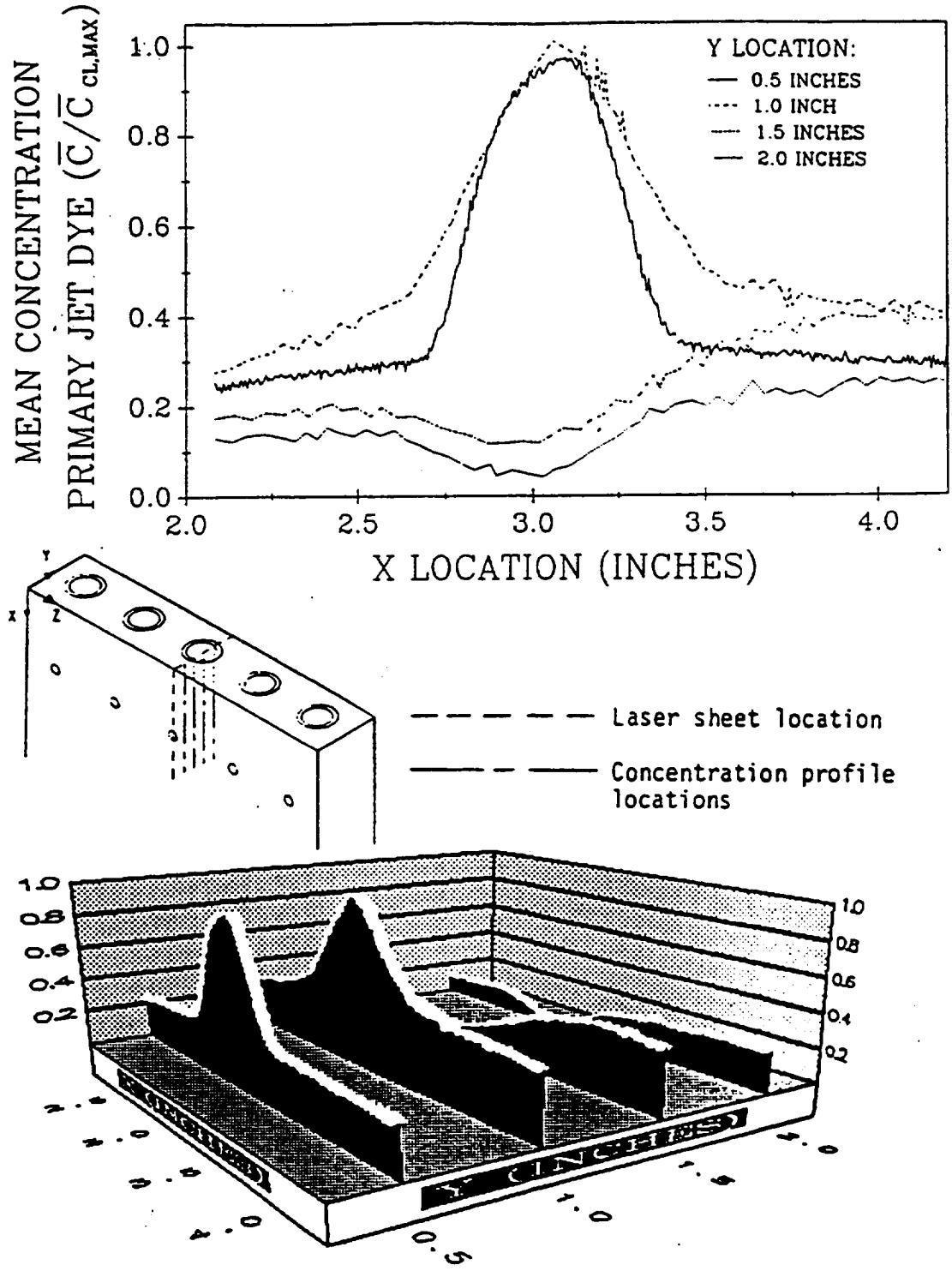

Figure 4.5. Mean Primary Jet Concentration without Annular Jet Flow (z = 7.5 inches)

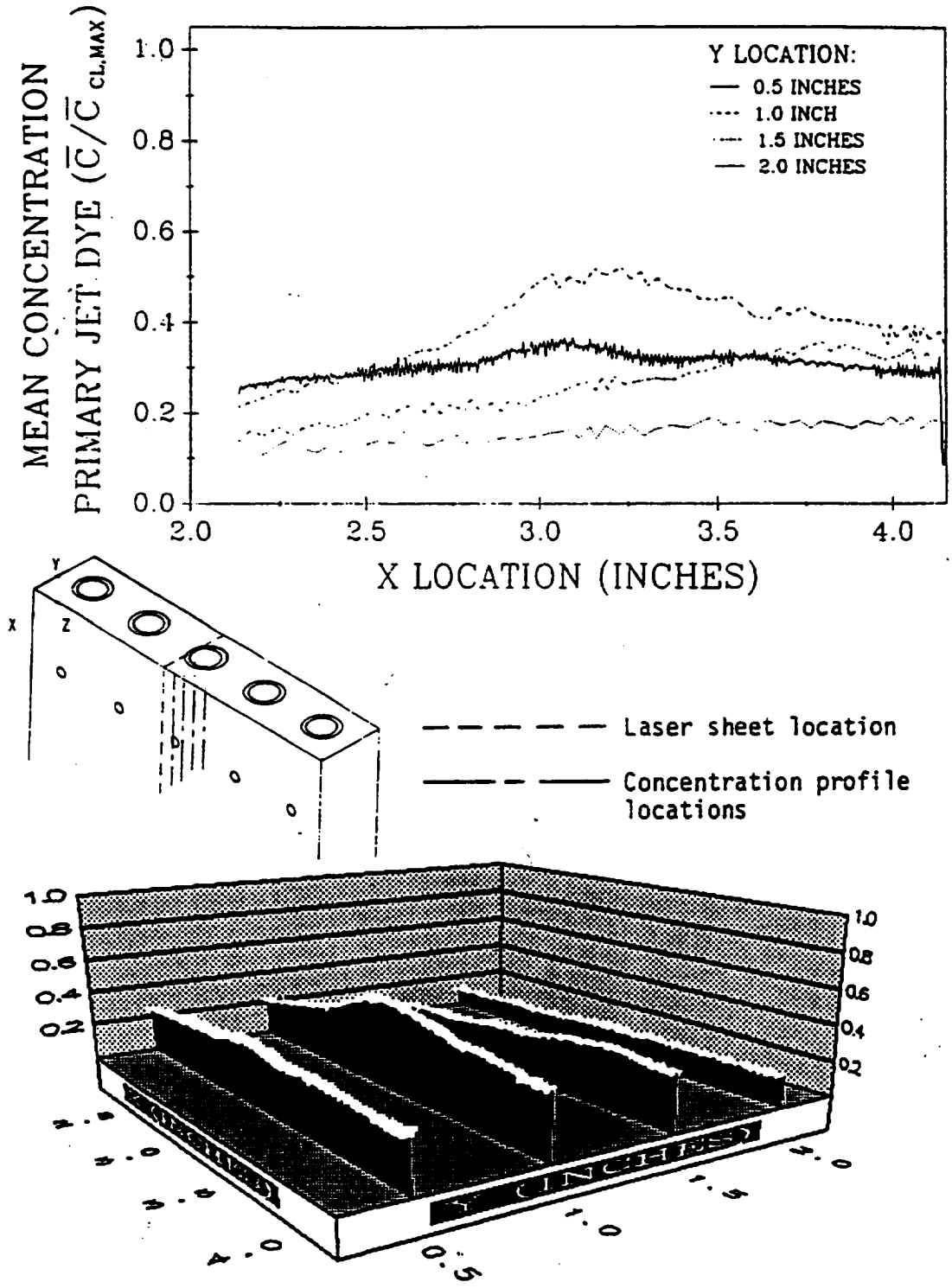

Figure 4.6. Mean Primary Jet Concentration without Annular Jet Flow (z = 7.0 inches)

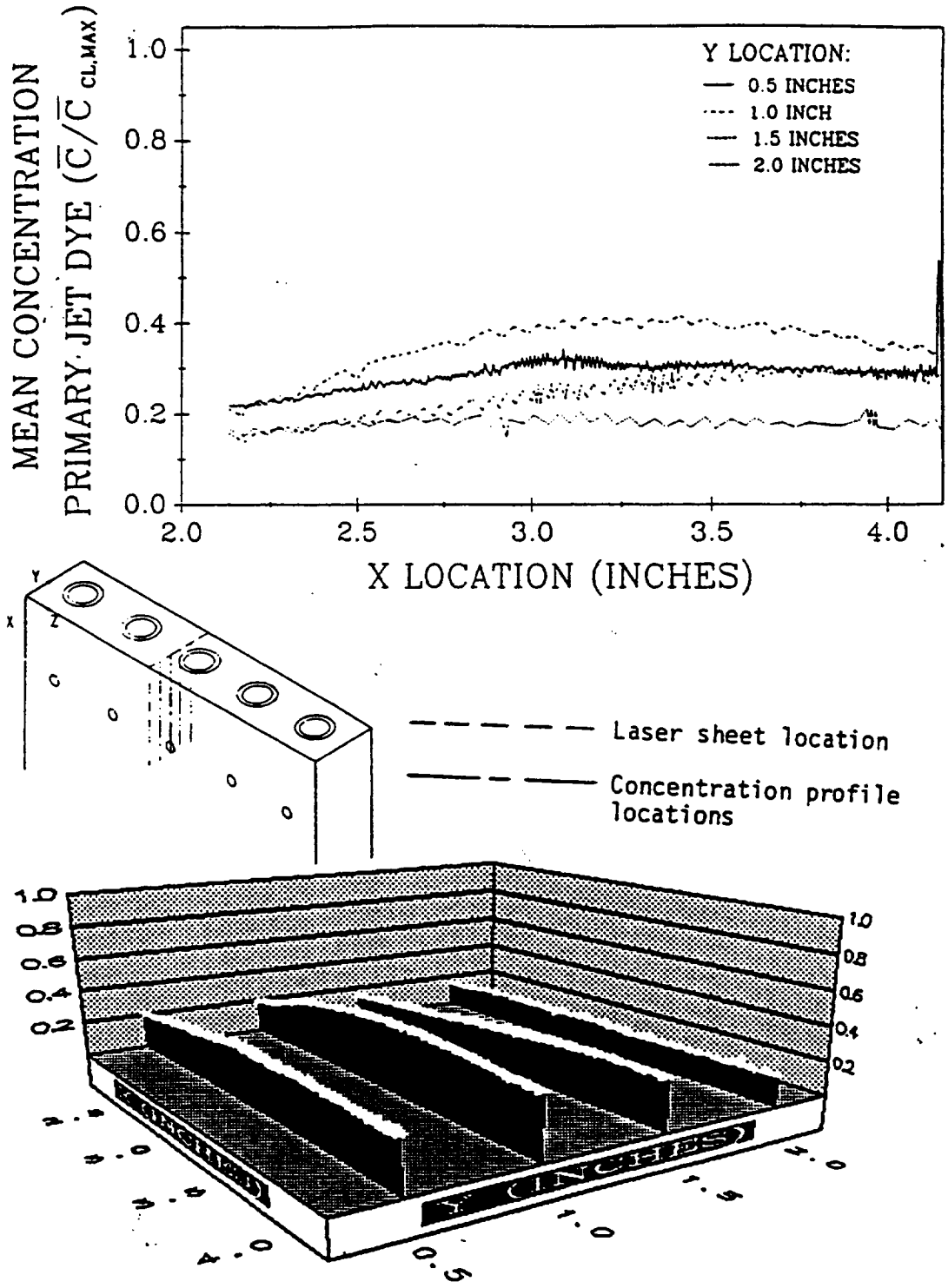

Figure 4.7. Mean Primary Jet Concentration without Annular Jet Flow (z = 6.5 inches)

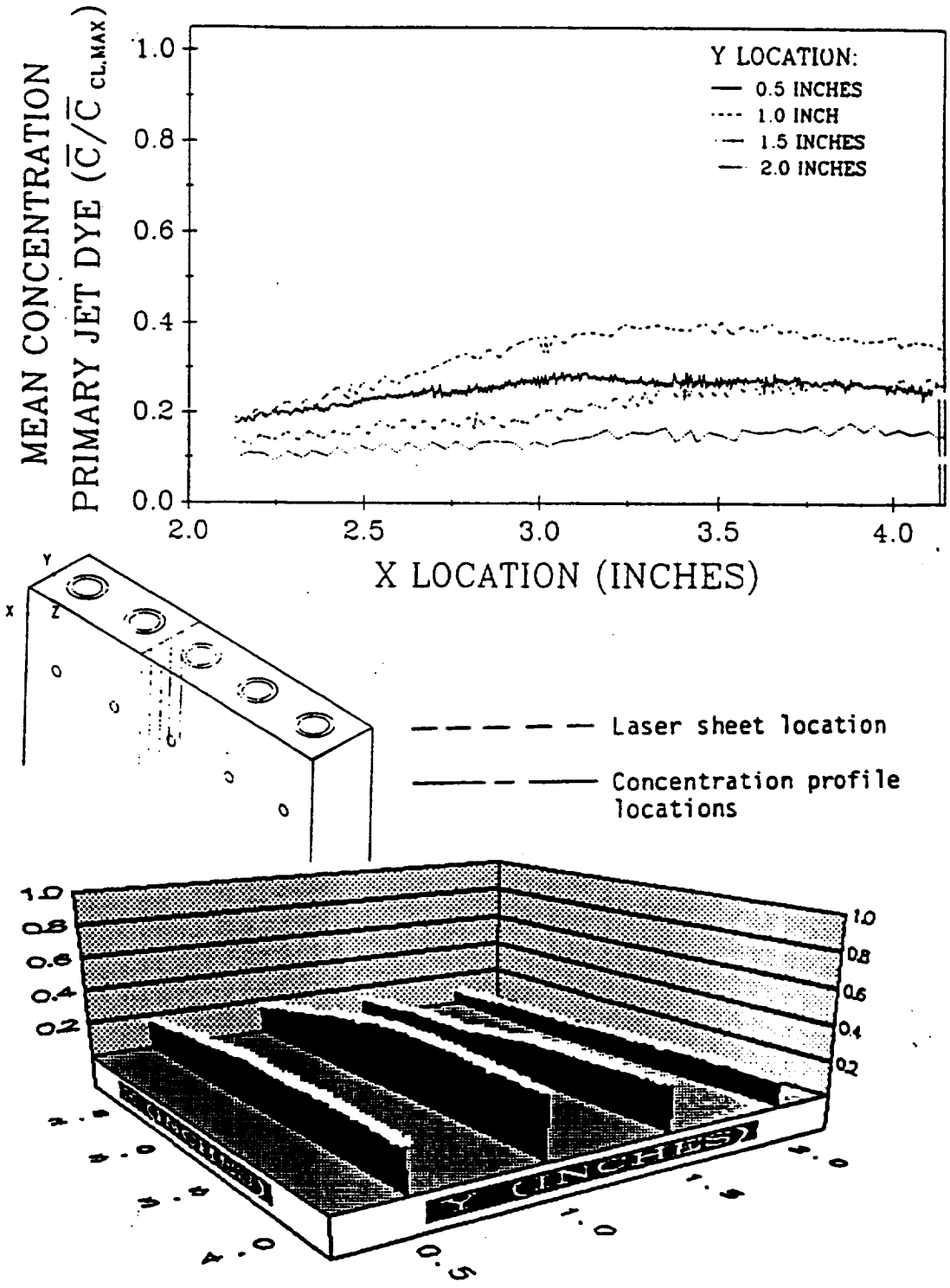

Figure 4.8. Mean Primary Jet Concentration without Annular Jet Flow (z = 6.0 inches)

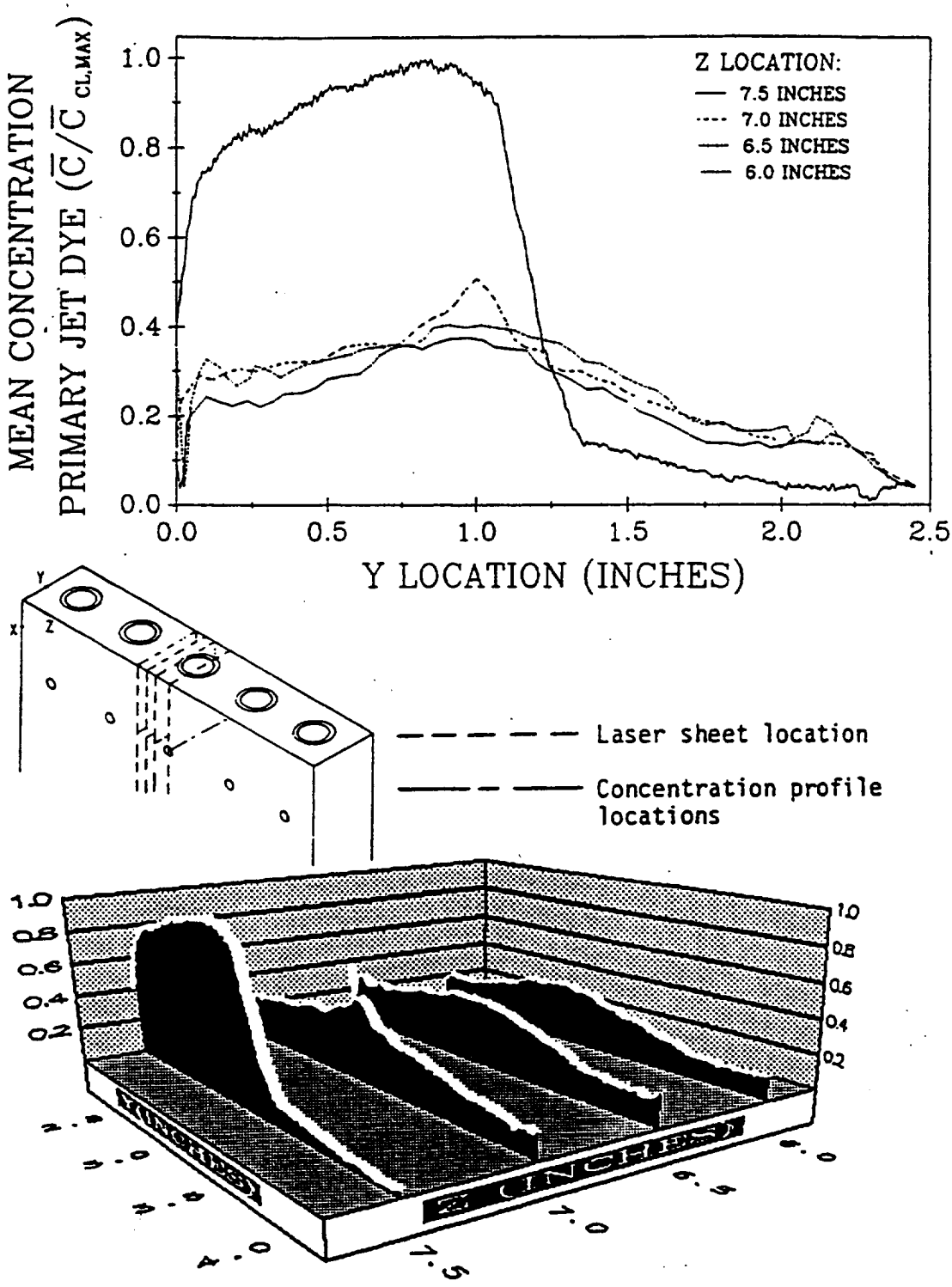

Figure 4.9. Mean Primary Jet Concentration without Annular Jet Flow (x = 3.0 inches)

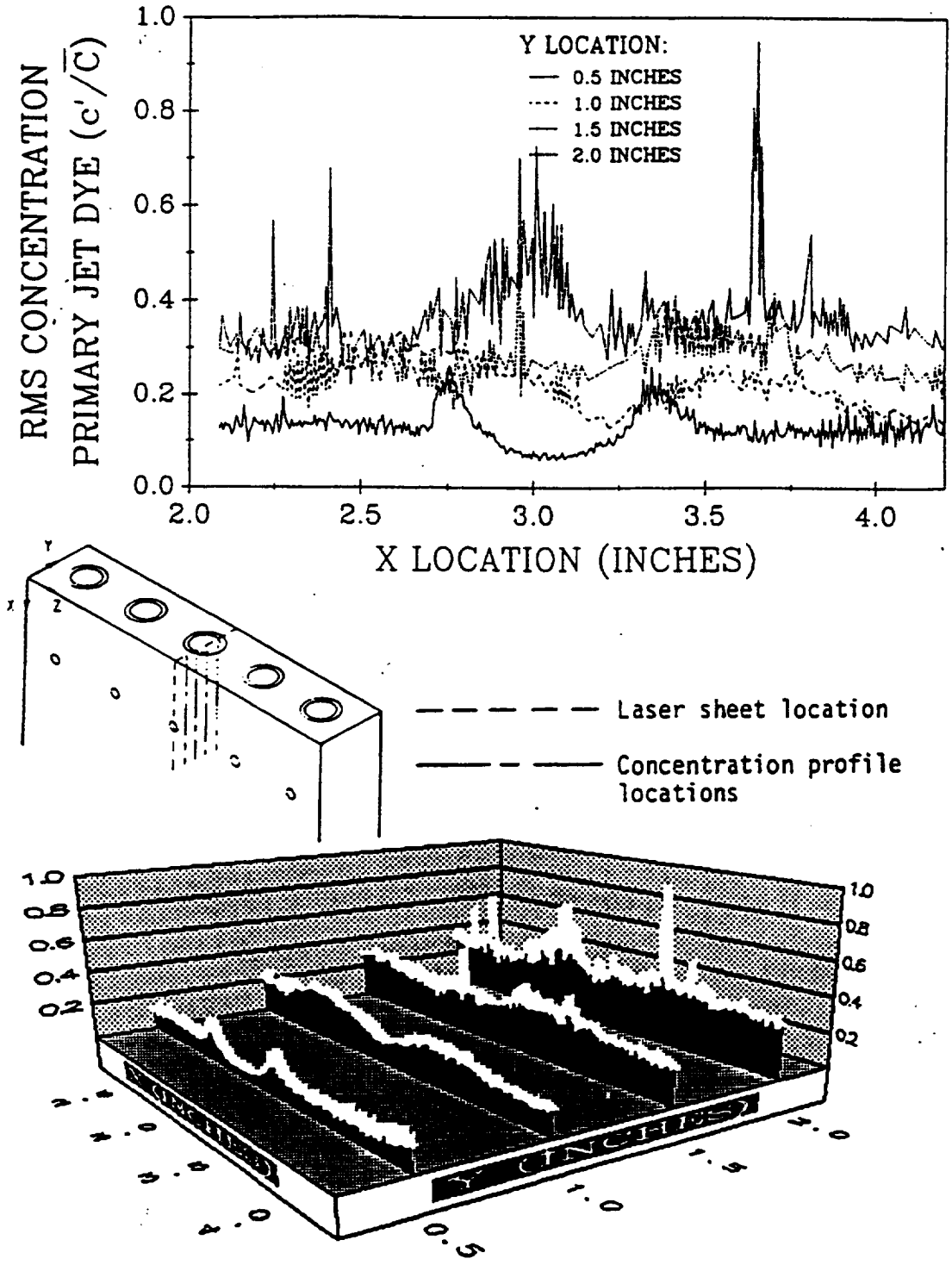

Figure 4.10. RMS Primary Jet Concentration without Annular Jet Flow (z = 7.5 inches)

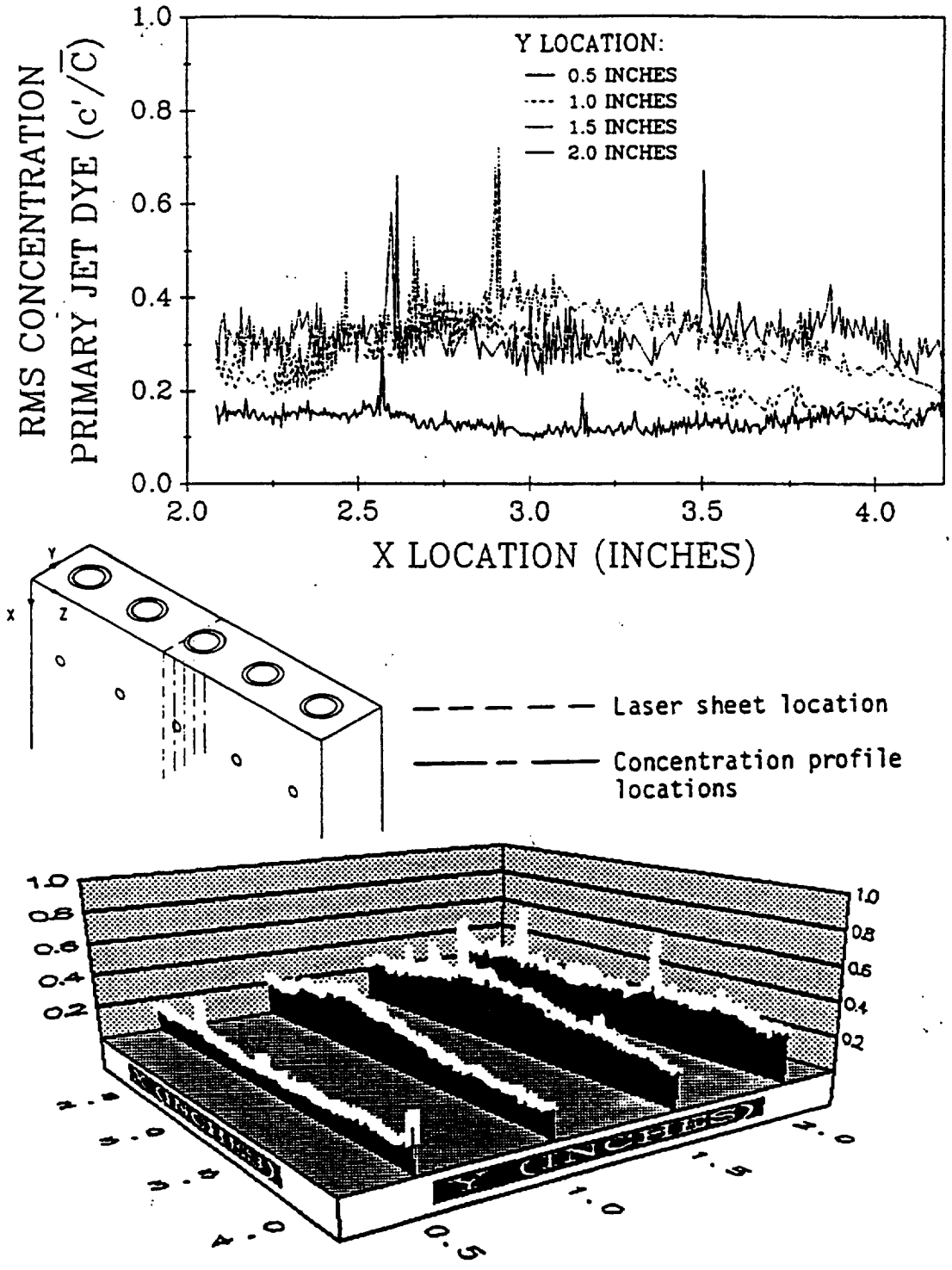

Figure 4.11. RMS Primary Jet Concentration without Annular Jet Flow (z = 7.0 inches)

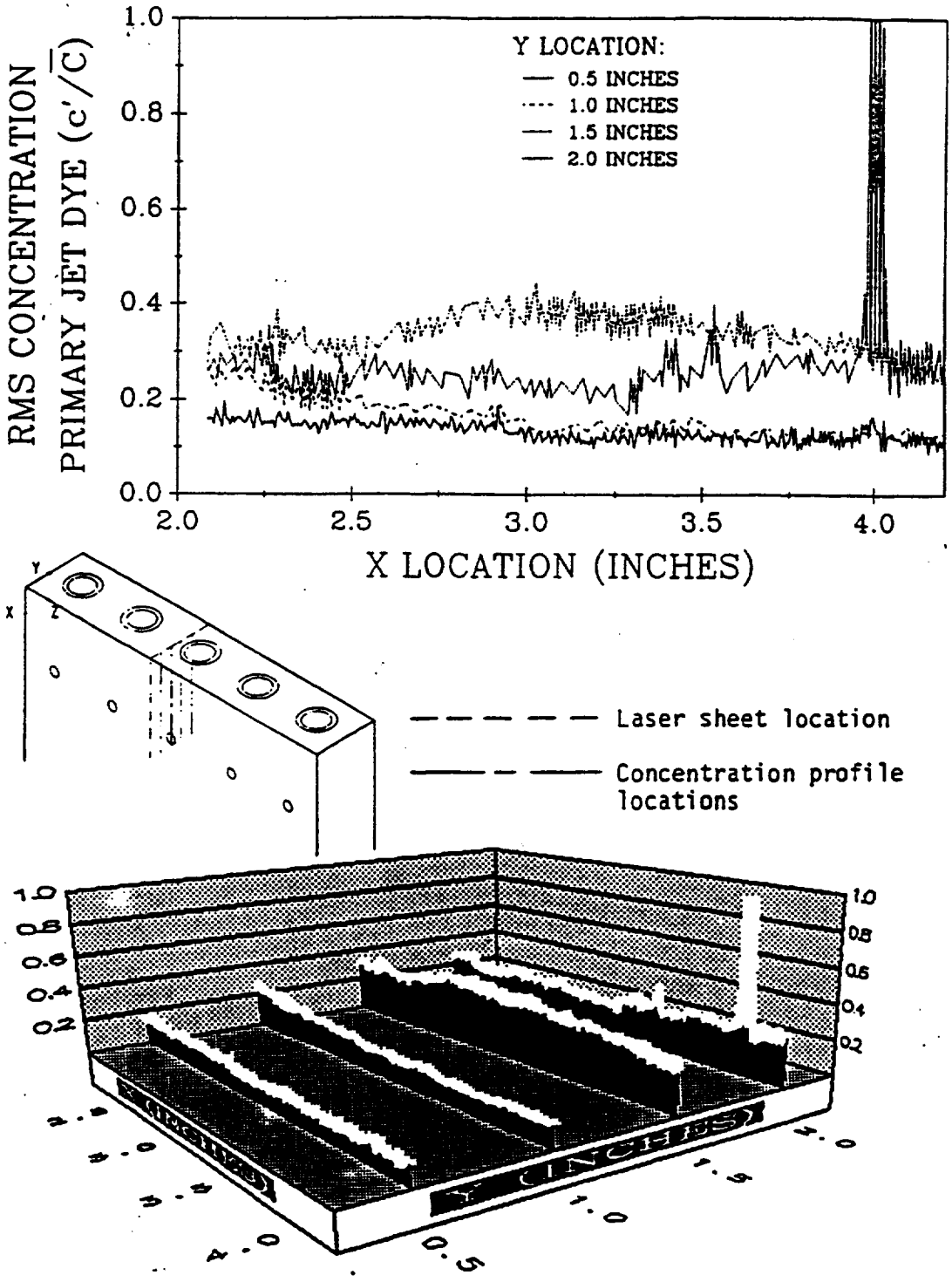

Figure 4.12. RMS Primary Jet Concentration without Annular Jet Flow (z = 6.5 inches)

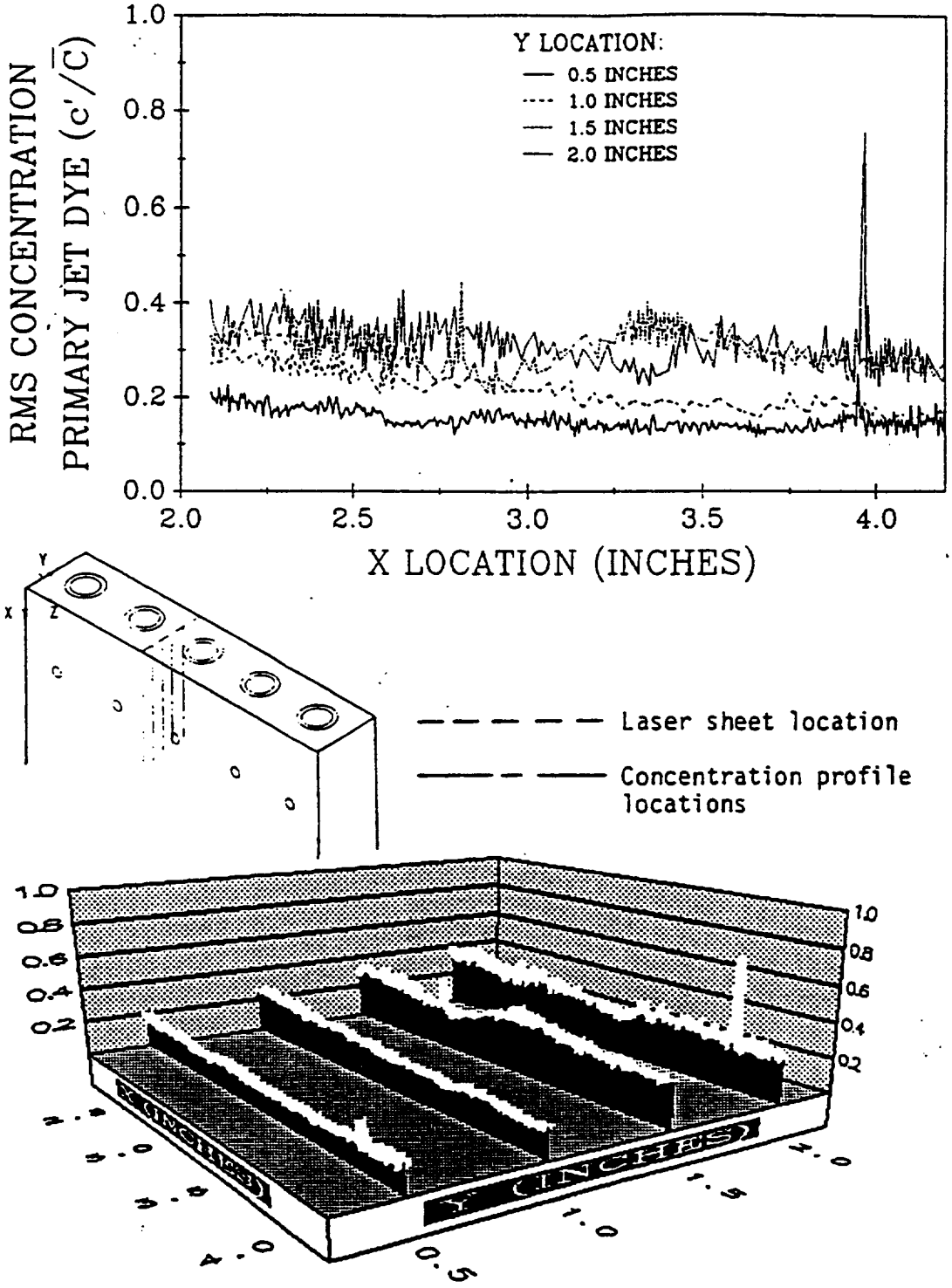

Figure 4.13. RMS Primary Jet Concentration without Annular Jet Flow (z = 6.0 inches)

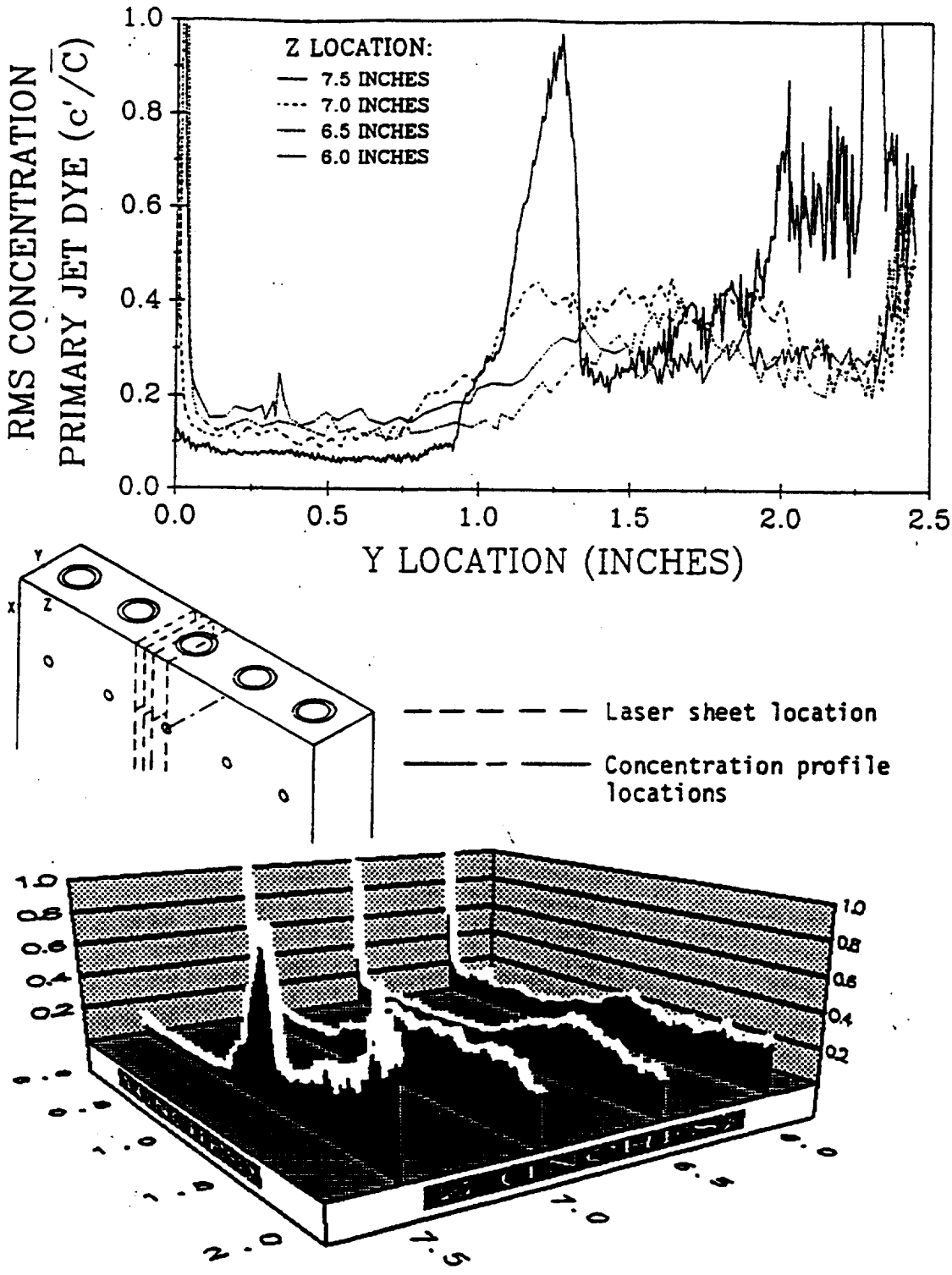

Figure 4.14. RMS Primary Jet Concentration without Annular Jet Flow (x = 3.0 inches)

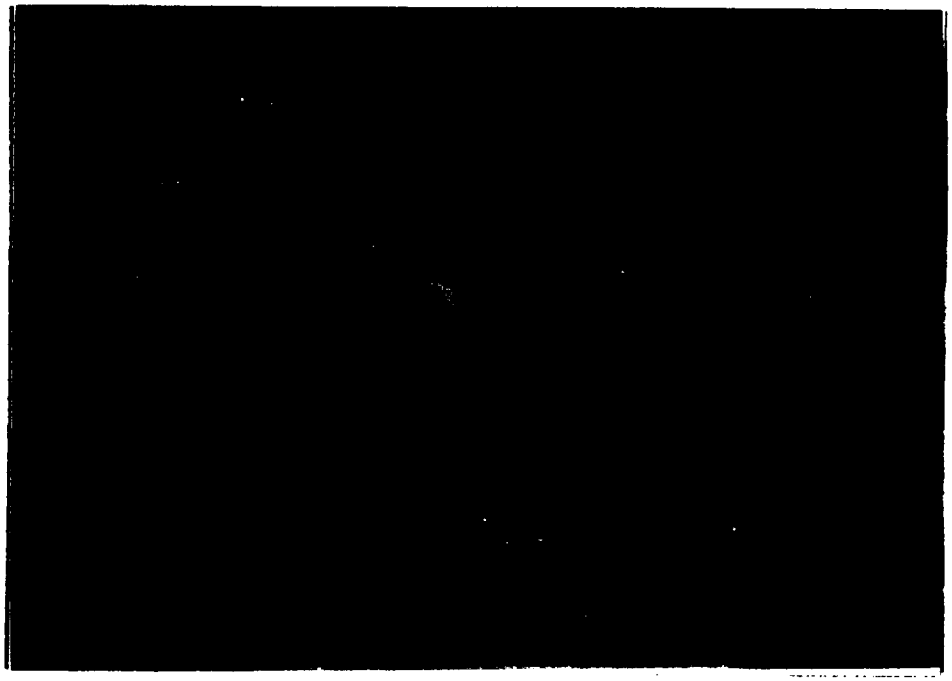

TE92-2373

Figure 4.15. Single Frame Primary Jet Concentration Field Visualization Image with Annular Jet Flow (z = 7.5 inches)

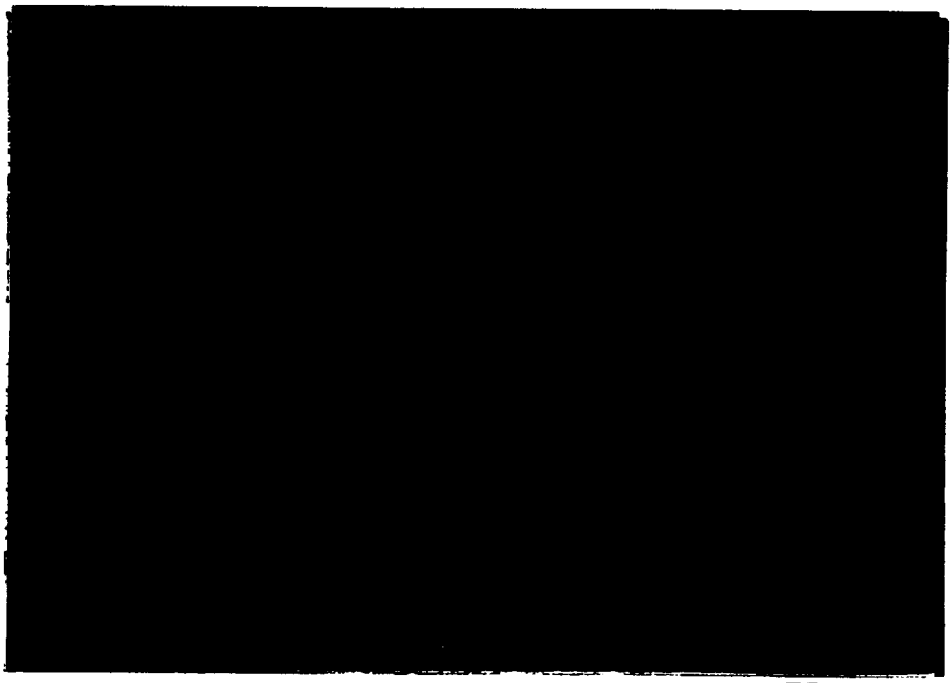

TE92-2374

Figure 4.16. 127 Frame Average Primary Jet Concentration Field Visualization Image with Annular Jet Flow (z = 7.5 inches)

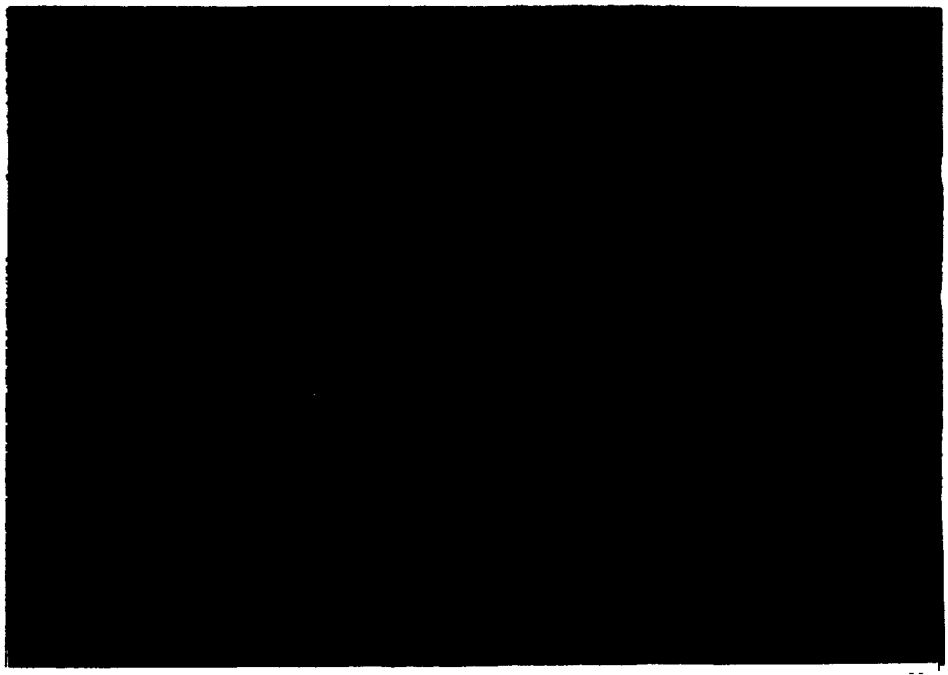

TE92-2375

Figure 4.17. Single Frame Primary Jet Concentration Field Visualization Image with Annular Jet Flow (z = 7.0 inches)

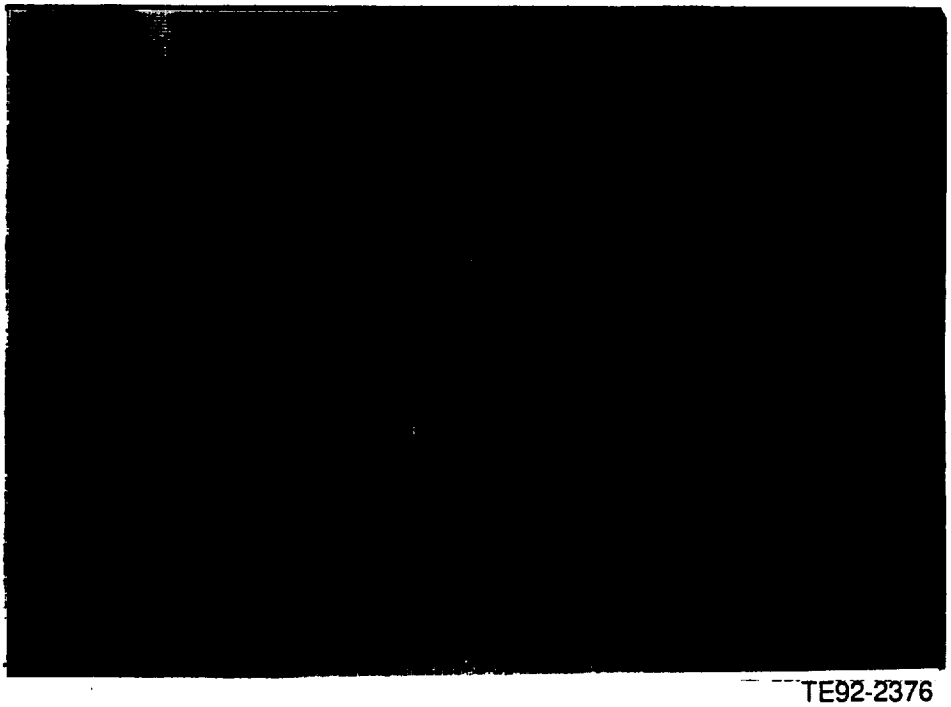

TE92-2376

Figure 4.18. 127 Frame Average Primary Jet Concentration Field Visualization Image with Annular Jet Flow (z = 7.0 inches)

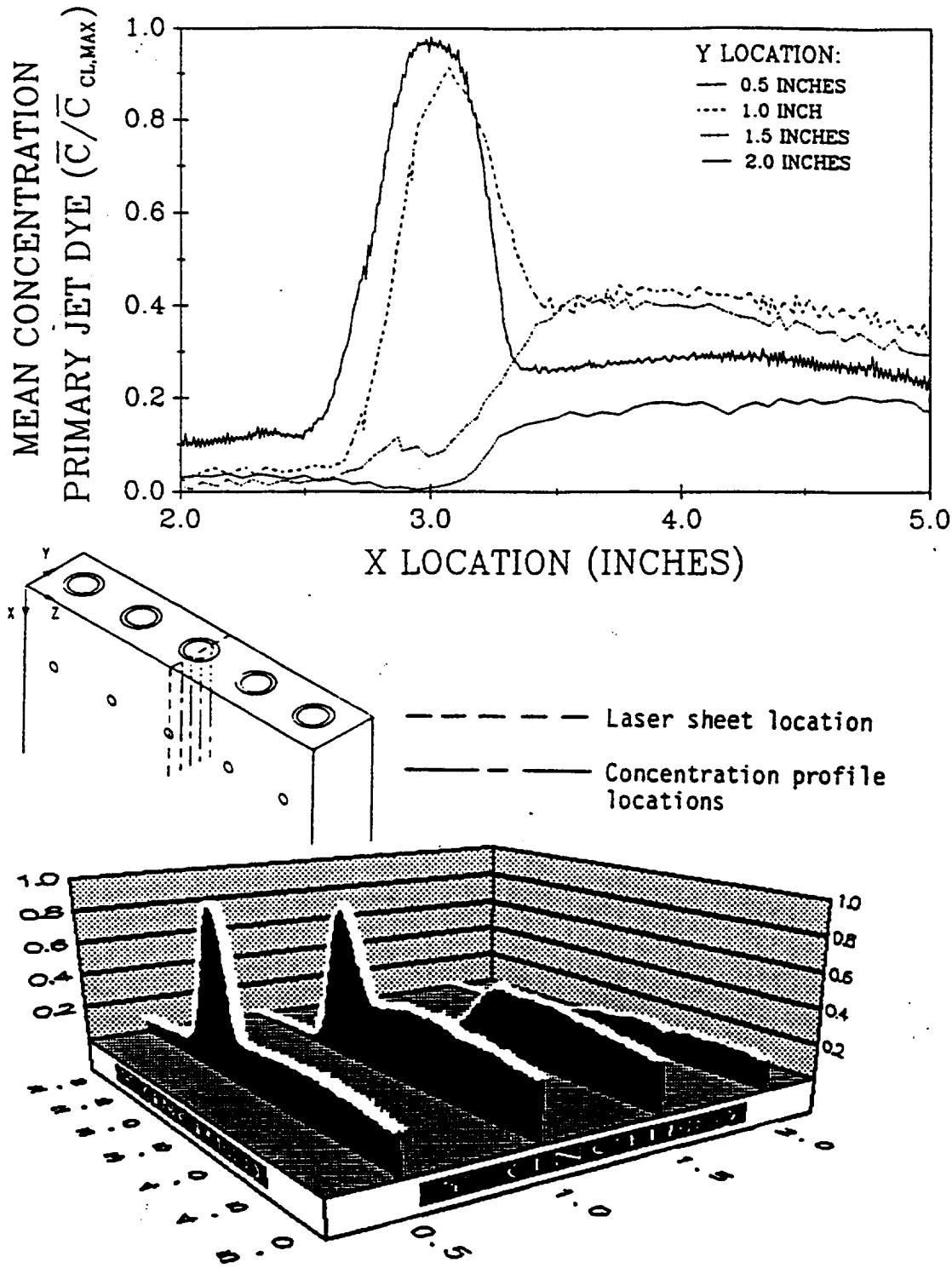

Figure 4.19. Mean Primary Jet Concentration with Annular Jet Flow (z = 7.5 inches)

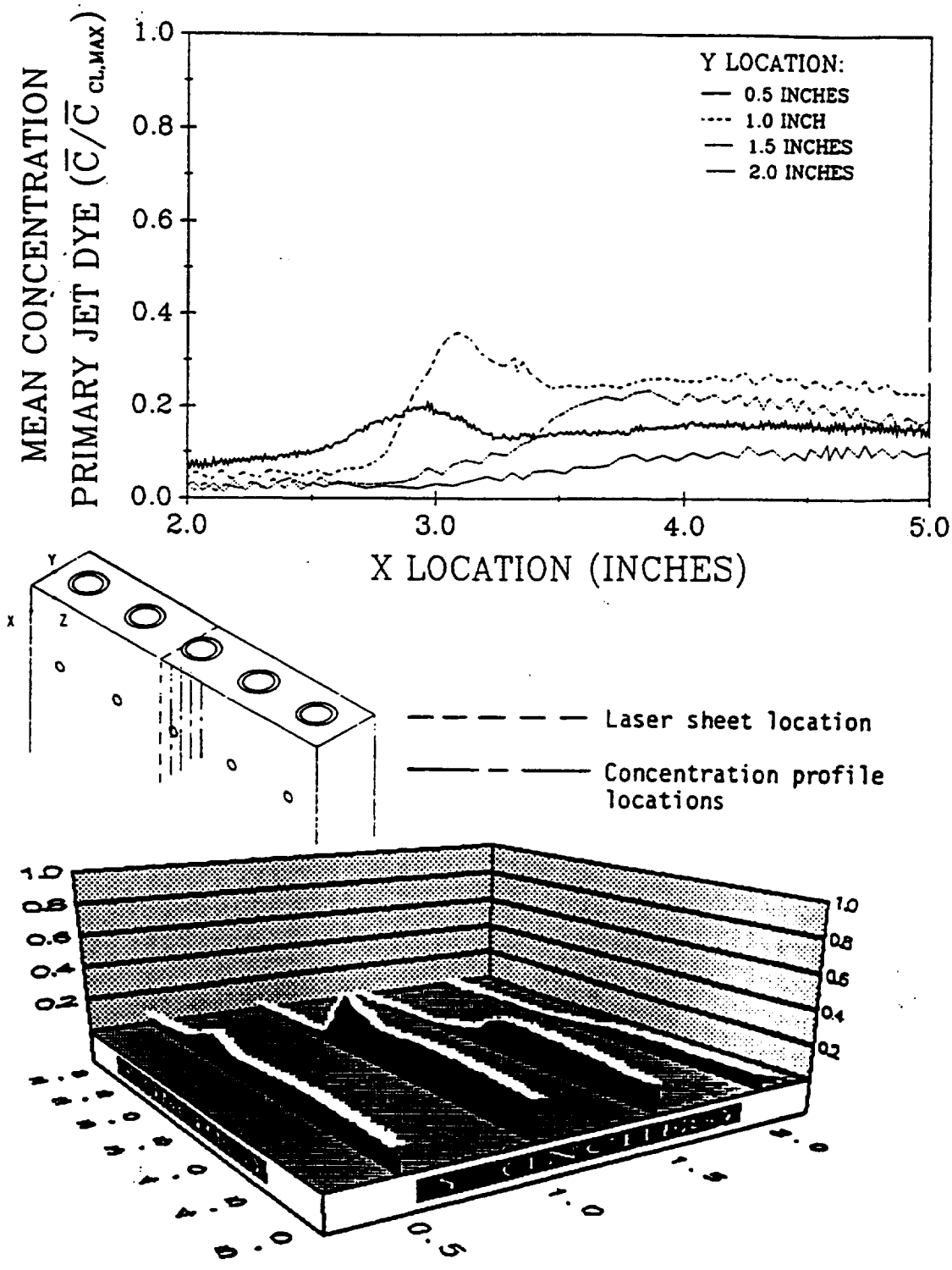

Figure 4.20. Mean Primary Jet Concentration with Annular Jet Flow (z = 7.0 inches)

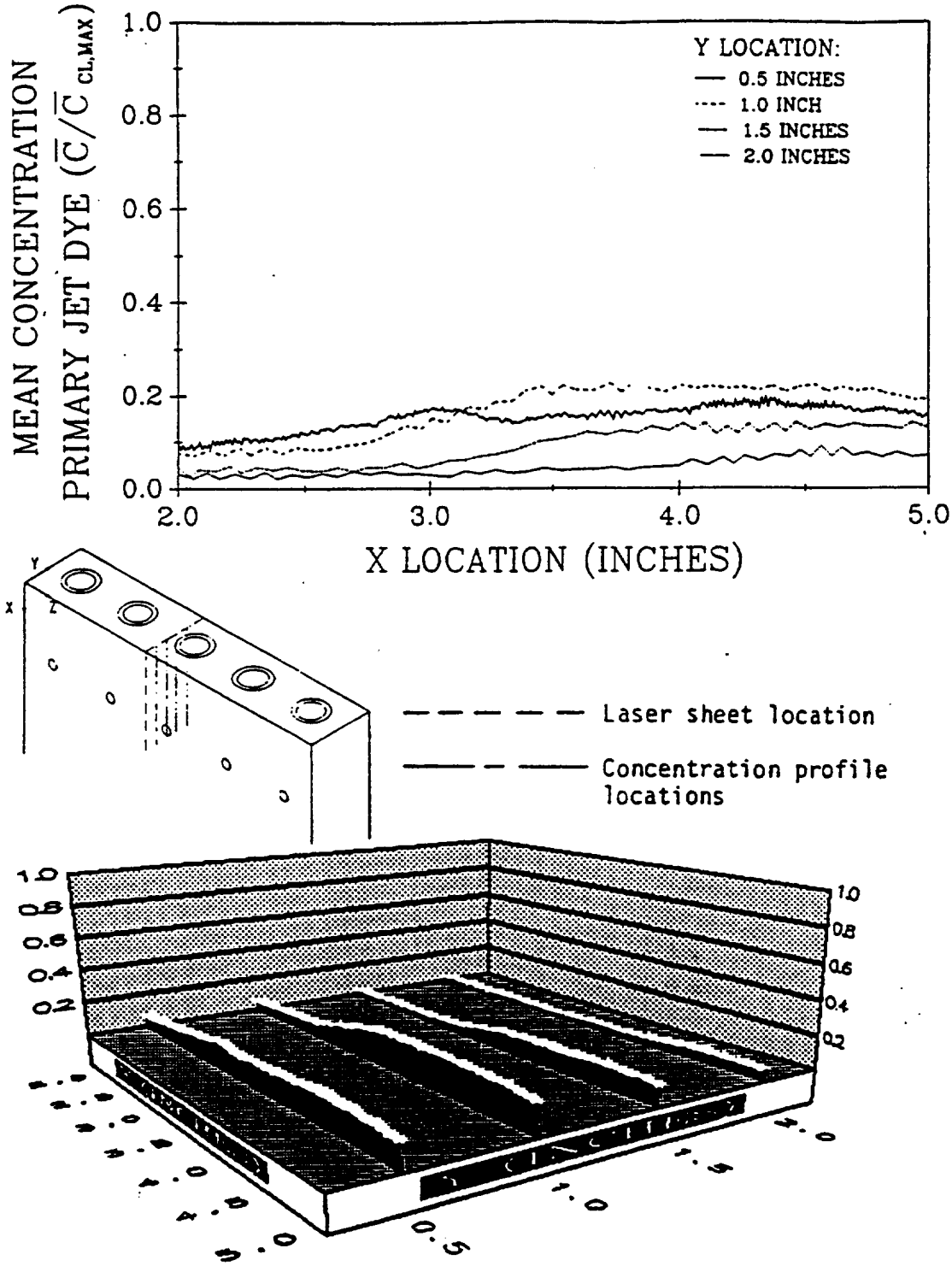

Figure 4.21. Mean Primary Jet Concentration with Annular Jet Flow (z = 6.5 inches)

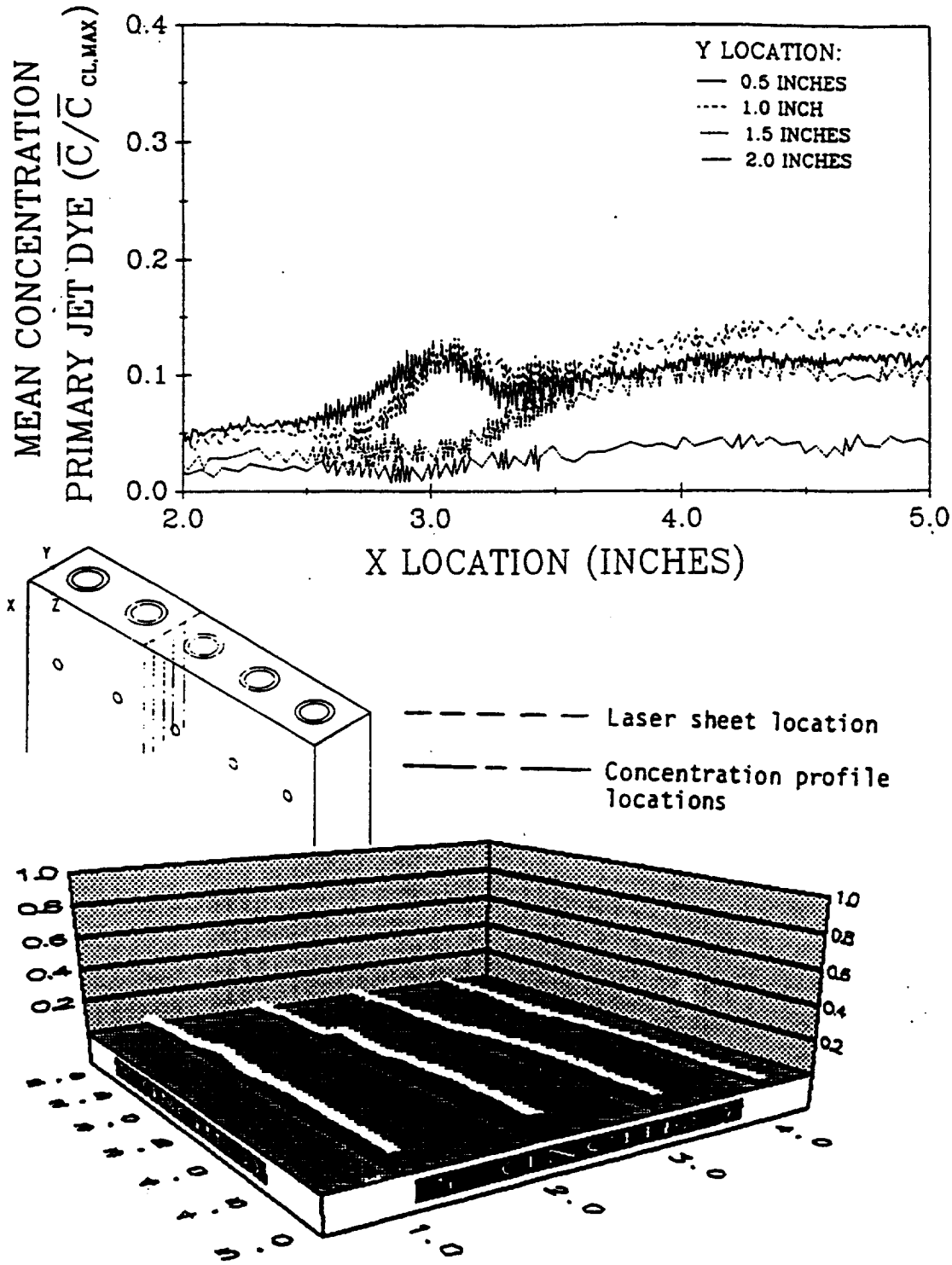

Figure 4.22. Mean Primary Jet Concentration with Annular Jet Flow (z = 6.0 inches)

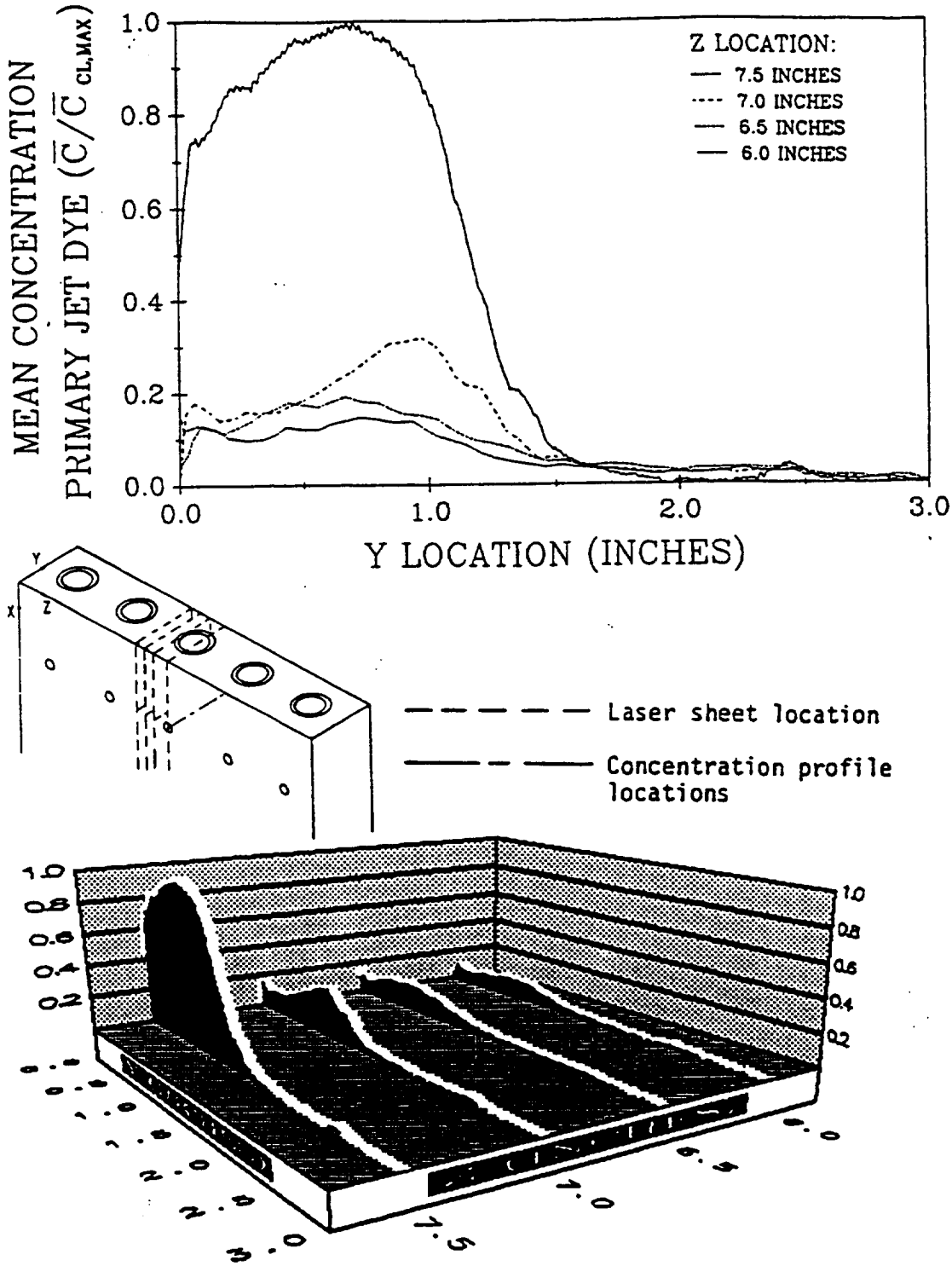

Figure 4.23. Mean Primary Jet Concentration with Annular Jet Flow (x = 3.0 inches)

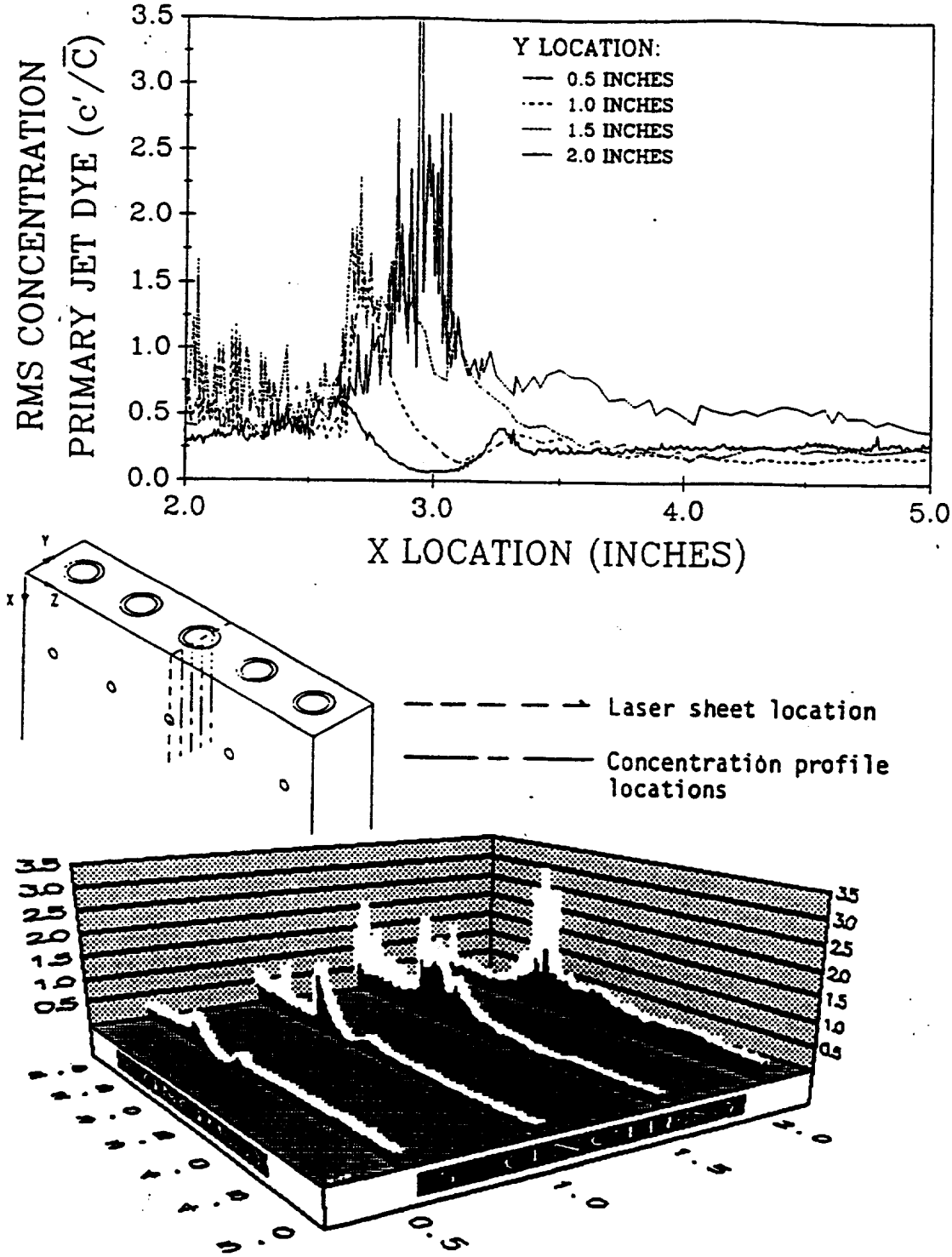

Figure 4.24. RMS Primary Jet Concentration with Annular Jet Flow (z = 7.5 inches)

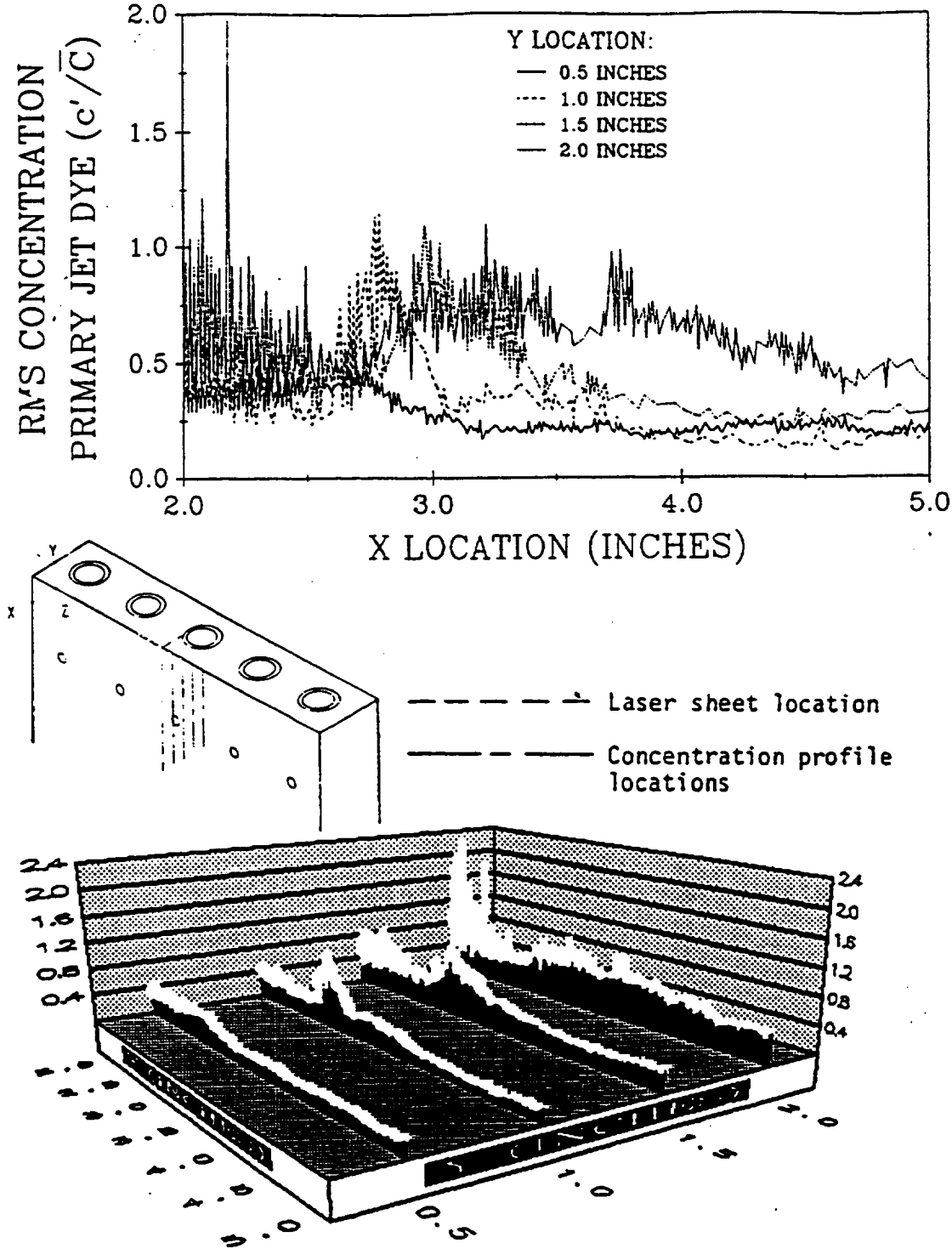

Figure 4.25. RMS Primary Jet Concentration with Annular Jet Flow (z = 7.0 inches)

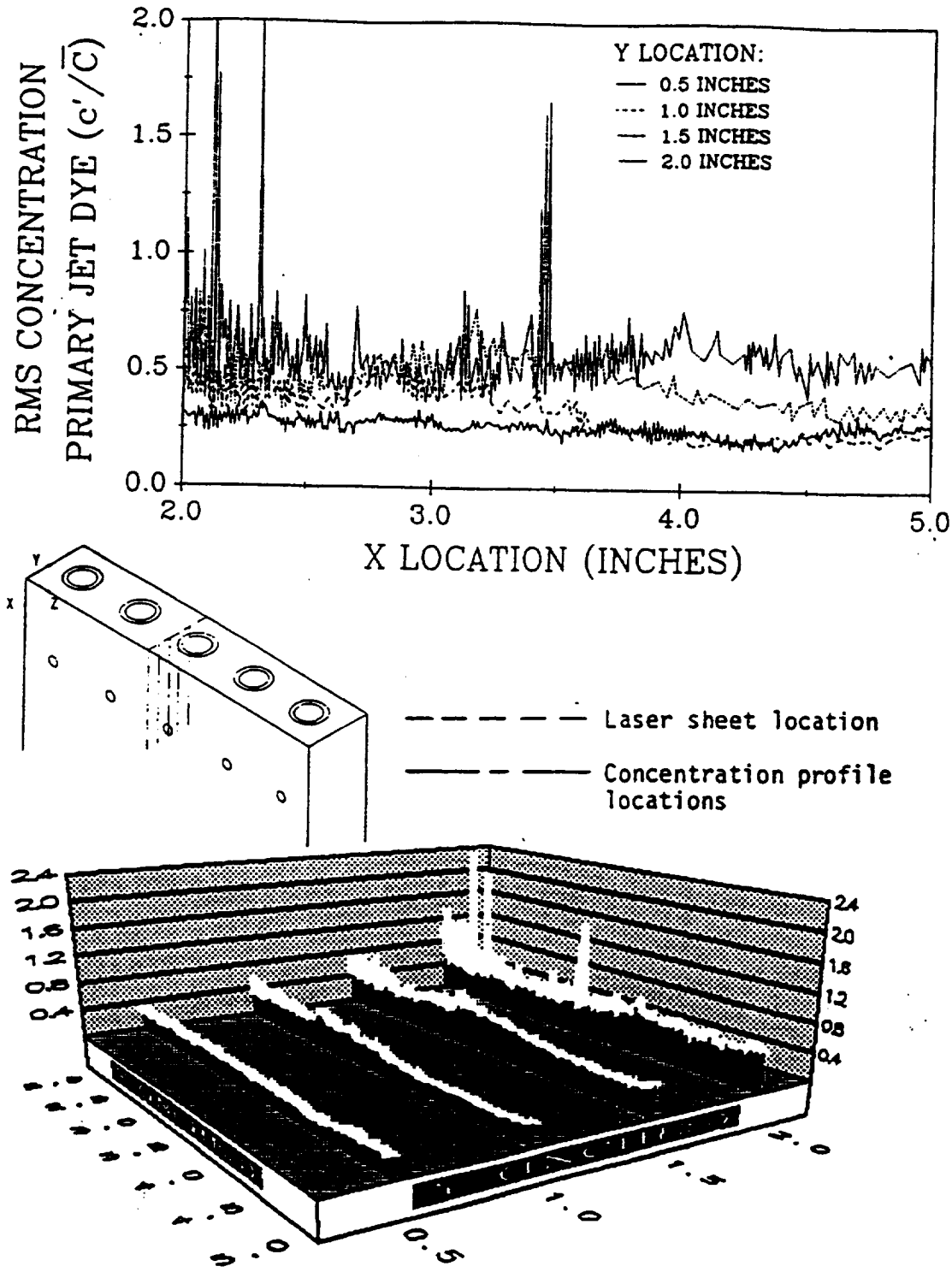

Figure 4.26. RMS Primary Jet Concentration with Annular Jet Flow (z = 6.5 inches)

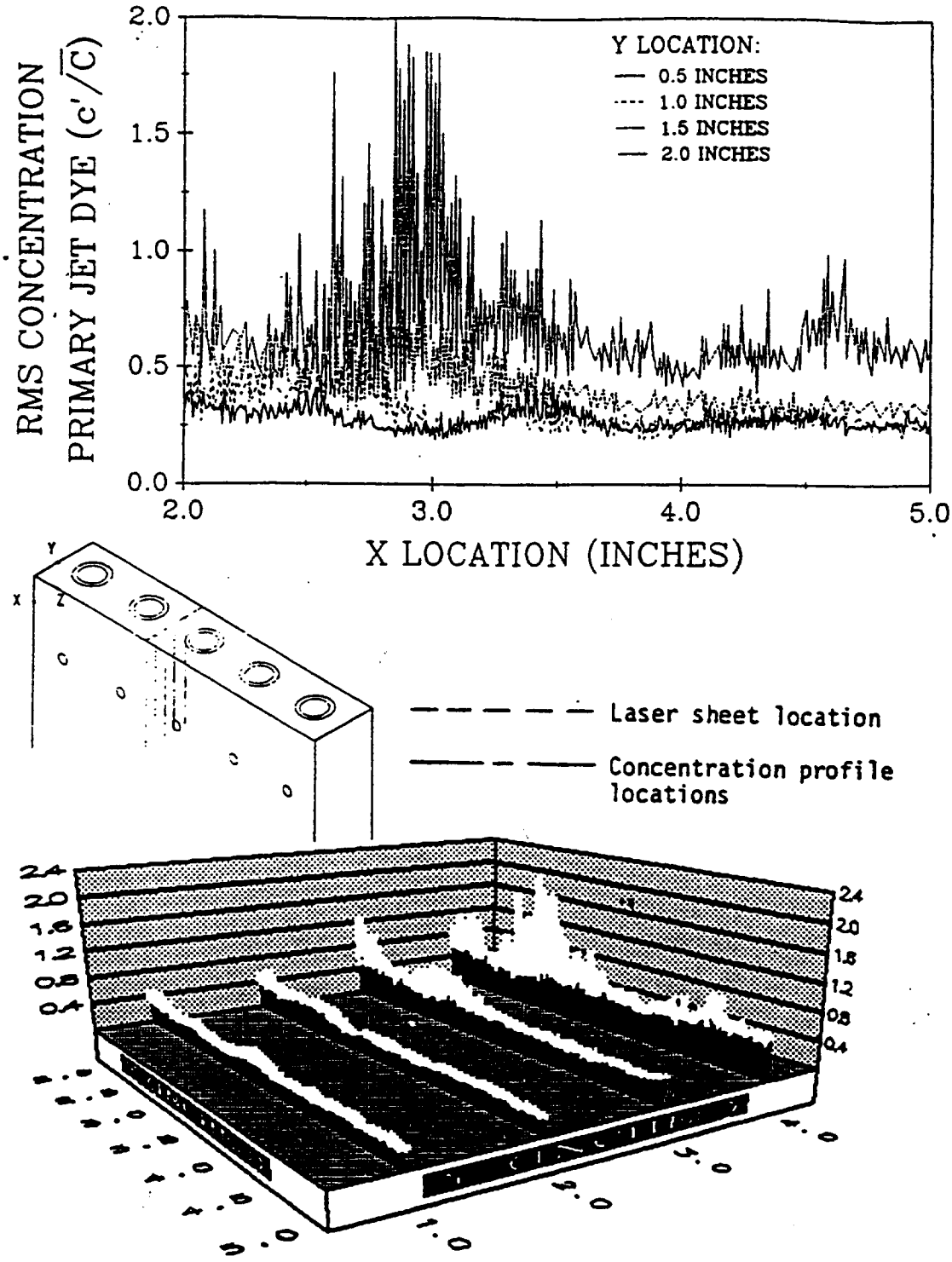

Figure 4.27. RMS Primary Jet Concentration with Annular Jet Flow (z = 6.0 inches)

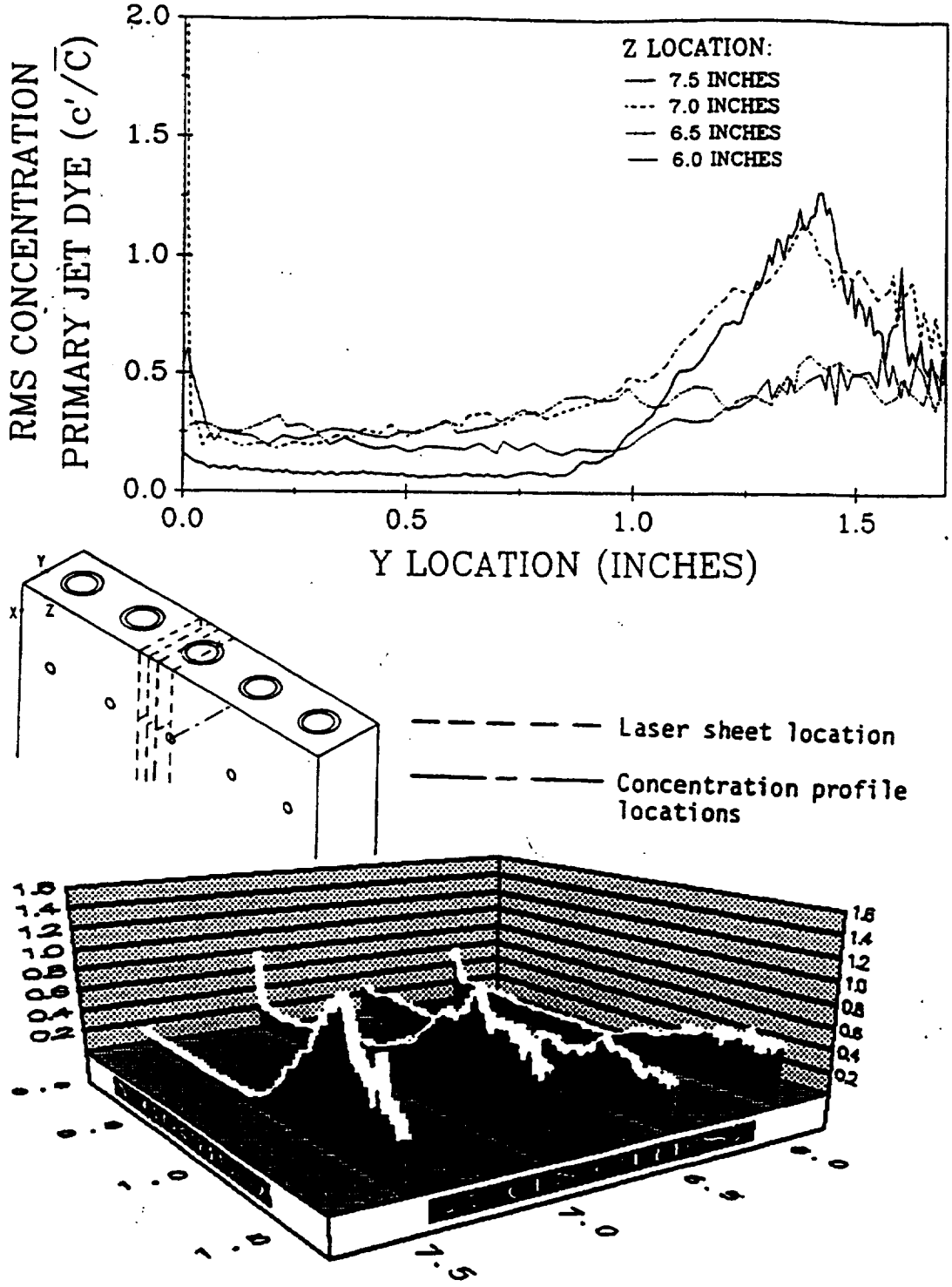

Figure 4.28. RMS Primary Jet Concentration with Annular Jet Flow (x = 3.0 inches)

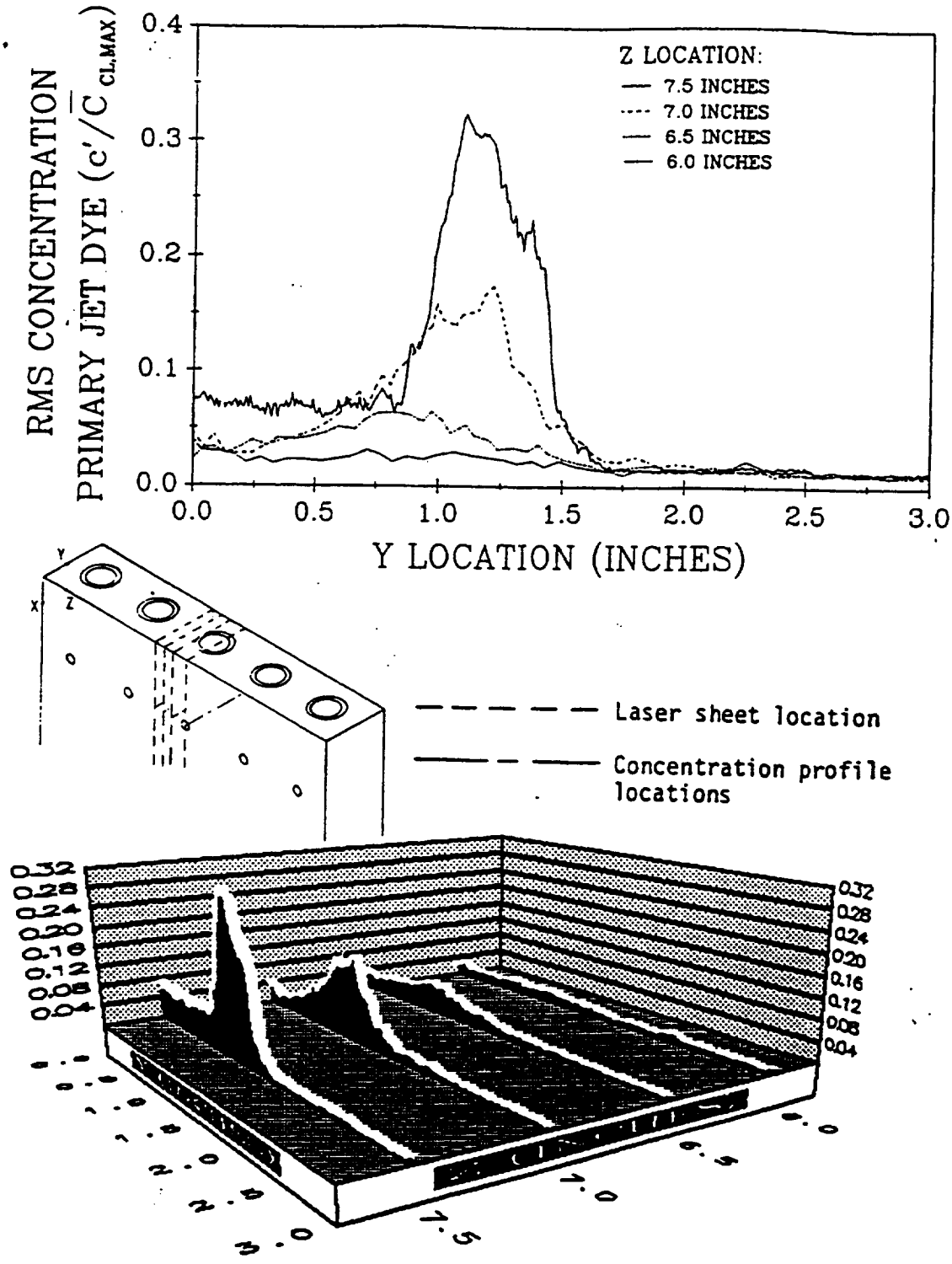

Figure 4.29. RMS Primary Jet Concentration Normalized by $\bar{C}_{CL,MAX}$ with Annular Jet Flow (x = 3.0 inches)

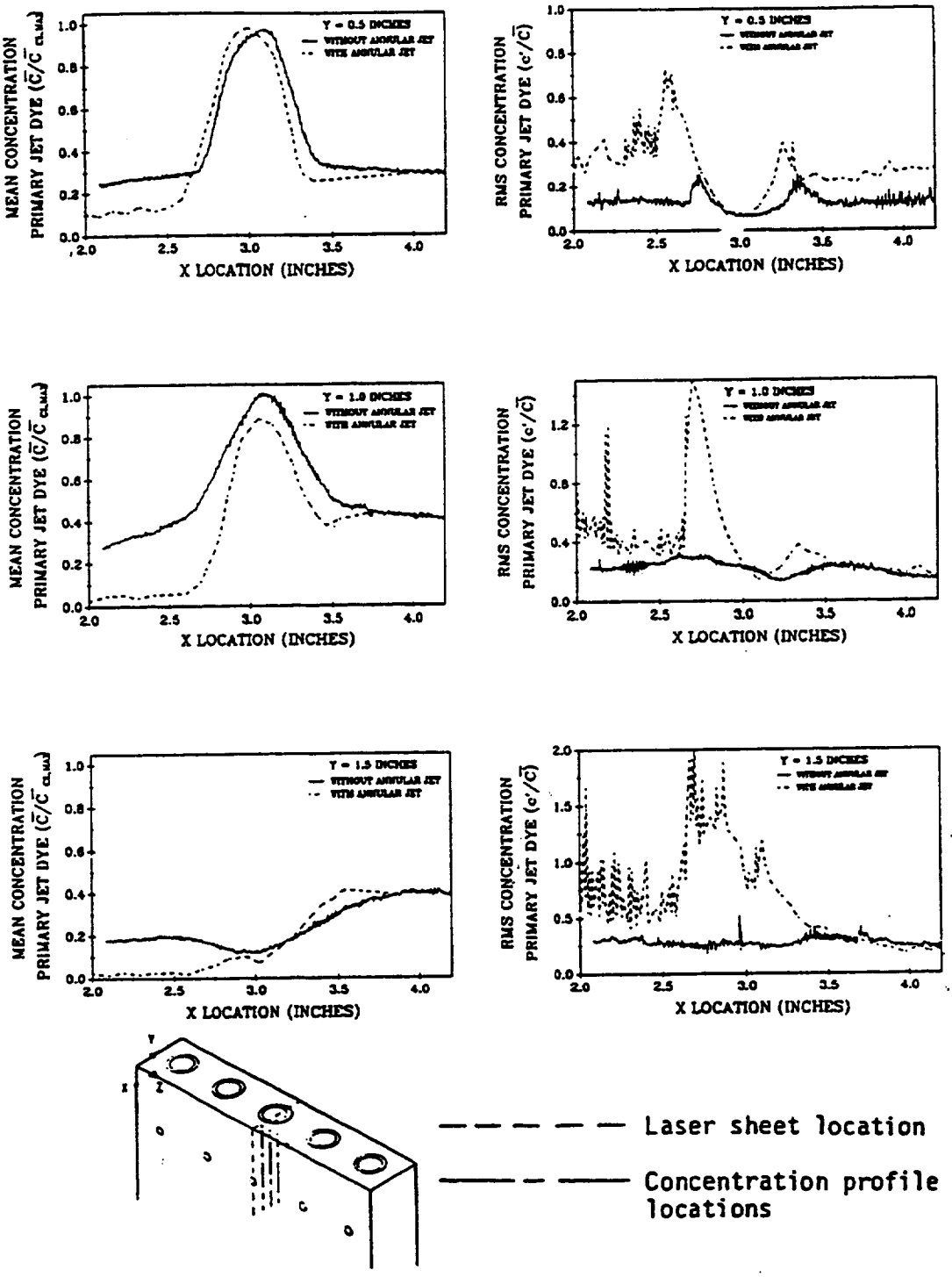

Figure 4.30. Comparison of Primary Jet Concentration with and without Annular Jet Flow (z = 7.5 inches)

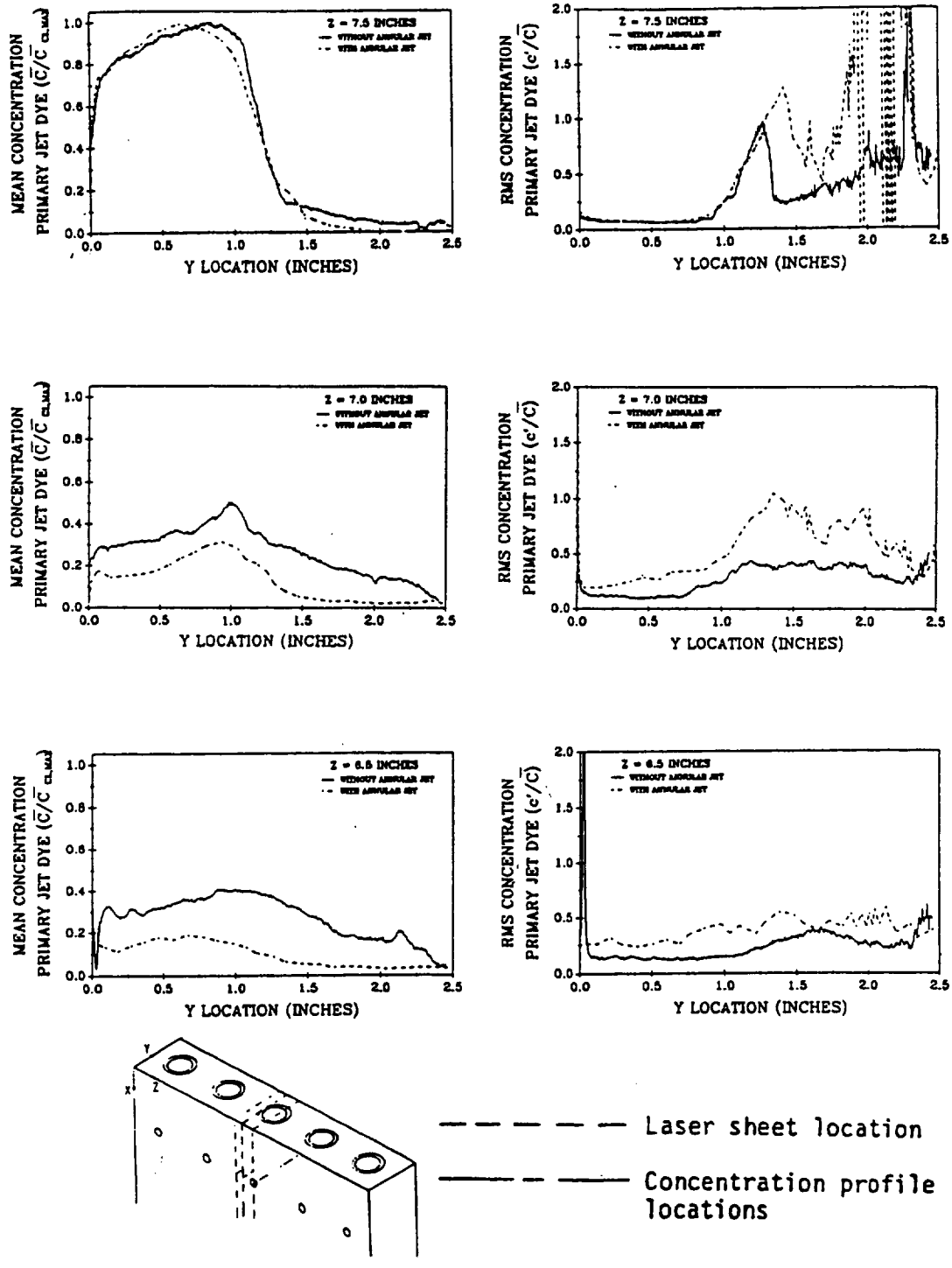

Figure 4.31. Comparison of Primary Jet Concentration with and without Annular Jet Flow (x = 3.0 inches)

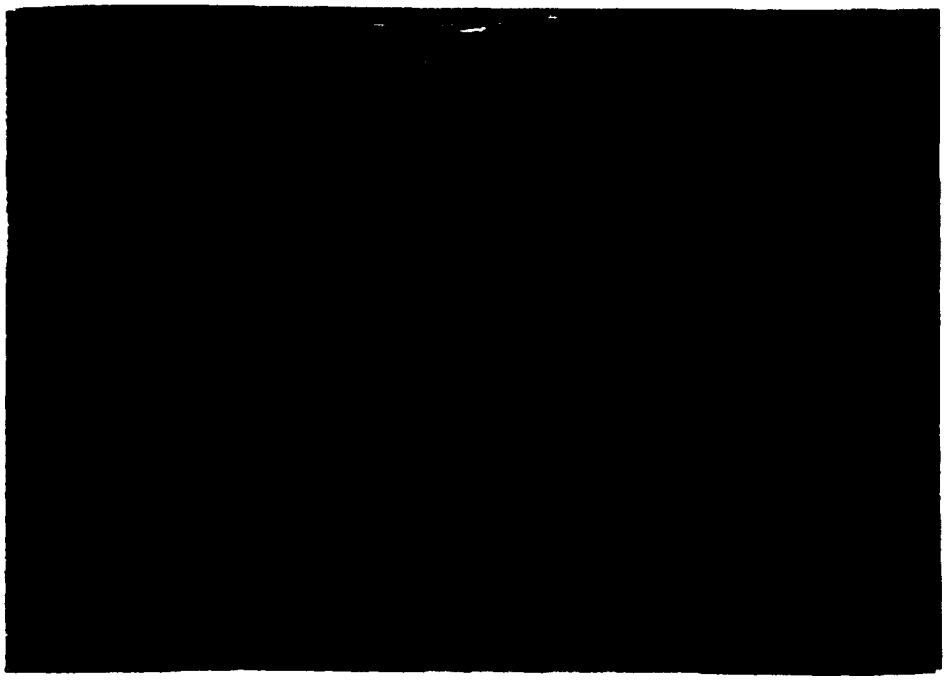

TE92-2390

Figure 4.32. Single Frame Annular Jet Concentration Field Visualization Image (z = 7.5 inches)

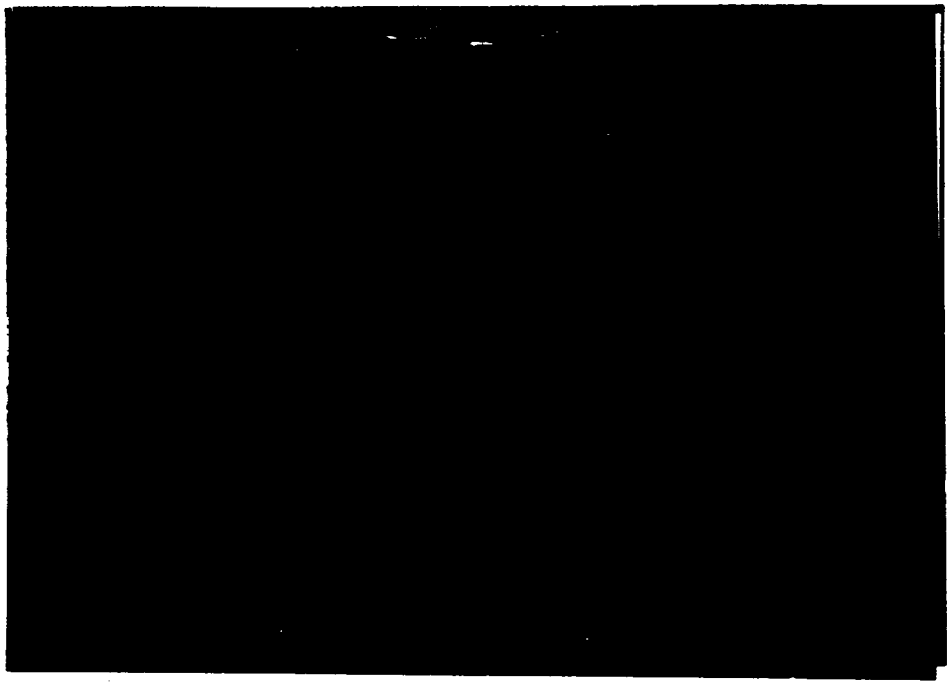

TE92-2391

Figure 4.33. 127 Frame Average Annular Jet Concentration Field Visualization Image (z = 7.5 inches)

TE92-2392

Figure 4.34. Single Frame Annular Jet Concentration Field Visualization Image (z = 7.0 inches)

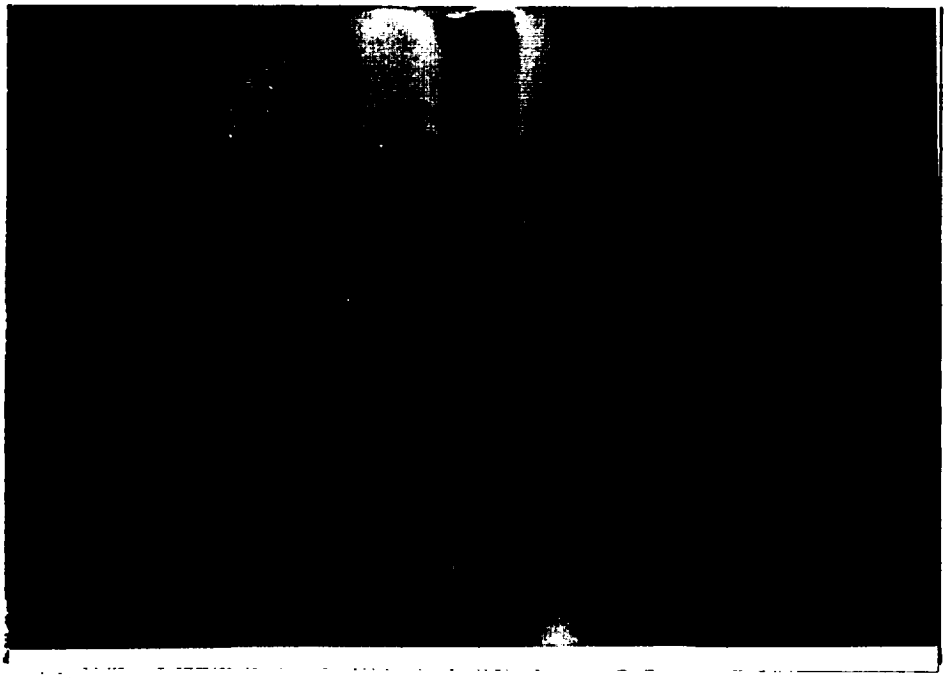

TE92-2393

Figure 4.35. 127 Frame Average Annular Jet Concentration Field Visualization Image (z = 7.0 inches)

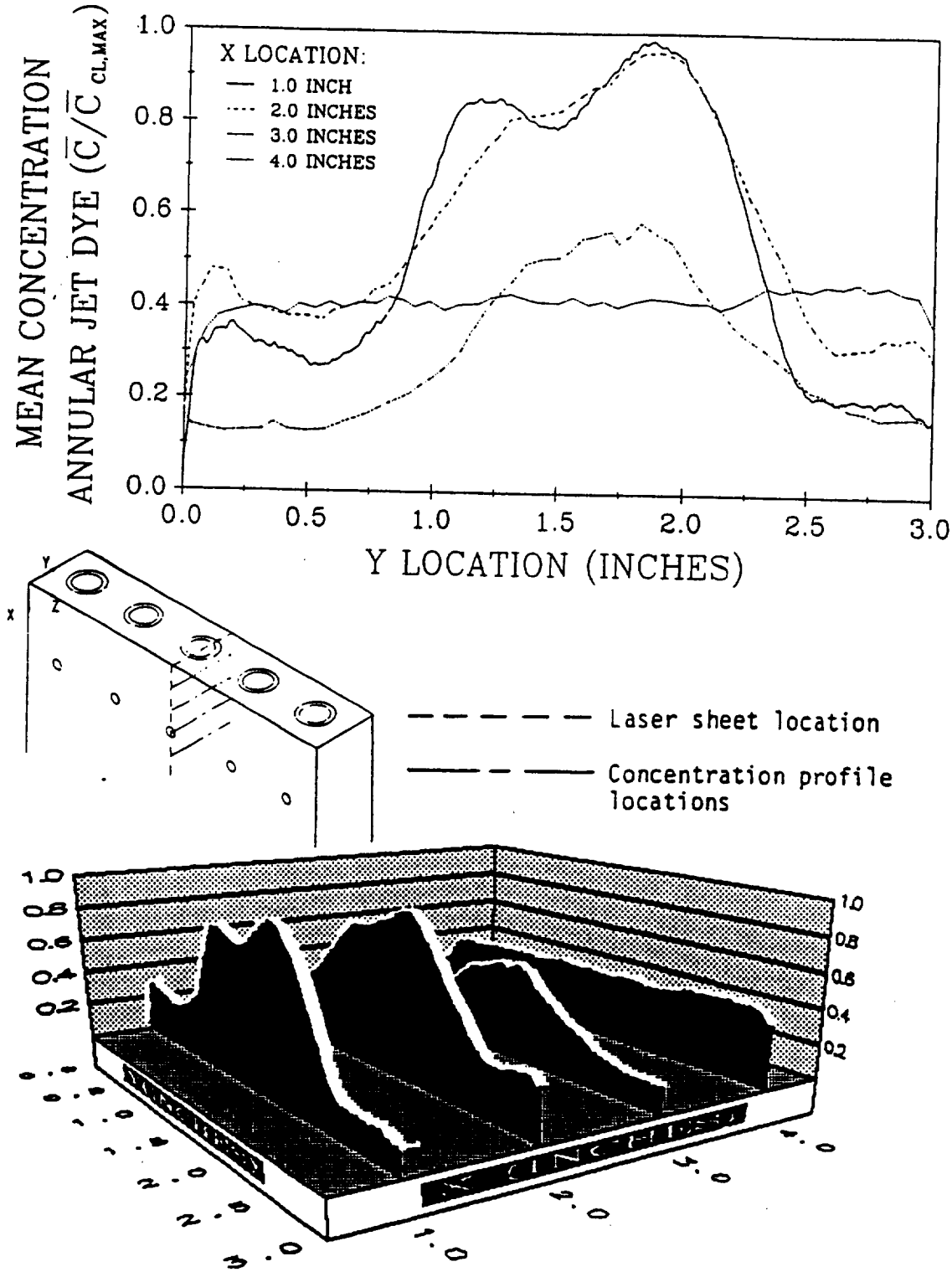

Figure 4.36. Mean Annular Jet Concentration (z = 7.5 inches)

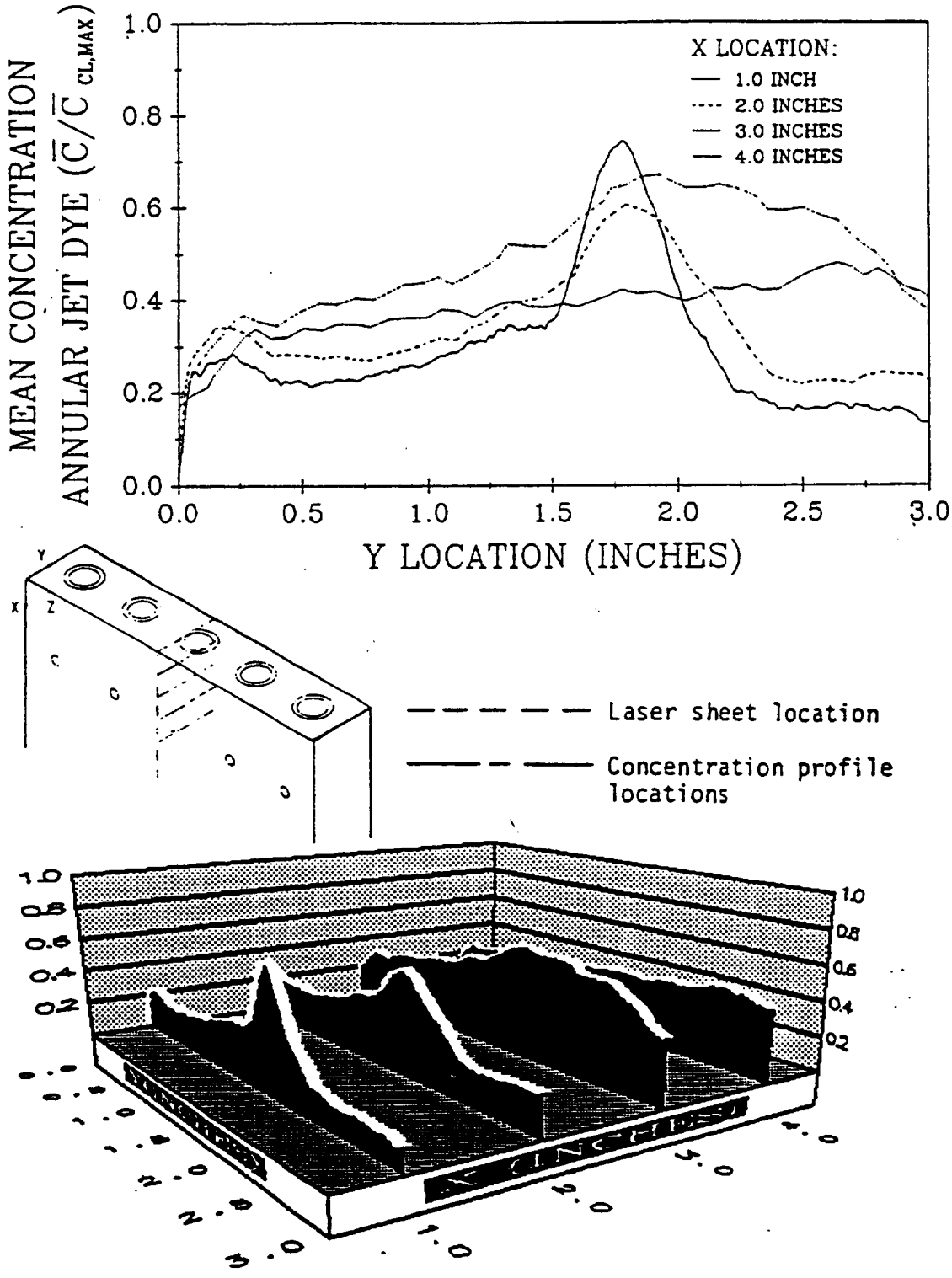

Figure 4.37. Mean Annular Jet Concentration (z = 7.0 inches)

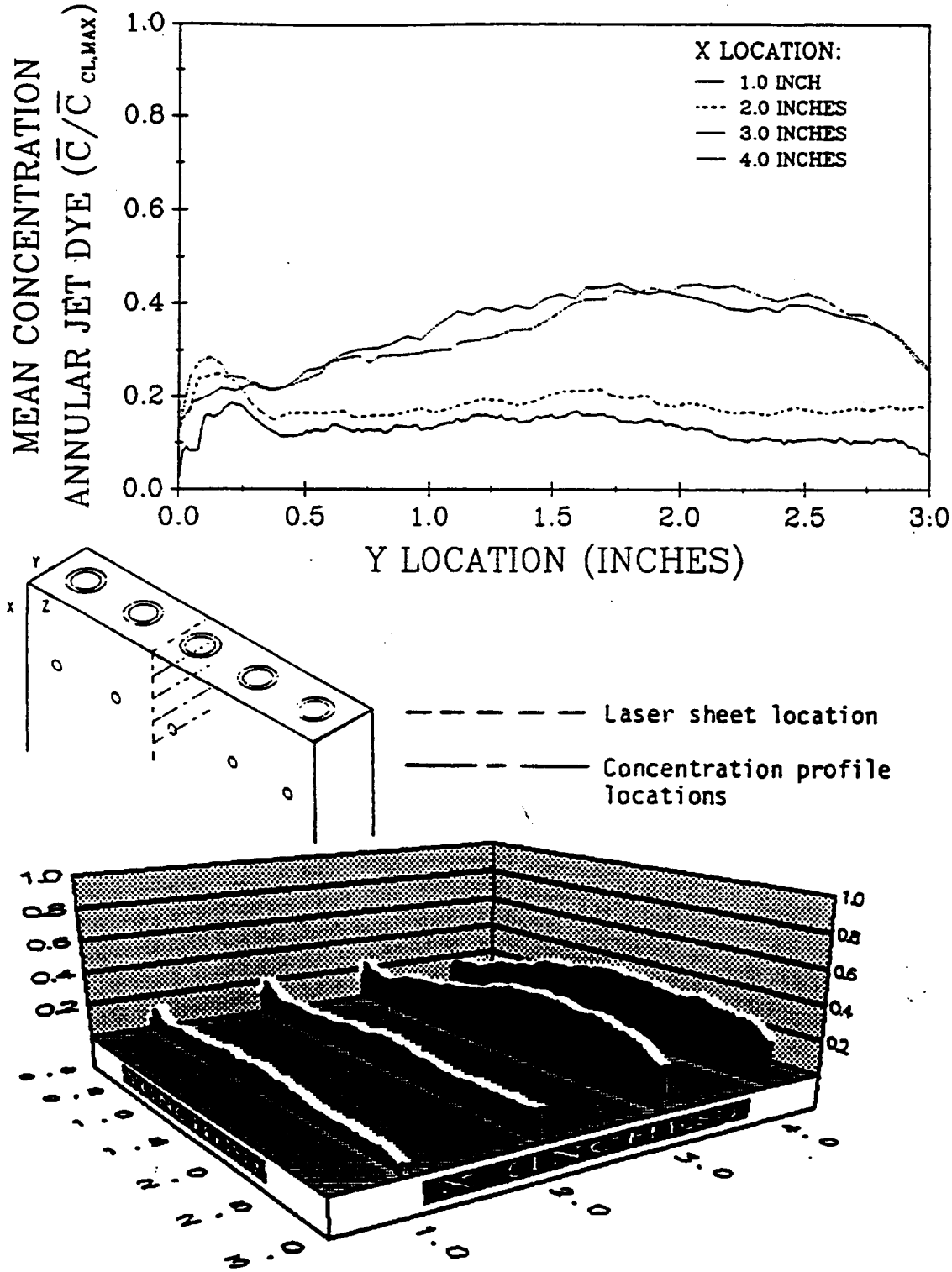

Figure 4.38. Mean Annular Jet Concentration (z = 6.5 inches)

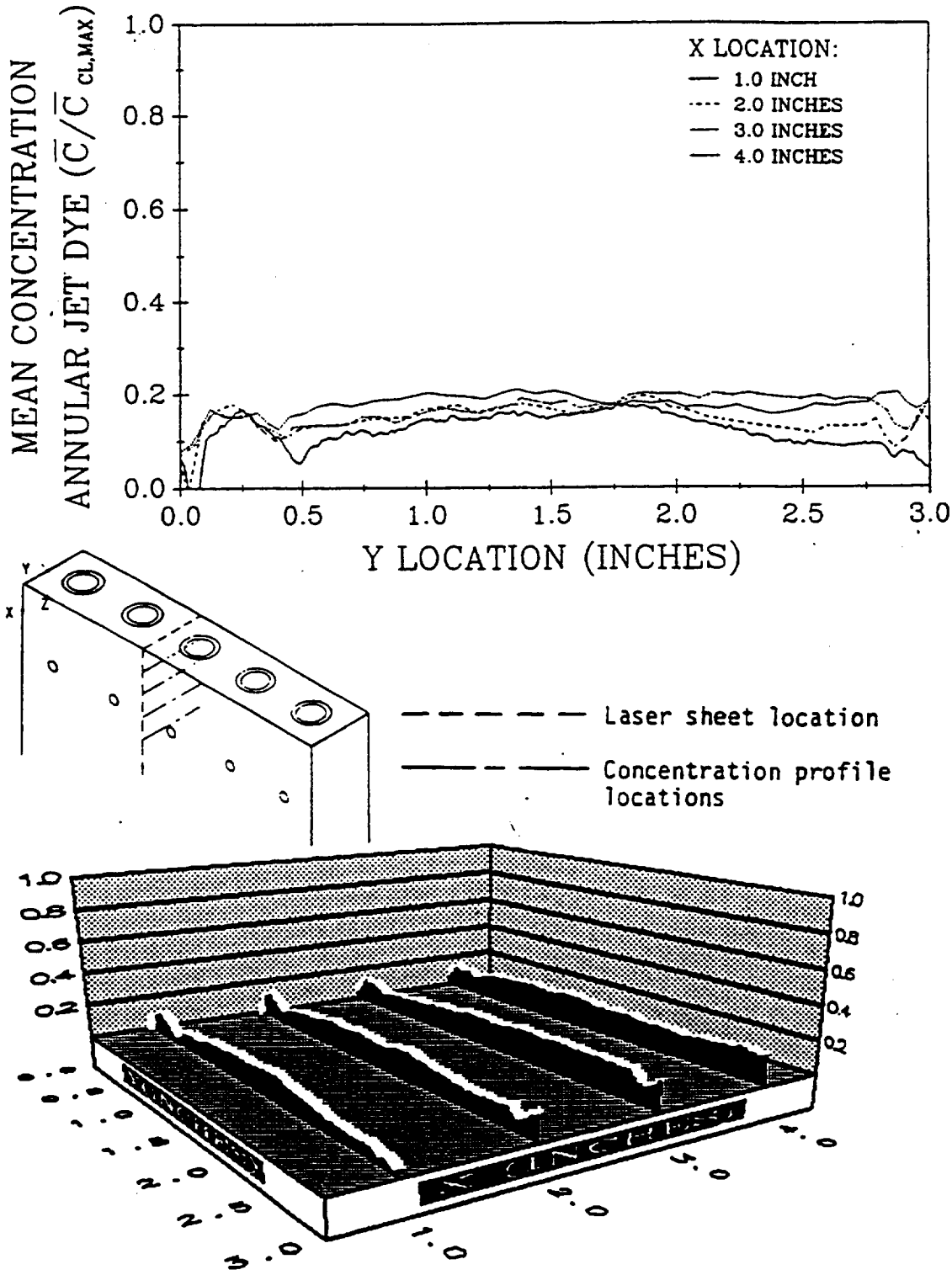

Figure 4.39. Mean Annular Jet Concentration (z = 6.0 inches)

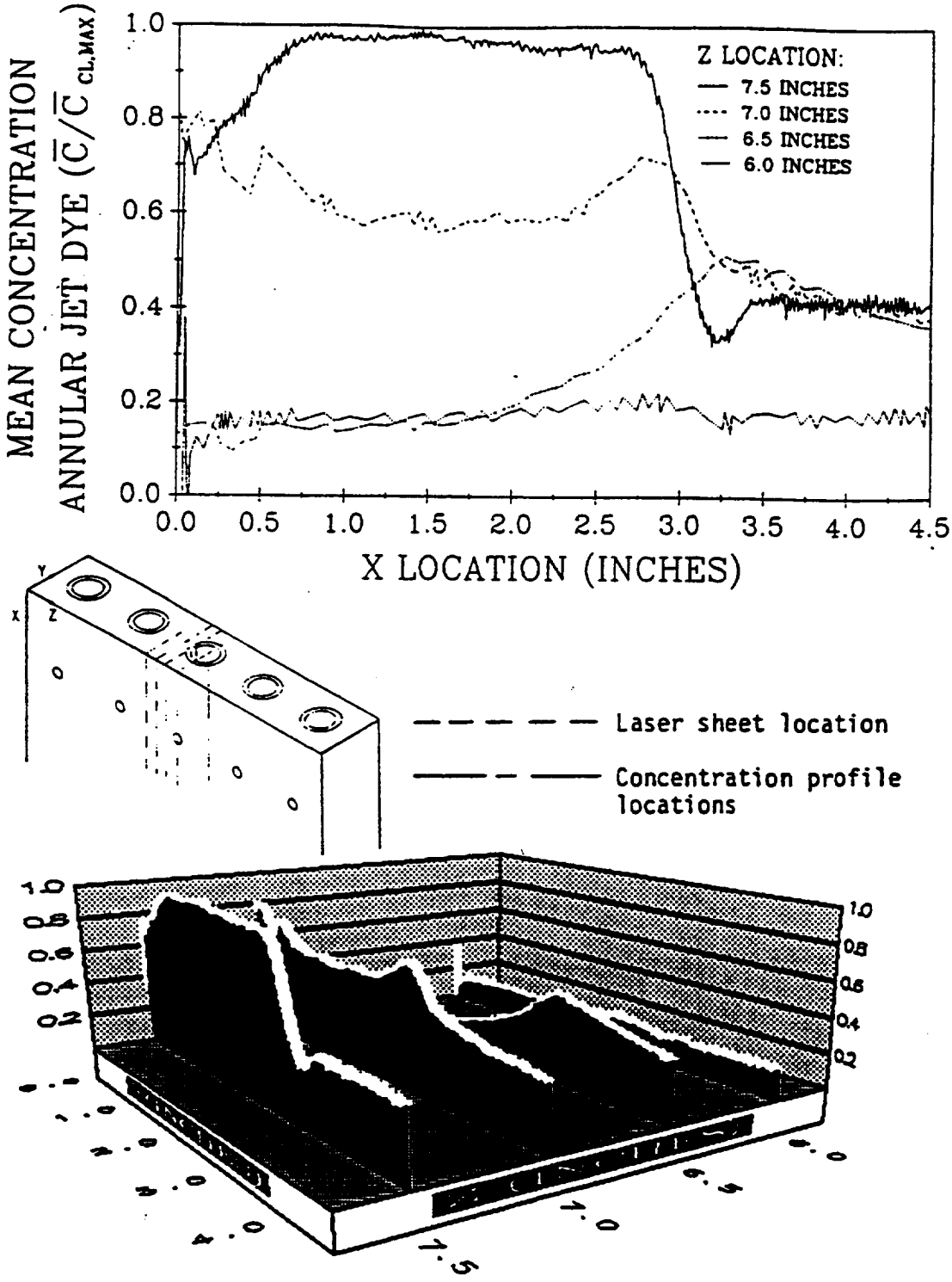

Figure 4.40. Mean Annular Jet Concentration (y = 1.5 inches)

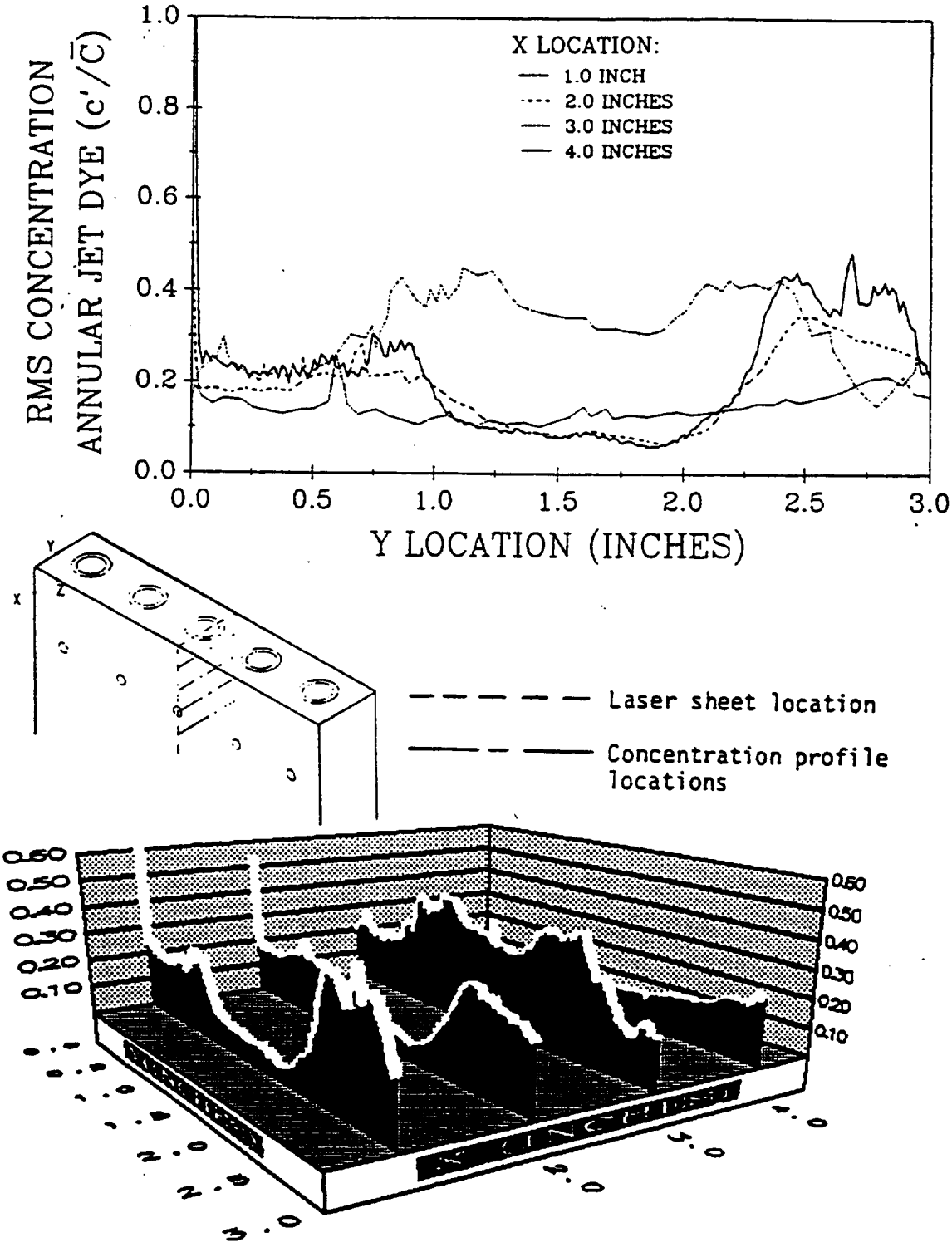

Figure 4.41. RMS Annular Jet Concentration (z = 7.5 inches)

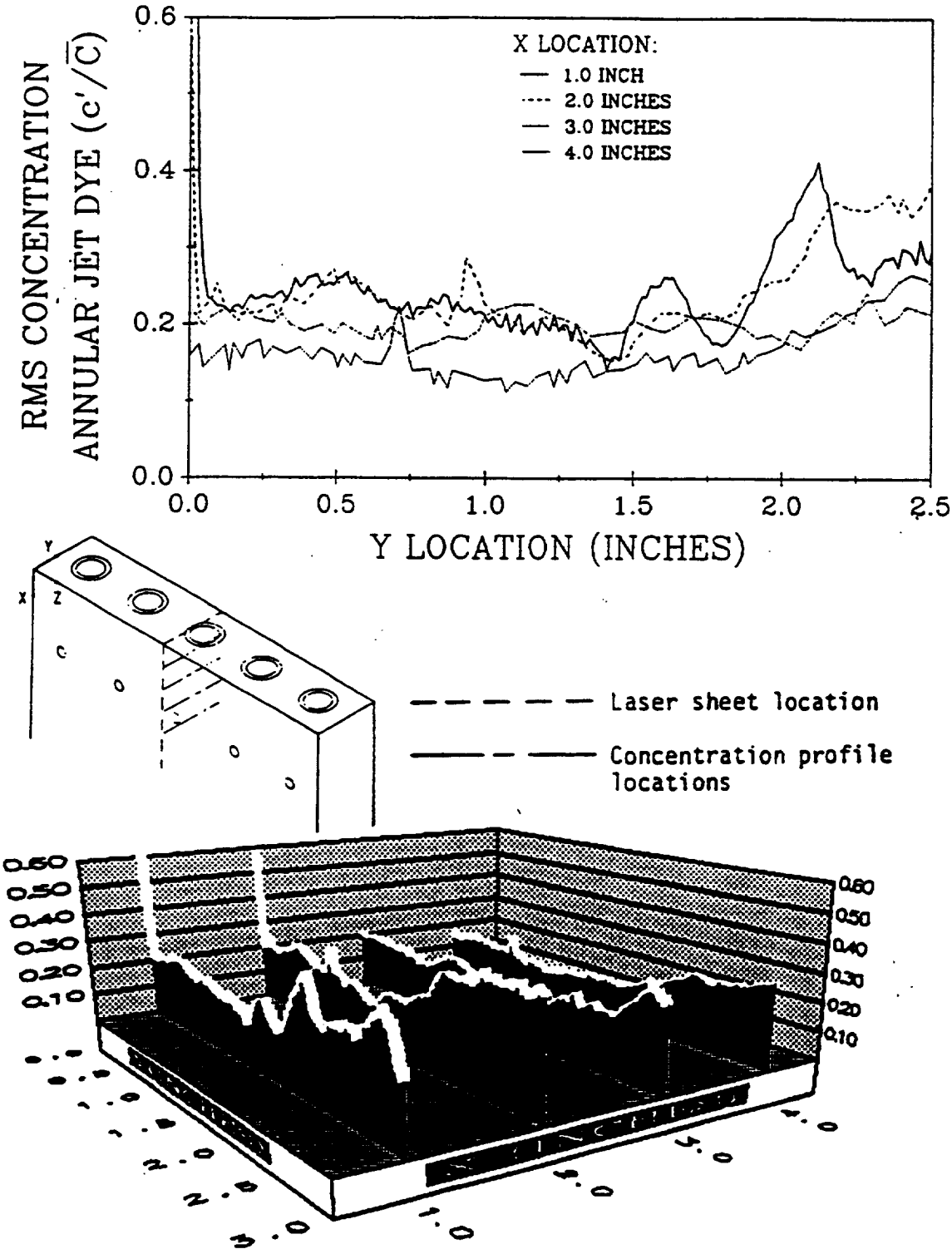

Figure 4.42. RMS Annular Jet Concentration (z = 7.0 inches)

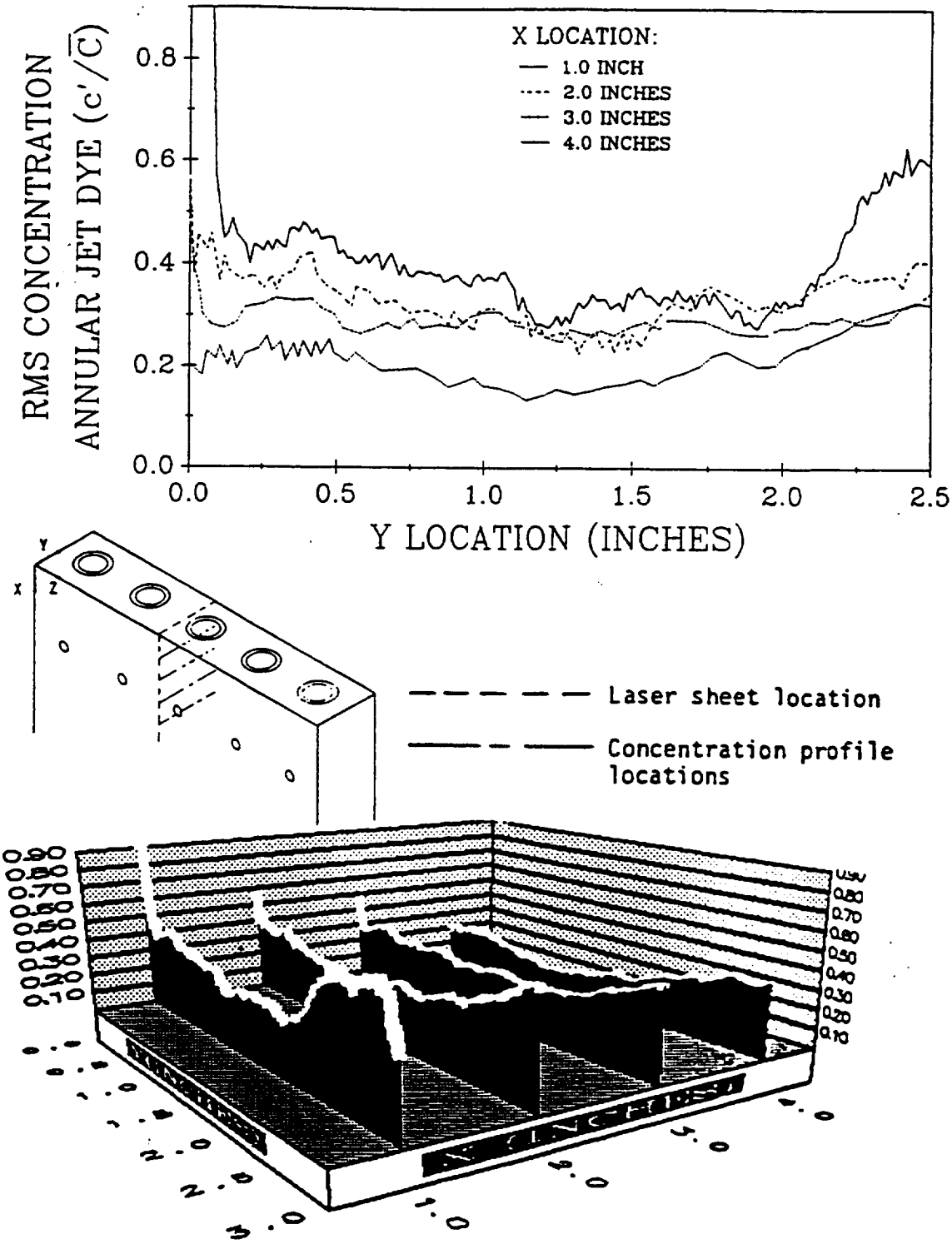

Figure 4.43. RMS Annular Jet Concentration (z = 6.5 inches)

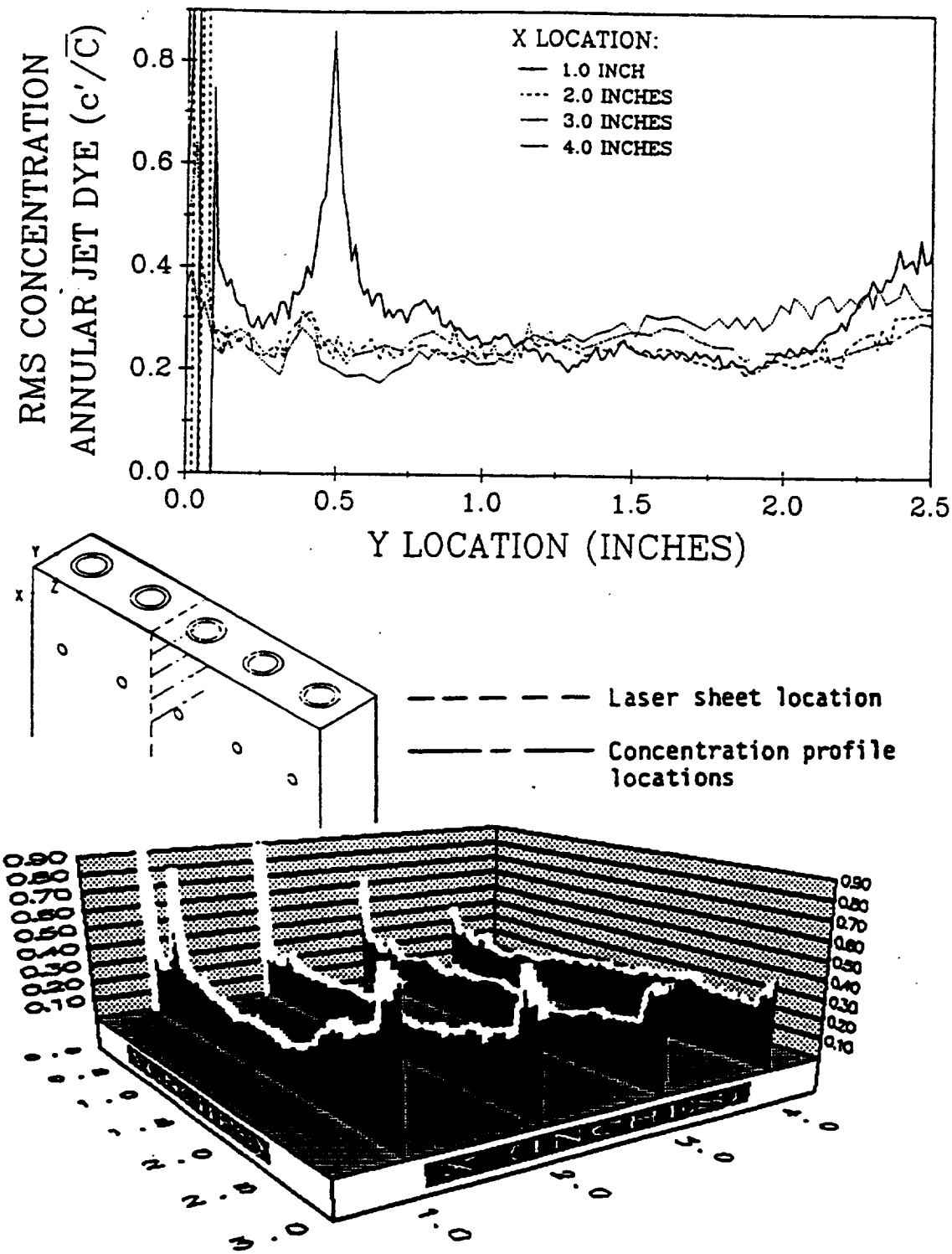

Figure 4.44. RMS Annular Jet Concentration (z = 6.0 inches)

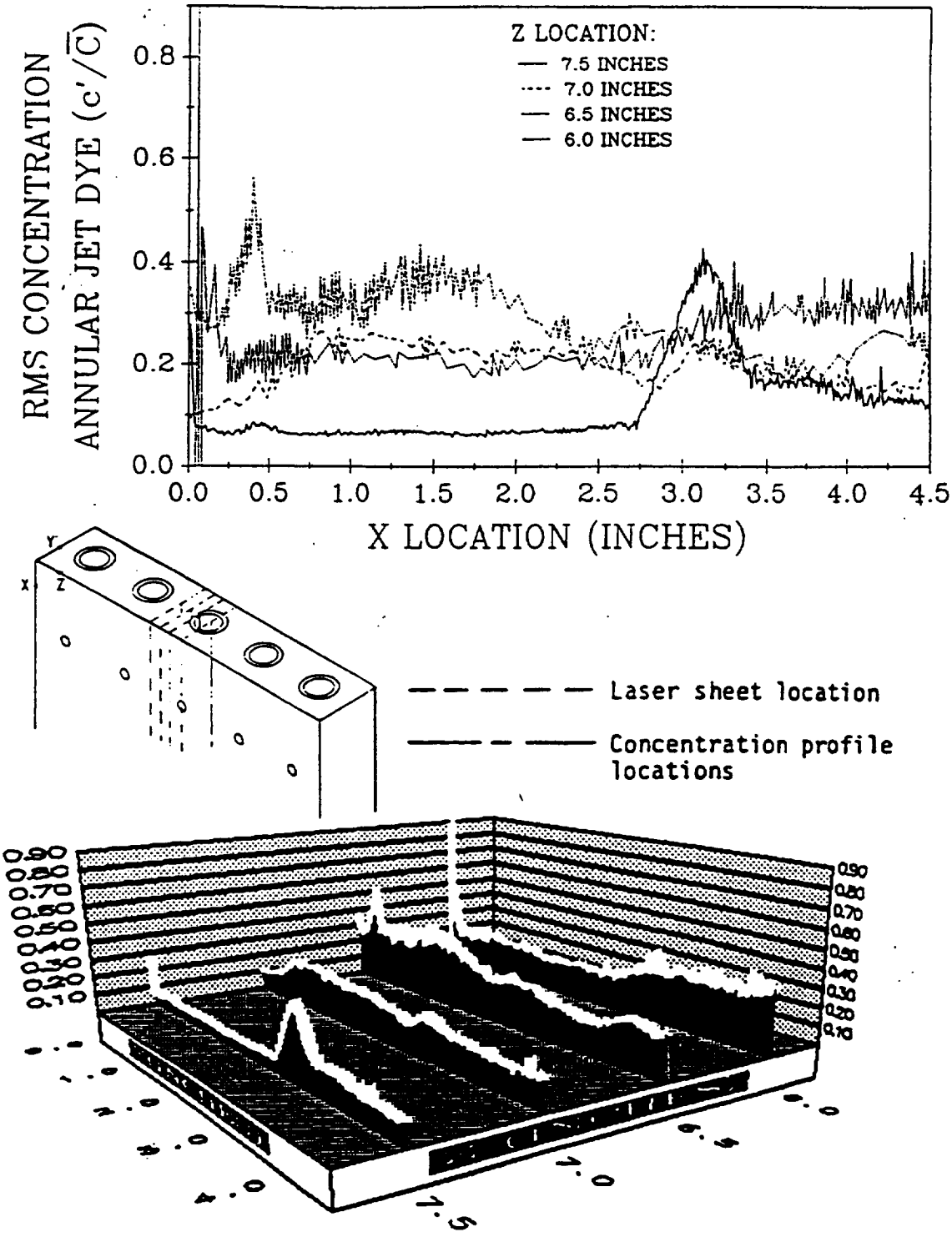

Figure 4.45. RMS Annular Jet Concentration (y = 1.5 inches)

LIST OF REFERENCES

1. Bálint, J. L., Ayrault, M., and Schon, J. P., "Quantitative Investigation of the Velocity and Concentration Fields of Turbulent Flows Combining Visualization and Image Processing," *Flow Visualization III, Proceedings of the Third International Symposium on Flow Visualization,* Sept. 1983, Univ. of Michigan, Ann Arbor, Michigan, Edited by W. J. Yang, Hemisphere Publishing Corp., Washington D. C.

2. Becker, H. A., Hottel, and Williams, G. C., "On the light-scatter technique for the study of turbulence and mixing," Journal of Fluid Mechanics, Vol. 30, part 2, pp. 259-284, 1967.

3. Becker, H. A., Hottel, H. C., and Williams, G. C., "The nozzle-fluid concentration field of the round, turbulent, free jet," Journal of Fluid Mechanics, Vol. 30, part 2, pp. 285-303, 1967.

4. Beer, J. M., and Chigier, N. A., *Combustion Aerodynamics,* Kreiger Publishing Co., Malabar, FL, 1983.

5. Birch, A. D., Brown, D. R., Dodson, M. G., and Thomas, J. R., "The turbulent concentration field of a methane jet," Journal of Fluid Mechanics, Vol. 88, part 3, pp. 431-449, 1978.

6. Borleteau, J-P., "Concentration Measurement with Digital Image Processing," ICIASF '83 Record, pp. 37-42, 1983.

7. Borrego, C. and Olivari, D., " A Method for the Measurements of Mixing Properties in a Flow," AGARD CP-281, *Testing and Measurement Techniques in Heat Transfer and Combustion,* September 1980.

8. Brandt, A., "Hydrodynamic flowfield imaging," *Flow Visualization III, Proceedings of the Third International Symposium on Flow Visualization,* Sept. 1983, Univ. of Michigan, Ann Arbor, Michigan, Edited by W. J. Yang, Hemisphere Publishing Corp., Washington D. C.

9. Chigier, N. A., and Beer, J. M., "The Flow Region Near the Nozzle in Double Concentric Jets," Transactions of the ASME, Journal of Basic Engineering, Vol. 86, pp. 797-804, 1964.

10. Dahm, W. J. A., and Dimotakis, P. E., "Measurements of Entrainment and Mixing in Turbulent Jets," AIAA 23rd Aerospace Sciences Meeting, Reno, Nevada, Jan., 1985, AIAA paper no. 85-0056.

11. Forstall, W. Jr. and Shapiro, A. H., " Momentum and Mass Transfer in Coaxial Gas Jets," ASME Transactions, Journal of Applied Mechanics, Vol. 17, pp. 399-408, 1950.

12. Hinze, J. O., *Turbulence,* McGraw-Hill, New York, 1975.

13. Koochesfahani, M. M., and Dimotakis, P. E., "Laser Induced Fluorescence Measurements of Concentration in a Plane Mixing Layer," AIAA 22nd Aerospace Sciences Meeting, Reno, Nevada, Jan., 1984, AIAA paper no. 84-0198.

14. Long, M. B., Chu, B. T., and Chang, R. K., "Instantaneous Two-dimensional Gas Concentration Measurements by Light Scattering," AIAA Journal, Vol. 19, No. 9, pp. 1151-1157, 1981.

15. Long, M. B., Webber, B. F., and Chang, R. K., "Instantaneous two-dimensional concentration measurements in flow by Mie scattering," Applied Physics Letters, Vol. 34, pp. 22-24, 1979.

16. Rosensweig, R. E., Hottel, H. C., and Williams, G. C., "Smoke-scattered light measurement of turbulent concentration fluctuations," Chemical Engineering Science, Vol. 15, pp. 111-129, 1961.

17. Seal, M. D. II, " An Experimental Study of Swirling Flows as Applied to Annular Combustors," MS Thesis, Purdue University, May 1988.

18. Squire, H. B. and Trouncer, J., "Round Jets in a General Stream," ARC Technical Report R&M No. 1974, 1944.

19. Tennekes, H. and Lumley, J. L., *A First Course in Turbulence,* MIT Press, Cambridge, Mass., 1973.

20. Vranos, A., and Liscinsky, D. S., "A Study of Turbulent Jet Mixing Through Planar Imaging and Gas Sampling," AIAA/SAE/ASME/ASEE 21st Joint Propulsion Conference, Monterey, Calif., July, 1985, AIAA paper no. 85-1444.

21. Walker, D. A., " A fluorescence technique for measurement of concentration in mixing liquids," Journal of Physics E: Scientific Instruments, Vol. 20, pp. 217-224, 1987.

APPENDIX

The effect of nonuniformities in the laser sheet and in the camera response were not accounted for in this thesis. In this appendix, those effects are investigated.

Uniform concentration fields were obtained in the model annular combustor test section by circulating a very dilute dye solution through the test rig. The fluorescent field was recorded for various uniform concentration levels. Dark response data were also recorded with no dye in the rig. These raw data are presented in figure A.1. The values on the vertical axis are the levels assigned by the image digitizer. The increase at the sides of the channel are due to the laser sheet reflecting from the plexiglass sides. This reflection results in a higher laser intensity near the wall.

Figure A.2 presents the profiles obtained for the different concentration levels by subtracting the dark response from the measured intensity field. This is the method of data correction which was used in this thesis. As expected, the profiles are fairly flat across the center portion of the channel (0.5" < y < 2.0"). The response at the sides is apparently non-linear since the profile drops off at each side. This could be due to a combination of the reflection from the plexiglass walls and nonuniformities in the camera response towards the edge of the image.

Long, Chu and Chang[14] suggest correcting for the camera's nonuniformities by recording an image of a uniform dilute concentration field and dividing the measured

image by this dilute response image. This is the second step of a two step correction which they used. The first step being the subtraction of the dark response mentioned above.

Figure A.3 presents the results after performing this two step correction. The lowest concentration level image was used for the dilute response. The drop at the sides is still apparent and is therefore probably due to the reflection from the plexiglass sides. The profiles over the center portion of the channel are fairly flat, but not significantly improved from those in figure A.2. Therefore, the single step correction used in this thesis is probably sufficient over the majority of the flow area. The near wall regions could possibly be improved by masking the laser sheet such that the visible sheet width is less than the flow channel width. The sheet must still be maintained much wider than the measurement area to reduce the Gaussian variation effects.

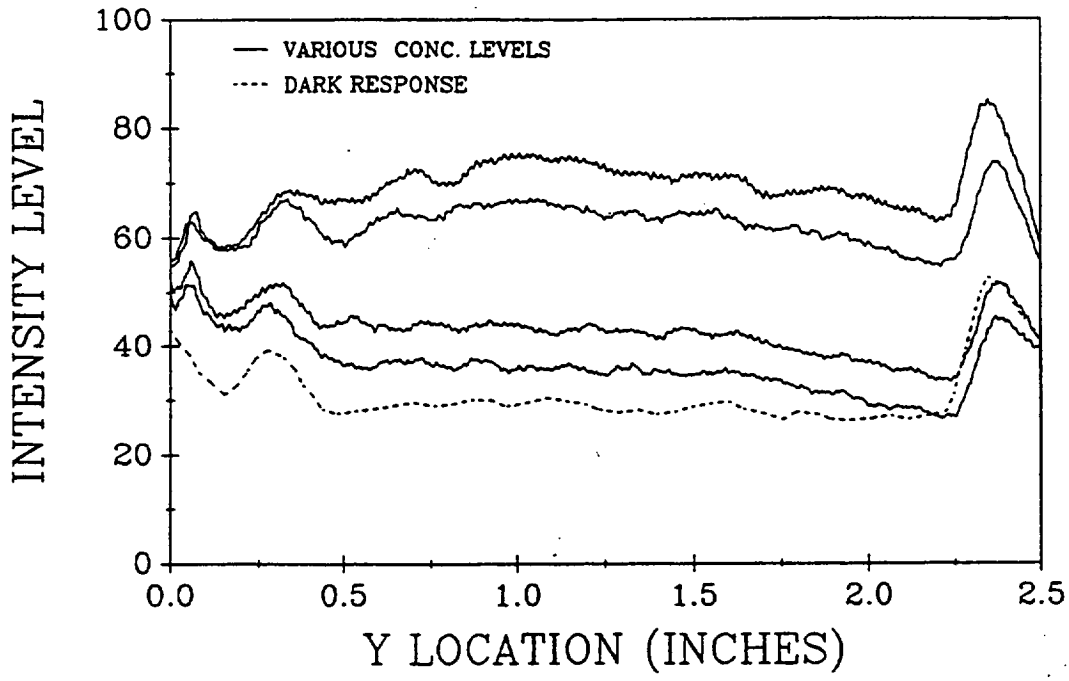

Figure A.1. Uniform Concentration Profiles, Raw Data

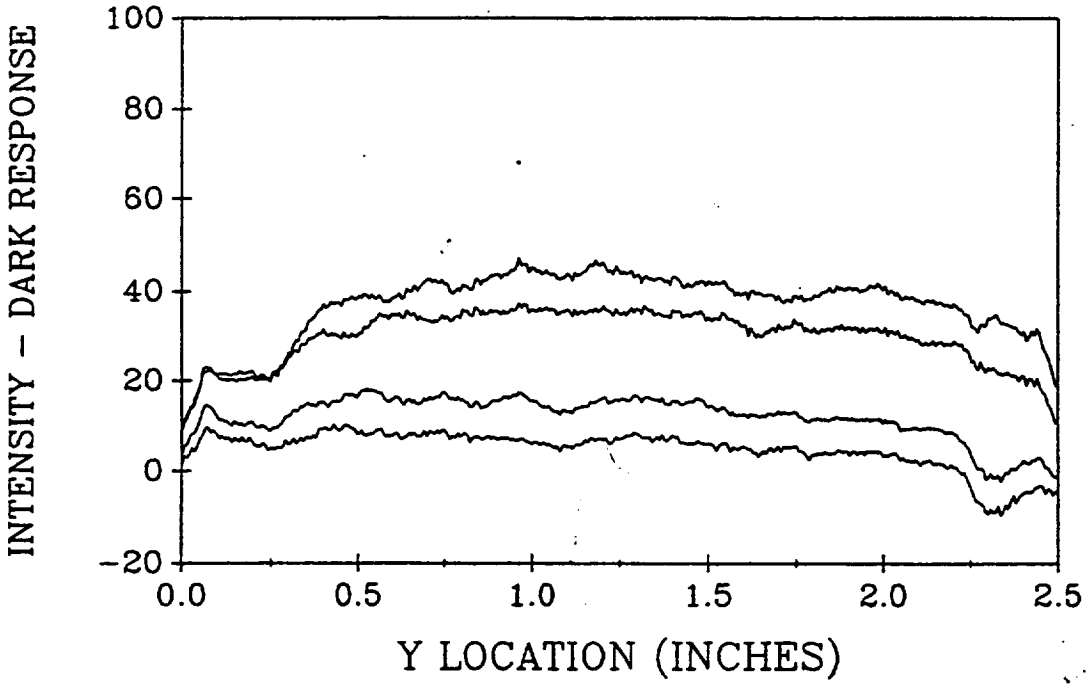

Figure A.2. Uniform Concentration Profiles, Dark Response Subtracted

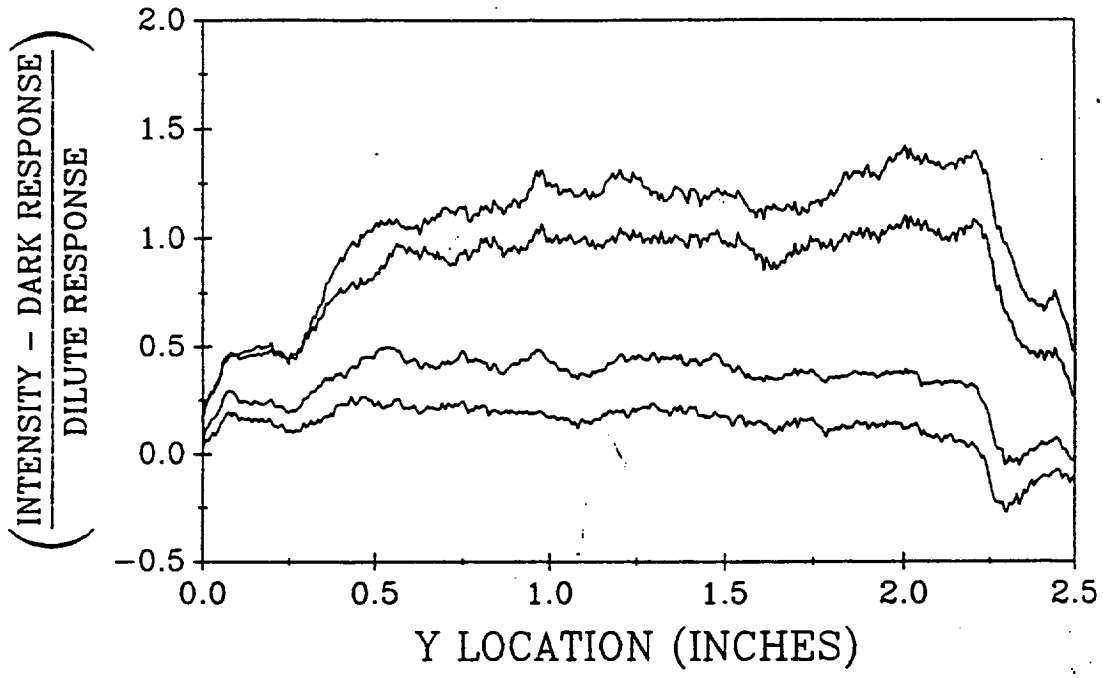

Figure A.3. Uniform Concentration Profiles, 2 Step Correction Applied

REPORT DOCUMENTATION PAGE

Form Approved
OMB No. 0704-0188

1. AGENCY USE ONLY (*Leave blank*)	2. REPORT DATE	3. REPORT TYPE AND DATES COVERED
	September 1996	Final Contractor Report

4. TITLE AND SUBTITLE

Concentration Measurements in a Cold Flow Model Annular Combustor Using Laser Induced Fluorescence

5. FUNDING NUMBERS

WU-505-62-21
C-NAS3-24350

6. AUTHOR(S)

Douglas C. Morgan

7. PERFORMING ORGANIZATION NAME(S) AND ADDRESS(ES)

Purdue University
West Lafayette, Indiana 47907

8. PERFORMING ORGANIZATION REPORT NUMBER

E-9864

9. SPONSORING/MONITORING AGENCY NAME(S) AND ADDRESS(ES)

National Aeronautics and Space Administration
Lewis Research Center
Cleveland, Ohio 44135-3191

10. SPONSORING/MONITORING AGENCY REPORT NUMBER

NASA CR-182252

11. SUPPLEMENTARY NOTES

This report was submitted as a thesis in partial fulfillment of the requirements for the degree Master of Science in Mechanical Engineering to Purdue University, West Lafayette, Indiana 47907. Project Manager, J.D. Holdeman, Internal Fluid Mechanics Division, NASA Lewis Research Center, organization code 2650, (216) 433-5846.

12a. DISTRIBUTION/AVAILABILITY STATEMENT

Unclassified - Unlimited
Subject Category 07

This publication is available from the NASA Center for Aerospace Information, (301) 621-0390.

12b. DISTRIBUTION CODE

13. ABSTRACT (*Maximum 200 words*)

A nonintrusive concentration measurement method is developed for determining the concentration distribution in a complex flow field. The measurement method consists of marking a liquid flow with a water soluble fluorescent dye. The dye is excited by a two dimensional sheet of laser light. The fluorescent intensity is shown to be proportional to the relative concentration level. The fluorescent field is recorded on a video cassette recorder through a video camera. The recorded images are analyzed with image processing hardware and software to obtain intensity levels. Mean and root mean square (rms) values are calculated from these intensity levels. The method is tested on a single round turbulent jet because previous concentration measurements have been made on this configuration by other investigators. The previous results were used to comparison to qualify the current method. These comparisons showed that this method provides satisfactory results. The concentration measurement system was used to measure the concentrations in the complex flow field of a model gas turbine annular combustor. The model annular combustor consists of opposing primary jets and an annular jet which discharges perpendicular to the primary jets. The mixing between the different jet flows can be visualized from the calculated mean and rms profiles. Concentration field visualization images obtained from the processing provide further qualitative information about the flow field.

14. SUBJECT TERMS	15. NUMBER OF PAGES
Turbulent viscous flow; Laser diagnostics; Laser induced fluorescence; Concentration measurements; Annular combustor	107
	16. PRICE CODE: A06

17. SECURITY CLASSIFICATION OF REPORT	18. SECURITY CLASSIFICATION OF THIS PAGE	19. SECURITY CLASSIFICATION OF ABSTRACT	20. LIMITATION OF ABSTRACT
Unclassified	Unclassified	Unclassified	